Thianthrene and Related Heterocycles: Metal Complexes, Radical Cation Salts and Semiconductors

DISSERTATION

zur Erlangung
des Doktogrades (Dr. rer. nat.)
der Mathematisch-Naturwissenschaftlichen Fakultät
der Rheinischen Friedrich-Wilhelms-Universität Bonn

vorgelegt von

Rachmat Triandi Tjahjanto, M. Sc.
aus
Makassar/Indonesien

Bonn 2009

Angefertigt mit Genehmigung der Mathematischen-Naturwissenschaftlichen Fakultät
der Rheinischen Friedrich-Wilhelms-Universität Bonn

1. Gutachter: Prof. Dr. Johannes Beck
2. Gutachter: Prof. Dr. Alexander C. Filippou

Tag der Promotion: 17.7.2009

Erscheinungsjahr: 2009

Diese Dissertation ist auf dem Hochschulschriftenserver der ULB Bonn unter
http://hss.ulb.uni-bonn.de/diss_online elektronisch publiziert.

Abstract

Liquid SO_2 was used as a solvent for complexation as well as redox reactions based on thianthrene and related heterocyclic molecules. With silver salt, AgX (X = BF_4^-, SbF_6^-), the complexes $[Ag_2(TA)_2][BF_4]_2 \cdot 3\,SO_2$ (**1**) and $[Ag_2(TA)_3][SbF_6]_2 \cdot 5\,SO_2$ (**2**), and with gold(III) chloride, the complex $[AuCl_2(TA)_2][AuCl_4]$ (**3**) were obtained. The oxidation products contain radical cations of thianthrene, $TA^{\cdot+}$, as found in the structure of $(TA^{\cdot})(HSO_4) \cdot H_2SO_4$ (**5**) and $(TA^{\cdot})[FeCl_4]$ (**6**), radical cation of selenanthrene in the structure of $(SA^{\cdot})[AlCl_4]$ (**8**) and $(SA^{\cdot})_2[SO_4(BF_3)_2]$ (**10**), and a structure with a bridging oxygen of μ-oxy-selenanthrene(2+), $SAO(HSO_4)_2$ (**9**). The reaction between thianthrene and aluminum chloride was also performed without solvent, resulting in an adduct $[AlCl_3(TA)]$ (**4**) and a unique thianthrene ”triple decker”, $(TA_3)[Al_2Cl_7]_2$ (**7**). An unexpected phenazine salt, $(H_2PAz)(HSO_4)_2$ (**11**) was obtained from phenazine in an oxidative environment. All compounds were examined by single crystal X-ray diffractometry. The gold and aluminum complexes were additionally characterized by UV-Vis, IR and Raman spectra, calorimetry and conductivity measurements. Cyclic voltammetry measurements of thianthrene in SO_2 at room temperature were performed using a self-made pressure-tight electrochemical cell and electrodes with the result that liquid SO_2 does not reduce the oxidation potential of thianthrene. The influence of SO_3, which is often present in liquid SO_2 as impurity, was also studied, confirming its role in the oxidation of thianthrene. The use of liquid SO_2 combined with weak coordinating anions allows complexation of silver ion with higher coordination number, bonded to thianthene via S atoms. SO_3 as an impurity in liquid SO_2 is the most probable source for oxidation reaction leading to the compounds containing radical cations. Thianthrene undergoes self-oxidation processes in the presence of $AlCl_3$, both with or without solvent. Close $TA \cdots TA$ arrangements in the crystal structures should be an indication of the electrical semiconductivity.

Preface

This dissertation is written to fulfill the the requirement for doctoral grade in Math and Natural Science from the Institute of Inorganic Chemistry of University of Bonn. It is based on a series of experimental works during the period from the very beginning of 2004 to the mid of 2008 in the Institute for Inorganic Chemistry, the University of Bonn. Most part of this dissertation is already reported, in short, in six workgroup seminars in the Institute and two poster presentations in *GDCh-Jahrestagung* in Aachen and in Ulm and one oral speech in Hirschegg, Austria. Besides, parts of it have been also published in three publications.

For all material supports and intensive supervisions during the period of doctoral program I thank Professor Dr. Johannes Beck as my supervisor and I thank Dr. Jörg Daniels for the crystal selections and measurements. Norbert Wagner, Volker Bendish, Marcus Zink, Doris Ernsthäuser, Dr. Ralf Weisbarth and Barbara Knopp are thanked for performing measurements in this work.

Parts of this dissertation are published in the following papers:

R. T. Tjahjanto and J. Beck, Synthesis and crystal structures of silver thianthrene complexes with weakly coordinating anions, *Zeitschrift für Naturforschung, B*, vol. 62, pp. 1291–1297, **2007**.

J. Beck, T. Bredow, and R. T. Tjahjanto, Thianthrene radical cation hexafluorophosphate, *Zeitschrift für Naturforschung, B*, vol. 64b, pp. 145–152, **2009**.

R. T. Tjahjanto and J. Beck, Synthesis and Characterization of Semiconductive Dichloridobis(thianthrene)gold(1+) tetrachloridoaurate(1–), *European Journal of Inorganic Chemistry*, 2524–2528, **2009**.

Contents

1 Introduction **1**

1.1 Thianthrene 1

1.2 Thianthrene radical cation 5

1.3 Sulfur dioxide, SO_2 9

1.4 Objectives 11

2 Experiments and Results **13**

2.1 Complexes of neutral thianthrene 13

2.1.1 Bis(μ-thianthrene-κ^2S)disilver(I) bis(tetrafluoridoborate) tri(sulfur dioxide) 13

2.1.2 Tris(μ-thianthrene-κ^2S)disilver(I) bis(hexafluoridoantimonate) penta(sulfur dioxide) 20

2.1.3 Dichloridobis(thianthrene)gold(1+) tetrachloridoaurate(1–) 29

2.1.4 Trichlorido(thianthrene)aluminium(III) 40

2.2 Thianthrene radical cation salts 51

2.2.1 Thianthreniumyl hydrosulfate 51

2.2.2 Thianthreniumyl tetrachloridoferrate(III) 59

2.2.3 Tris(thianthrene)(2+) bis(heptachloridodialuminate) 64

2.3 Other related salts 71

2.3.1 Selenanthreniumyl tetrachloridoaluminate 71
2.3.2 μ-oxy-selenanthrene(2+) bis(hydrosulfate) 77
2.3.3 Bis(selenanthreniumyl) bis(trifluoridoborate)(tetraoxidosulfate)(2–) mono(sulfur dioxide) 82
2.3.4 Phenazinediium bis(hydrosulfate) 88
2.4 Analytical experiments 94
2.4.1 Qualitative analyses 94
2.4.2 Gravimetry 98
2.4.3 Coloration 101
2.4.4 Cyclic voltammetry 103

3 General Discussion 107
3.1 The solvent influence 107
3.2 The oxidation reaction in liquid SO_2 109
3.3 The reaction with aluminum chloride 110
3.3.1 What oxidizes thianthrene? 110
3.3.2 A suggestion for the reaction mechanism 111
3.4 Electrical conductivity 112

4 Summary 115

A Experimental work 119
A.1 Chemicals 119
A.2 Instruments 122
A.3 Laboratory equipment 122
A.3.1 Vacuum line installation 122
A.3.2 Glove box 123
A.3.3 H-shaped vessel 124
A.4 Methods 124

A.4.1 Crystal selection under inert conditions 124
A.4.2 Electrical conductivity measurements 126
A.4.3 Electrochemical technique 126

B Software **128**

Chapter 1

Introduction

1.1 Thianthrene

Thianthrene (TA) is a heterocyclic compound with two sulfur atoms connecting two benzene rings in form of a tricyclic molecule. It was reported for the first time in 1868 as a pyrolysis residue of sodium benzenesulfonate in a copper retort.[1] The yellow colored distillation product of this residue crystallized as colorless plates which was analyzed as C_6H_4S and initially termed as phenylene sulfide. Later on, the molecular weight determination showed the compound to be $C_{12}H_8S_2$ and was named, therefore, diphenylenedisulfide.[2] Twenty eight years after the first synthesis a new name was given, thianthrene, for its similarity to anthracene.[3]

There are several literature reports explaining how thianthrene can be synthesized. Synthesis methods up to 1960 were already comprehensively reviewed including more than 50 reports.[4] The brief explanations below are taken from the mentioned literature, only to show the most important of the available methods.

The reaction mechanism of the historical synthetic procedure is uncertain, and gives a low yield and can only be written as:

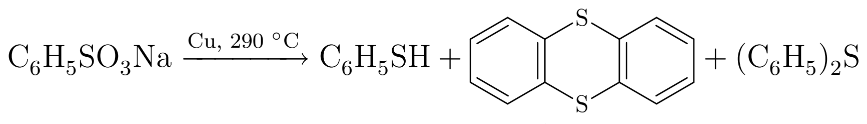
C6H5SO3Na
Cu, 290 °C
C6H5SH +
S
S
+ (C6H5)2S

A convenient synthesis method involves benzene, sulfur monochloride and aluminum chloride as the catalyst:

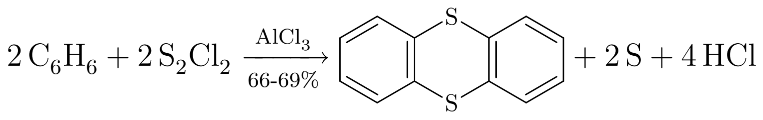
2 C6H6 + 2 S2Cl2
AlCl3
66-69%
S
S
+ 2 S + 4 HCl

The mechanism of this reaction was not clear. Another group proposed the reaction to involve diphenylsulfide as an intermediate, and another one confirmed the idea through similar method. It was then proposed that the diphenylsulfide reacts with sulfur slowly to thianthrene, and, also releases H_2S:

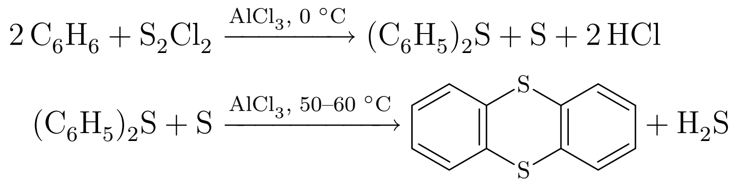
2 C6H6 + S2Cl2
AlCl3, 0 °C
(C6H5)2S + S + 2 HCl
(C6H5)2S + S
AlCl3, 50–60 °C
S
S
+ H2S

The reaction between diphenylsulfide and sulfur forming thianthrene is described to be quite slow. The analogous reaction using sulfur dichloride provides a lower yield (50%).

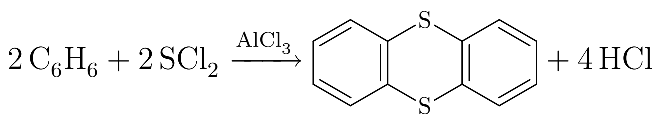
2 C6H6 + 2 SCl2
AlCl3
S
S
+ 4 HCl

Heating benzene with sulfur without any catalyst yields 20–30% thianthrene.

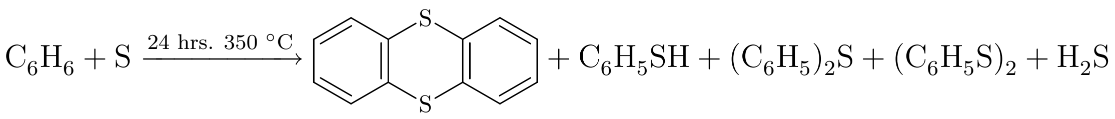
C6H6 + S
24 hrs. 350 °C
S
S
+ C6H5SH + (C6H5)2S + (C6H5S)2 + H2S

The pyrolysis of diphenyl disulfide achieves a higher yield of thianthrene, 60%. A radical mechanism is proposed for this reaction.[5]

$$C_6H_5SSC_6H_5 \xrightarrow{288\ ^\circ C} 2\,C_5H_5S\cdot$$

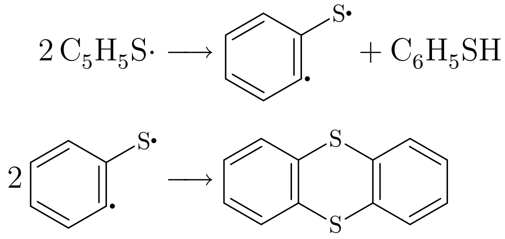

The thianthrene molecule (Fig. 1.1) is bent at the S· · · S axis by 127° and 128° according to crystal structure determinations at 163 K and 295 K, respectively. However, the conformation of thianthrene in solution is different with a wider dihedral angle, due to solvent interaction with S, a low energy flapping vibration about the S· · · S axis and solvent interaction with the aromatic rings.[6] All reported theoretical calculations on the configuration of thianthrene are consistent with the experimental structure.[7–13]

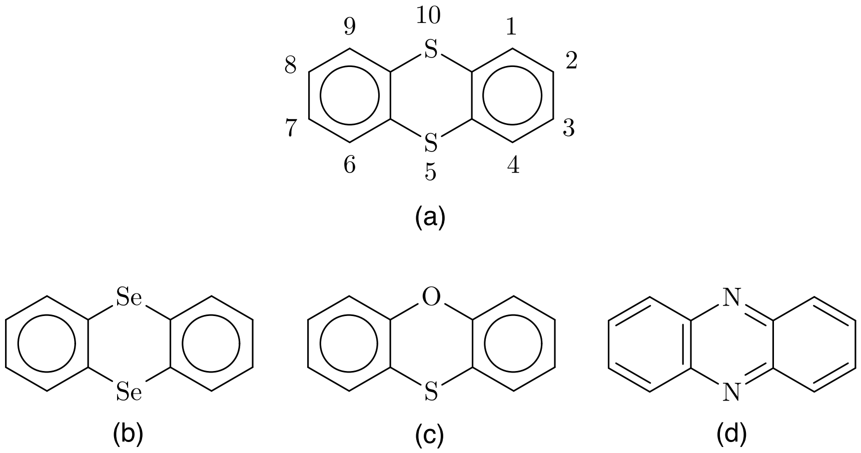

(a)

(b) (c) (d)

Figure 1.1: Molecular formula of thianthrene (a), including the atom numbering scheme (according to *Chemical Abstracts*) and some of its substitution derivates; selenanthrene (b), phenoxathiin (c) and phenazine (d).

Substitution of H atoms or addition of atoms at the S atom leading to thianthrene derivates change slightly the dihedral angle of the thianthrene skeleton, as long as the aromatic rings are not distorted. But if double bonding oxygen atoms replace the H's at position 1, 4, 6, and 9, or the C atoms on that position are substituted by N, the dithiin core becomes planar.[14] Several other heterocyclic molecules derived from anthracene with one or both of the *meso* CH group replaced by any of N, or O are planar, but folded if at least one of the substituents is S, Se or Te.[15] In case of the chalcogenanthrene series the folding of the molecule increases with the molar mass of the chalcogen atom.[13,16]

Alternative names for thianthrene are dibenzo-1,4-dithiadiene, dibenzo-1,4-dithiin, di-*o*-phenylene sulfide, and diphenylenedisulfide. Dithiin is referred to the central ring of the thianthrene molecule. Substitution of H atoms or addition at the S atom gives derivates still bearing the name thianthrene. For example, thianthrene dioxide and tetroxide are thianthrene derivates with two or four oxygen atoms bound at the S atoms, respectively. 2,3,7,8-Tetramethoxythianthrene is a thianthrene derivate with four methoxy groups bound to the corresponding C atoms. Basically, the central ring determines the name of the compound. For example, if both S atoms are replaced with Se, the resulting molecule is called selenanthrene, replacement with N gives phenazine and replacement with S and O simultaneously gives phenoxathiin (Fig. 1.1).

Thianthrene is commercially available as a crystalline white powder with a purity of 97%. Re-crystallization from toluene/ethanol is in general sufficient for obtaining a starting material pure enough for further reactions. Thianthrene is a non toxic material and is not attributed with any warning symbol.

Having two accessible sulfur atoms, thianthrene was formerly expected to serve as a mono- as well as a bidentate ligand towards metal ions.[14] The results from earlier attempts to prepare complexes of thianthrene with nickel,[18] palladium and platinum,[19] ruthenium,[20] silver, rhodium, iridium and gold,[21] the last mentioned

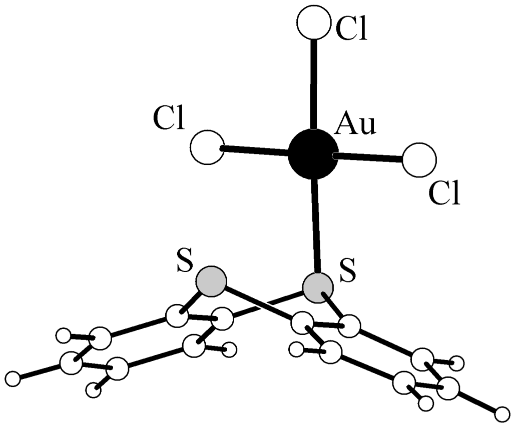

Figure 1.2: The structure of the thianthrene-gold(III)chloride complex.[17]

with crystallographic support[17] (Fig. 1.2), however, indicate that thianthrene behaves preferably as a monodentate ligand. By means of Job's method[22] and microanalysis the ratio of metal to ligand in the Pt(II) or Pd(II) complexes are known to vary with the solvent used.[19] While these two metals form complexes up to 1:2 metal to ligand ratio, iridium is found to form complexes with a 1:3 metal to ligand ratio.[21] The only characterized compound containing TA as a bidentate ligand, is the dimeric bis(μ-η^2-thianthrene)disilver(I) bis(perchlorate)[23] (Fig. 1.3). In the structure, each silver ion is coordinated by two sulfur atoms of one thianthrene and two carbon atoms of another thianthrene. Additionally, there is an Ag–O coordination by the perchlorate anion. However, the distance between the coordinating O atom to an Ag atom of the next dimer is only slightly longer, giving rise to a one-dimensional, infinite polymer.

1.2 Thianthrene radical cation

Since in the very beginning of its chemistry, thianthrene has been characterized as a colorless compound, which dissolves in concentrated sulfuric acid giving a purple colored solution, which in lower concentration appears red. When water is added, the color disappears and a white crystalline precipitate is produced.[1] Nowadays, the

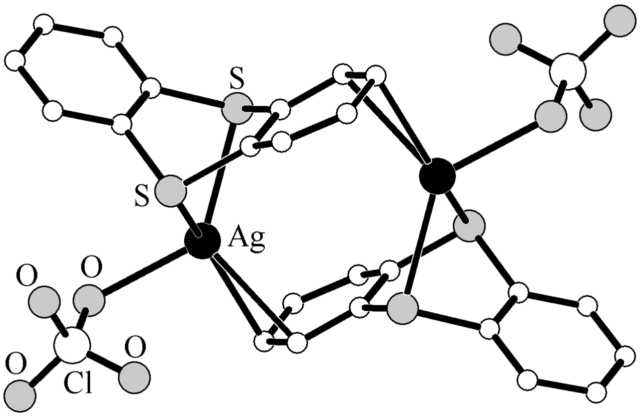

Figure 1.3: Bis(μ-η^2-thianthrene)disilver(I) bis(perchlorate),[23] a dimer with a center of inversion. Hydrogen atoms are not shown.

purple color is associated to oxidized thianthrene in form of the radical cation.

The development of radicals, detectable by EPR spectroscopy, originating from the reaction of aromatic compounds with aluminum chloride is already known, and has also been observed for thianthrene. Studies have already been undertaken showing that thianthrene reacts with $AlCl_3$ in a solid state mixture as well as in many organic solvents. If thianthrene and anhydrous aluminum chloride are heated in the temperature range from 60 to 180 °C and cooled to room temperature, a deeply colored solid forms, which has no paramagnetism,[24] while in solvents like benzene, chloroform or methylene chloride, red solutions with paramagnetic EPR absorption were formed.[25] Furthermore, aluminum chloride and thianthrene react in nitrobenzene to give a brownish purple solution, similar to that made in sulfuric acid, indicating the similarity of both products.[26]

If thianthrene is oxidized to its radical cation, the molecule obtains a planar or almost planar shape although the π-electron number of the molecule does not meet Kekulé's $4n + 2$ rule for an aromatic system. Thianthrene derivates behave in the same manner.[9,27–29] An earlier report based on EPR observations suggested that the distribution of free spin over both sulfur atoms and the carbon atoms, C2, C3,

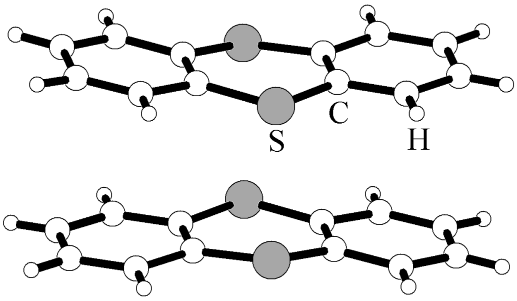

Figure 1.4: The structure of thianthrene radical ion dimer in the structure of thianthrene radical cation tetrachloridoaluminate.[9]

C7 and C8 implies the planarity.[30] A crystal structure determination showed a 174° dihedral angle of oxidized thianthrene and the theoretical calculations resulted in 180° with D_{2h} symmetry using semi-empirical PM3 as well as *ab initio* methods.[9,11,13] Furthermore, it was shown that the monovalent radical cations form pairs in all cases, as determined by the crystal structure determination (Fig. 1.4),[9] voltammetry experiments,[31,32] and theoretical calculation.[33]

A recent report showed the crystallographic structure of tris(thianthrene)(2+) bis(dodecamethylcarba–*closo*–dodecaborate) dichloromethane tetrasolvate with a flat thianthrene molecule located between two other molecules, each with a 170° dihedral angle. The S$\cdots$S axes of the two outer molecules are parallel while the one of in the middle is fixed with a tilt of 90° with respect to the two outer ones. This unique trimer carries two positive charges (Fig. 1.5).[34]

The high number of various reactions for obtaining thianthrene radical cations is a sign of the ease of the oxidation. Until now, however, not all reactions are explainable. Thianthrene is converted to its oxidized state when mixed with the *one-electron-oxidation-system* $AlCl_3/CH_2Cl_2$,[9] with concentrated sulfuric acid or undistilled trifluoroacetic acid,[35] with aluminum chloride in benzene, chloroform[25] or nitrobenzene,[26] with antimony pentachloride in chloroform[36] or in methylene chloride,[37] or by electrochemical methods.[33,38,39] Thianthrenium trichlorodiiodide was prepared by mixing

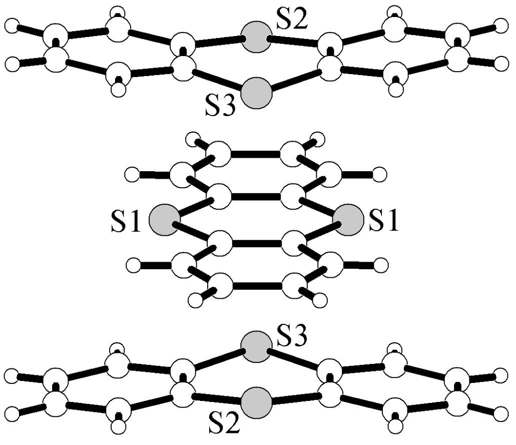

Figure 1.5: Tris(thianthrene)(2+), a trimer with an inversion center in the structure of tris(thianthrene)(2+) bis(dodecamethylcarba–*closo*–dodecaborate) dichloromethane tetrasolvate.[34] The anion and solvate molecules are omitted.

solutions of thianthrene and iodine chloride in dry carbon tetrachloride.[40] A mixture of thianthrene and its monoxide react with perchloric acid in nitromethane to give thianthrenium perchlorate, and the analogous reaction occurred with fluoroboric acid as well.[41] The same product also emerged when only thianthrene is mixed with perchloric acid in hot acetic anhydride.[42] Nitrosonium tetrafluoroborate in acetonitrile was employed to produce the related thianthrene radical salts.[43,44]

The electrochemistry of thianthrene also has a long history, giving support to the experimental observations. In an earlier study, the radical cation of thianthrene was suggested to be paired as $(TA^{\cdot +})_2$ and no sign of discrete paramagnetic species $[(TA)_2^{\cdot}]^+$ was observed.[45] Cyclic voltammetry experiments of thianthrene performed in several organic solvents showed the oxidation potential to vary with the solvent used.[39] Additionally, the result of the oxidation in liquid SO_2 was incomparable due to the different reference electrodes used.[31,46] Further investigation with faster scan rates proved not only the reversibility of thianthrene radical dimerization[33] but even the existence of a dimer composed of a radical cation and a neutral molecule $[(TA)_2^{\cdot}]^+$.[32] $(TA^{\cdot})[FeCl_4]$ and $(TA^{\cdot})[GaCl_4]$ synthesized electrochemically in acetonitrile have been used as radical transfer reagents.[38] Recently, reports on electrochemical experiments showed that thianthrene can be used as a homogenous redox catalyst to study reaction mechanisms.[47,48] Thianthrene can be incorporated in a polymer as a hole transfer layer in *light emitting diodes* (LED).[49]

1.3 Sulfur dioxide, SO_2

Liquid sulfur dioxide is a toxic, dipolar, nonionic solvent. It has a high heat of evaporation (25 kJ mol^{-1}), boils at –10.08 °C and melts at –75.52 °C (the boiling point given is calculated for 1.01325 bar, using the vapor pressure equation in literature.)[50] The vapor pressure of the liquid as a function of temperature is shown in Fig. 1.6, the correlation between density, viscosity and temperature in Fig. 1.7. Both curves are derived from literature.[51] Passing gaseous SO_2 through concentrated sulfuric acid and storage over P_4O_{10} prior to use is a common procedure for the removal of SO_3 and water, respectively.[52] On laboratory scale, SO_2 is conveniently synthesized from $NaHSO_3$ and H_3PO_4. Liquid SO_2 dissolves many organic and inorganic compounds which are summarized in the literature.[51]

Handling liquid SO_2 for daily laboratory work is comparable to other common organic solvents. SO_2 needs to be cooled to low temperature where the vapor pressure is also low, for example to –40 °C where a vapor pressure of only 0.2 bar is present. However, working in pressure-tight vessels allows generally experiments to be done at room temperature. –60 °C is a suitable condensation temperature of a SO_2 gas flow from a reservoir into a pre-evacuated reaction vessel. Distillation and re-concentration can be performed inside a closed vessel and removing the solvent is easily performed by slight opening of the valve and releasing SO_2 it in form of gas.

Thianthrene dissolves in liquid SO_2 in form of bright to dark yellow solution depending on the concentration although it was once reported as being insoluble.[53]

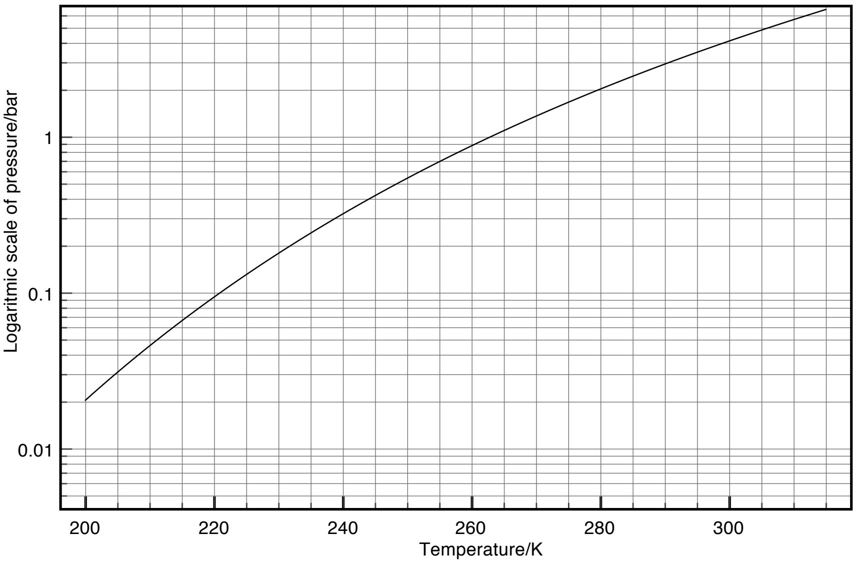

Figure 1.6: Curve of vapor pressure of SO_2 derived from literature.[51] The investigation ranges from –70° to +40 °C (203–313 K) which corresponds to 0.02 to 6.22 bar.

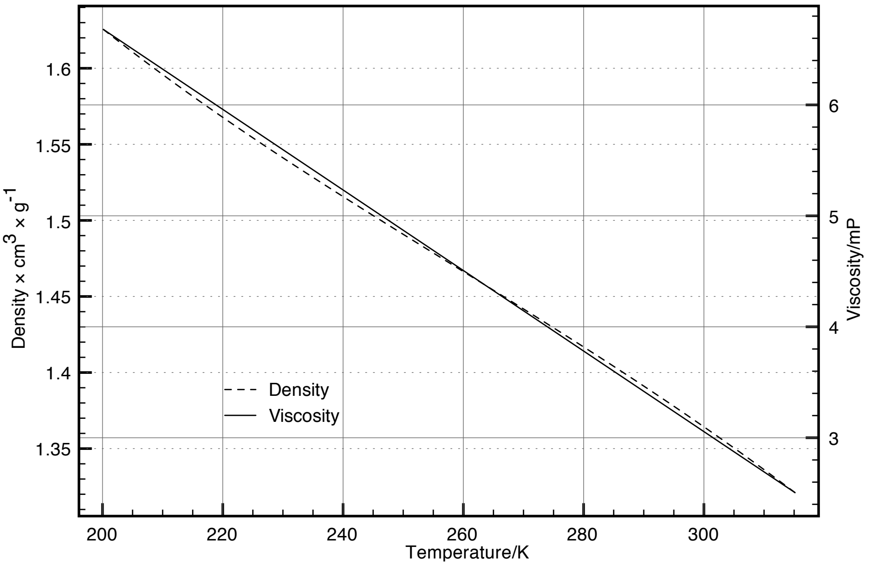

Figure 1.7: Curve of density and viscosity of SO_2 derived from literature.[51] The laboratory work ranges from –70° to +40 °C (203–313 K) which corresponds to 1.61 to 1.32 g/cm^3 and 6.57 to 2.58 mP, respectively.

1.4 Objectives

The coordination behavior of thianthrene has been in the focus of this laboratory work. The influence of weakly coordinating anions and a weakly coordinating solvent has been studied involving silver and gold metal ions. The basic of ligand exchange reactions is that the 'stronger' ligand replaces the 'weaker' one from the metal center. The use of SO_2 as the solvent increases the coordinating tendency of TA towards metal ions since the poorly coordinating SO_2 forms very labile $[M(SO_2)_y]^{x+}$ complexes and keeps metal ions in a highly reactive, almost uncoordinated or naked form, hence prone to ligand attack.

The redox properties of TA are also of interest. Though various reactions to produce thianthrene radical ions have been described, only two crystal structure determinations of compounds bearing thianthrenium ions were available in the literature. Additionally, there was an "old puzzle" about the radical formation from thianthrene and aluminum chloride. For these reasons, efforts to perform oxidation reactions has been a part of this work including electrochemical experiments.

The experiments performed dealt mainly with thianthrene, but its analogues, selenanthrene (SA) and phenazine, were also involved.

Chapter 2

Experiments and Results

2.1 Complexes of neutral thianthrene

Among many thianthrene complexation reactions described in the literature no reaction has been made in liquid SO_2 as the solvent. Additionally, no complexation reaction is described without the use of a solvent. Present laboratory work results reveal new structures related to experiments under both conditions. These are $[Ag_2(TA)_2][BF_4]_2 \cdot 3\,SO_2$ (**1**), $[Ag_2(TA)_3][SbF_6]_2 \cdot 5\,SO_2$ (**2**), $[AuCl_2(TA)_2][AuCl_4]$ (**3**) and $[AlCl_3TA]$ (**4**).

2.1.1 Bis(μ-thianthrene-κ^2S)disilver(I) bis(tetrafluoridoborate) tri(sulfur dioxide)

Preparation

$AgBF_4$ (45 mg, 0.23 mmol) and thianthrene (50 mg, 0.23 mmol) were placed separately in two branches of an H-shaped vessel under argon atmosphere and under protection from sunlight. The solvent was condensed into the branch containing TA under cooling with a mixture of ethanol and dry ice. The two valves were closed and after reaching room temperature the color of the solution of thianthrene in liquid

SO_2 was yellow and that of the silver salt was colorless with most of the salt remaining undissolved. The reaction was then initiated by pouring the yellow thianthrene solution into the other branch where silver salt was placed. In about a minute the color of the solution was pink, and colorless crystals appeared after one day. Single crystal selection was done under inert conditions with the cold oil method (see A.4.1, p. 124). The crystal structure solution was done using the direct method[54] and H atoms were added in calculated positions and fixed on the C atoms of the benzene rings during the refinement process.

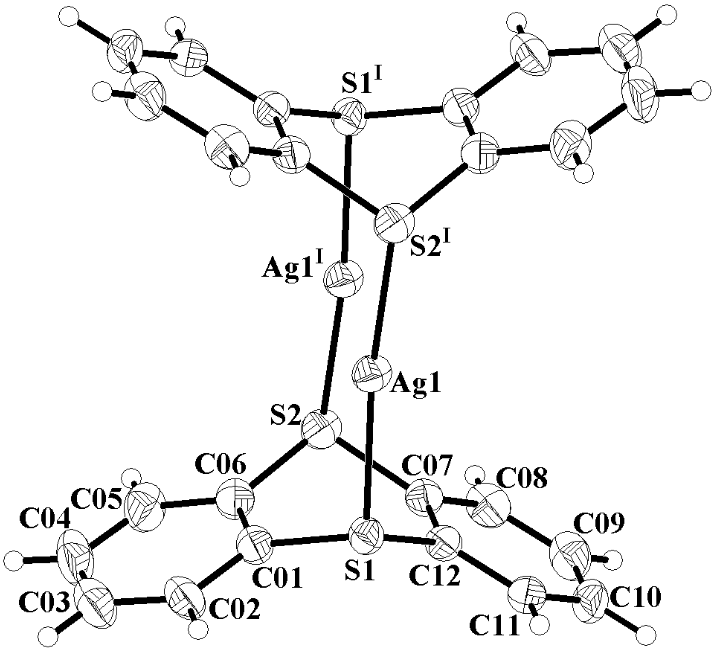

Figure 2.1: An individual complex in the structure of $[Ag_2(TA)_2][BF_4]_2 \cdot 3\,SO_2$. Thermal displacement ellipsoids are scaled to include 50% probability. Symmetry operation I = 1.5-x, 0.5-y, 1-z.

Structure

The crystal structure of bis(μ-thianthrene-κ^2S)disilver(I) bis(tetrafluoridoborate) tri-(sulfur dioxide), $[Ag_2(TA)_2][BF_4]_2 \cdot 3\,SO_2$ (**1**) consists of dinuclear complex cations, tetrahedral $[BF_4]^-$ anions and three SO_2 molecules per formula unit. Fig. 2.1 shows the structure of the $[Ag_2(TA)_2]^{2+}$ coordination unit. The tetrafluoroborate ion and the two independent SO_2 molecules are shown in Figure 2.2 and 2.3, respectively. Selected structural parameters are listed in Table 2.1. The $[Ag_2(TA)_2]^{2+}$ complexes are built up from two TA units each bridging two Ag^+ ions. The complex ion has a crystallographic inversion center, but the overall symmetry is only slightly distorted from the ideal point group D_{2h} symmetry. Each Ag^+ ion is almost linearly coordinated by two S atoms with an angle S1–Ag–S2 = 171.0°. The two S–Ag–S units are bent inwards resulting in an Ag$\cdots$Ag separation of 2.925 Å and considerably shorter than the S1$\cdots$S2 separation which is 3.264 Å. The Ag–S bond lengths differ slightly from each other, they are 2.47 and 2.48 Å. The TA ligand molecules have dihedral angles of 133.0° and are thus comparable with the uncoordinated molecule.

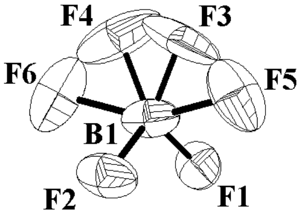

Figure 2.2: The BF_4 unit in $[Ag_2(TA)_2][BF_4]_2 \cdot 3\,SO_2$ is shown as a superimposition of two orientations. F3, F4, F5 and F6 are each refined as a half occupied atoms. Thermal displacement ellipsoids are scaled to include 50% probability.

The $[BF_4]^-$ anion and one of the two SO_2 molecules show disorder. In the structure refinements the "smeared" electron density around the B atom was refined assuming two fully occupied and four half occupied F atom positions. For the SO_2 molecule located on a special position on a twofold axis (O3–S4–O4), two half occupied closely neighboring O positions were refined. Both units, $[BF_4]^-$ and $S(4)O_2$, appear to occupy statistically two positions with B and S4 as the pivot atoms, since reasonable B–F and S–O bond lengths and F–B–F and O–S–O angles are present. Selected bond lengths and angles in structure **1** are listed in Table 2.2 and Table 2.3, respectively.

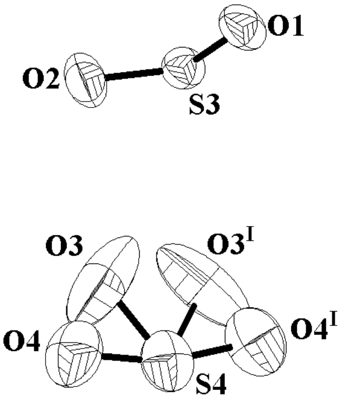

Figure 2.3: The SO_2 units in $[Ag_2(TA)_2][BF_4]_2 \cdot 3\,SO_2$, one of them is shown as a superimposition of two orientations. O3 and O4 are each refined as a half occupied. Thermal displacement ellipsoids are scaled to include 50% probability. Symmetry operation I = 2-x, y, 1.5-y.

Up to now, no Ag^+ complex with coordinated SO_2 has been isolated.[55] Even in this structure, it is uncertain to say whether the SO_2 is coordinated to Ag^+ or not, since the bond and angle parameters of SO_2 in this complex are similar to that of free ligand.[51] Both S–O distances are the same, but in the case of coordinated ligand they should be distinguishable between the bridging S–O and the terminal one.[55] However, taking into account all Ag–O and Ag–F distances up to 3 Å as weak bonds, each Ag^+ ion gains – besides the two Ag–S bonds – two additional Ag–O and three Ag–F contacs. Two SO_2 molecules act as bridging ligands, each with one O atom coordinated to both Ag^+ ions of one complex. The Ag–F interactions link the $[Ag_2(TA)_2]^{2+}$ complexes to one dimensional chains, which run along the crystallographic *b*-axis (Fig. 2.4). The Ag^+ ions in the $[Ag_2(TA)_2]^{2+}$ complexes, hence, are additionally weakly coordinated by O atoms of SO_2 molecules and by F atoms of $[BF_4]^-$ anions.

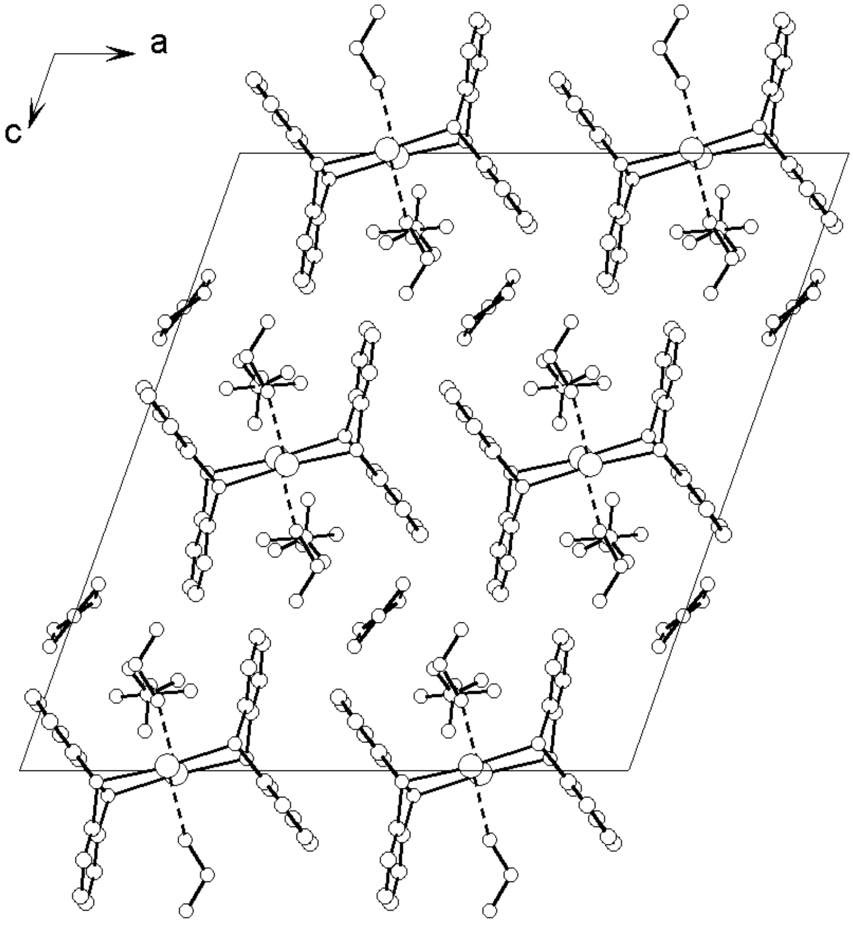

Figure 2.4: View of the unit cell of $[Ag_2(TA)_2][BF_4]_2 \cdot 3\,SO_2$ along *b*-axis. H atoms are omitted for clarity, the dotted line represents weak interaction between SO_2 molecule through O atom and Ag ions.

Table 2.1: Details of structure determination for $[Ag_2(TA)_2][BF_4]_2 \cdot 3\,SO_2$.

Formula	$C_{24}H_{16}Ag_2B_2F_8O_6S_7$
Cell lengths	$a = 21.0045(6)$ Å, $b = 7.4553(2)$ Å, $c = 22.6024(6)$ Å
Cell angles	$\beta = 109.649(1)°$
Volume of unit cell	3333.32(16) $Å^3$
Number of formula units, Z	4
Density (calc.), ρ	2.021 g cm^{-3}
Absorption coefficient, μ	1.698 mm^{-1}
Absorption correction	Multiscan[56] (empirical correction)
Crystal system, space group	monoclinic, $C2/c$ (15)
Diffractometer	KappaCCD
Radiation, wave length (λ)	Mo–Kα, 0.71073 Å
Temp. of measurement, T	153 K
Range of data collection	$2.92° < \theta < 27.43°$
hkl range	$-27 \leqslant h \leqslant 27$; $-9 \leqslant k \leqslant 9$; $-29 \leqslant l \leqslant 29$
Number of data collected	45162
Number of ind. refl., R_{merge}	3804, 0.1283
Number of refined parameters	249
Ratio reflections/parameters	15.28
R values	$wR(F^2) = 0.0762$
	$R(\|F\|) = 0.0528$ for all 3804 refl.
	$R(\|F\|) = 0.0338$ for 3011 refl. with $F_0 > 4sig(F_0)$
GooF	1.112
Largest electron density difference peak and hole	+0.58/-0.60 $eÅ^{-3}$

Table 2.2: List of selected bond lengths/Å in $[Ag_2(TA)_2][BF_4]_2 \cdot 3\,SO_2$.

Ag1–S2^{I}	2.4747(9)	S2–C06	1.775(4)	C01–C06	1.396(5)
Ag1–S1	2.4810(9)	F1–B1	1.363(5)	C02–C03	1.378(6)
Ag1–Ag1^{I}	2.9250(5)	F2–B1	1.357(5)	C03–C04	1.374(7)
O1–S3	1.420(3)	F3–F4	1.116(11)	C04–C05	1.388(6)
O2–S3	1.420(3)	F3–F5	1.233(11)	C05–C06	1.396(5)
O3–O4	1.125(15)	F3–B1	1.242(7)	C07–C08	1.393(5)
O3–S4	1.438(10)	F4–F6	1.262(12)	C07–C12	1.393(5)
O4–S4	1.375(8)	F4–B1	1.269(7)	C08–C09	1.371(5)
S1–C01	1.770(4)	F5–B1	1.565(8)	C09–C10	1.395(6)
S1–C12	1.772(3)	F6–B1	1.537(8)	C10–C11	1.378(5)
S2–C07	1.771(3)	C01–C02	1.390(5)	C11–C12	1.390(5)

Table 2.3: List of selected bond angles/° in $[Ag_2(TA)_2][BF_4]_2 \cdot 3\,SO_2$.

S2–Ag1–S1	171.04(3)	F4–B1–F1	116.7(4)	C04–C05–C06	119.7(4)
S2–Ag1–Ag1^{I}	93.08(2)	F2–B1–F1	114.0(3)	C01–C06–C05	119.3(3)
S1–Ag1–Ag1^{I}	94.62(2)	F3–B1–F6	104.5(7)	C01–C06–S2	121.8(3)
C01–S1–C12	101.48(16)	F2–B1–F6	92.9(4)	C05–C06–S2	119.0(3)
C01–S1–Ag1	105.73(11)	F1–B1–F6	100.9(4)	C08–C07–C12	119.5(3)
C12–S1–Ag1	109.80(11)	F4–B1–F5	103.3(7)	C08–C07–S2	118.6(3)
C07–S2–C06	101.56(16)	F2–B1–F5	94.4(4)	C12–C07–S2	122.0(2)
C07–S2–Ag1^{I}	107.38(11)	F1–B1–F5	98.7(4)	C09–C08–C07	120.3(4)
C06–S2–Ag1^{I}	109.68(11)	C02–C01–C06	120.1(3)	C08–C09–C10	120.4(3)

O1–S3–O2	117.99(19)	C02–C01–S1	118.1(3)	C11–C10–C09	119.6(3)
O4–S4–O3^{I}	116.5(9)	C06–C01–S1	121.8(3)	C10–C11–C12	120.3(3)
F3–B1–F2	118.7(5)	C03–C02–C01	120.0(4)	C11–C12–C07	119.9(3)
F4–B1–F2	122.2(5)	C04–C03–C02	120.3(4)	C11–C12–S1	118.3(3)
F3–B1–F1	119.1(5)	C03–C04–C05	120.6(4)	C07–C12–S1	121.8(2)

2.1.2 Tris(μ-thianthrene-κ^2S)disilver(I) bis(hexafluoridoantimonate) penta(sulfur dioxide)

Preparation

$AgSbF_6$ (79.4 mg, 0.23 mmol) and thianthrene (50 mg, 0.23 mmol) were placed separately in two branches of an H-shaped vessel under argon atmosphere and under protection from intensive sunlight. About 30 mL of SO_2 was then condensed into the branch containing TA under cooling with a mixture of ethanol and dry ice. The two teflon valves were closed and after reaching room temperature TA dissolved completely to give a yellow solution. The solution was then poured into the other branch of the vessel containing the silver salt. The vessel was shaken, the salt dissolved and the solution darkened within some hours. The final color was pink to light violet. Colorless crystals began to grow on the walls of the vessel after one day. Single crystal selection was done under inert conditions with the cold oil method (see A.4.1, p. 124). The crystal structure solution was done using the direct method[54] and H atoms were added in calculated positions and fixed on the C atoms of the benzene rings during the refinement process.

Structure

The crystal stucture of tris(μ-thianthrene-κ^2S)disilver(I) bis(hexafluoridoantimonate) penta(sulfur dioxide), $[Ag_2(TA)_3][SbF_6]_2 \cdot 5\,SO_2$ (**2**) consists of a dinuclear complex

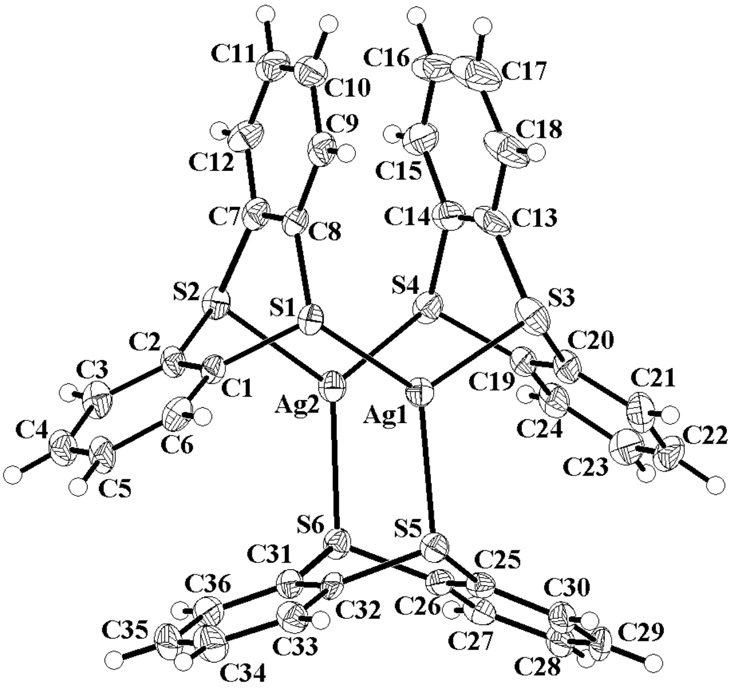
C11
C10
C16
C17
C9
C18
C12
C15
C7
C8
C14
C13
S2
S1
S4
S3
C2
C20
C3
C1
C21
Ag2
Ag1
C19
C4
C6
C24
C22
C23
C5
S6
S5
C31
C25
C36
C30
C32
C26
C35
C29
C33
C27
C34
C28

Figure 2.5: The $[Ag_2(TA)_3]^{2+}$ unit in the structure of $[Ag_2(TA)_3][SbF_6]_2 \cdot 5\,SO_2$. Thermal displacement ellipsoids are scaled to include 50% probability. H atoms are drawn with arbitrary radii.

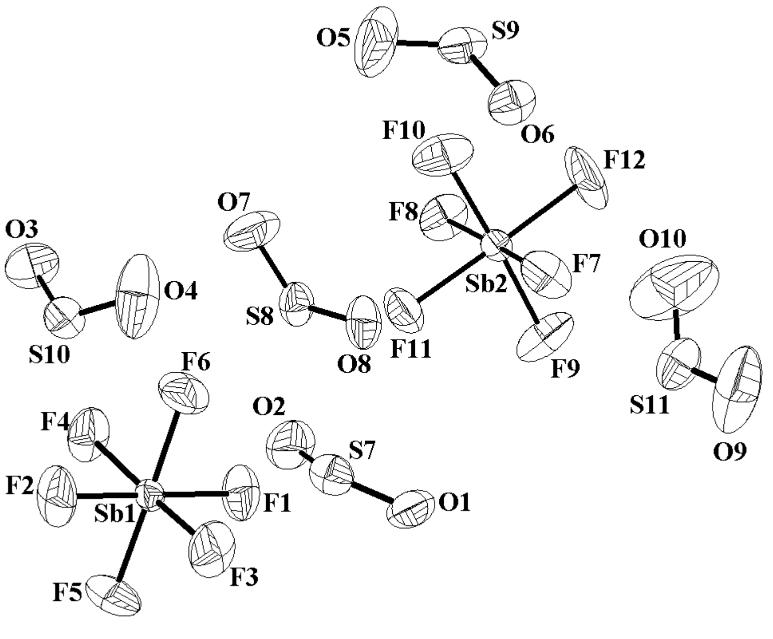
O5
S9
F10
O6
F12
O7
F8
O3
O10
F7
O4
Sb2
S8
S10
F11
O8
F9
F6
S11
O2
F4
S7
O9
F2
F1
Sb1
O1
F3
F5

Figure 2.6: Two independent $[SbF_6]^-$ ions and the five independent SO_2 molecules in the structure of $[Ag_2(TA)_3][SbF_6]_2 \cdot 5\,SO_2$. Thermal displacement ellipsoids are scaled to include 50% probability.

cation, two octahedral $[SbF_6]^-$ anions, and five SO_2 molecules per formula unit. Fig. 2.5 illustrates the structure of the $[Ag_2(TA)_3]^{2+}$ complex unit, and Fig. 2.6 shows the two crystallographically independent $[SbF_6]^-$ anions and the five independent SO_2 molecules with the atom numbering scheme. Table 2.4 lists selected structural parameters.

The $[Ag_2(TA)_3]^{2+}$ complex consists of three TA units each bridging two Ag^+ ions. The dihedral angle of the ligands is similar to that of the free thianthrene. Despite exhibiting no crystallographic symmetry, the complex deviates only slightly from ideal D_{3h} symmetry with the threefold rotation axis running along the Ag1–Ag2 axis. Each Ag^+ ion has a trigonal coordination environment by three sulfur atoms of three TA molecules. The two Ag^+ ions are located close to the centers of the triangular faces of a distorted trigonal prism built up from the six sulfur atoms of the three thianthrene molecules.

It is remarkable that the two Ag^+ ions are shifted by 0.159 Å (Ag1) and 0.192 Å (Ag2) out of the plane of the three coordinating sulfur atoms towards each other, resulting in an $Ag\cdots Ag$ separation of 2.911 Å, explicitly shorter than the average $S\cdots S$ separation, which amounts to 3.277 Å. Although the $Ag\cdots Ag$ separation is longer than the sum of the ionic radii of Ag^+ ($2r = 2.46$ Å[57]), it is within the range of assumed significant $d^{10}\cdots d^{10}$ interactions in Ag(I) compounds.[58,59] The Ag–S bond lengths are in the narrow range from 2.520 to 2.543 Å, with an average of 2.533 Å, considerably shorter than in the related complexes $[Ag_2(TA)_2][ClO_4]_2$ (Ag–S = 2.631 and 2.791 Å)[23] and in the chainlike polymer based on thianthrenophane $[Ag(TA{-}C(CH_3){=}C(CH_3))_2][ClO_4]$ (Ag–S = 2.81 Å),[60] but longer than that of in the structure **1**.

The TA molecules bound to Ag in the structure **2** show dihedral angles (132.62°, 132.89° and 130.53°) between the phenyl rings comparable with uncoordinated TA (127°).[19] This minute flattening of the ligand molecules is accompanied by longer S–

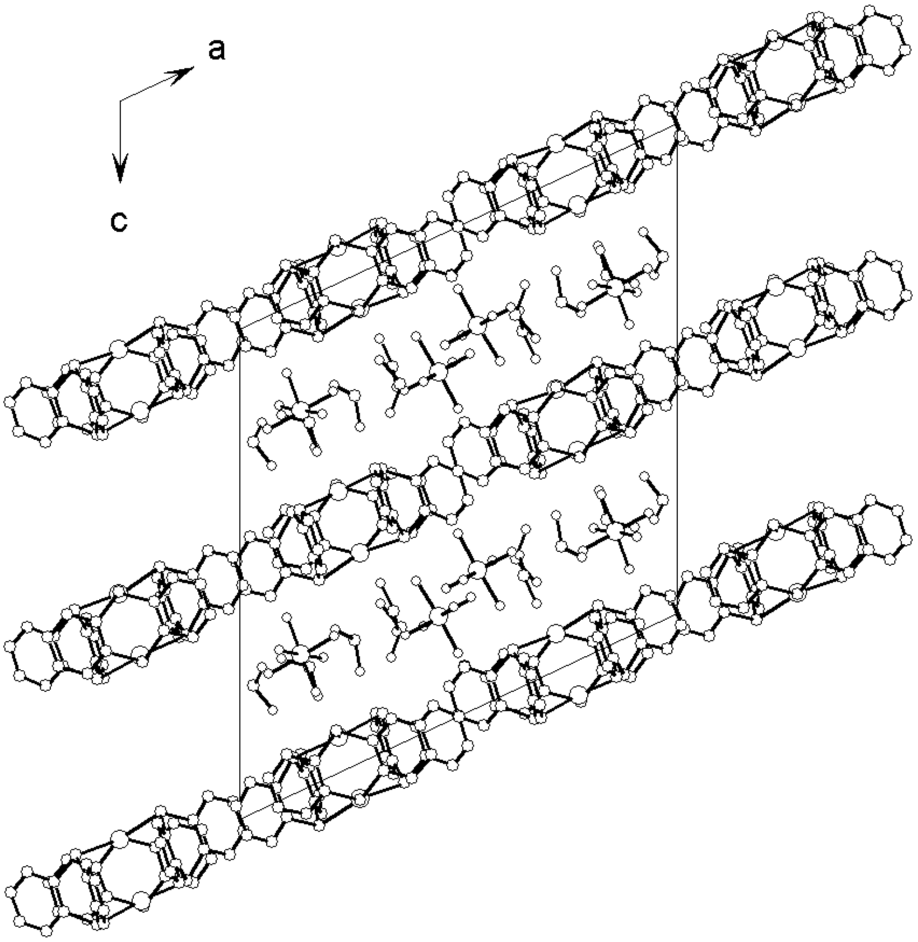

Figure 2.7: View of the unit cell of $[Ag_2(TA)_3][SbF_6]_2 \cdot 5\,SO_2$ along the *b*-axis. H atoms are omitted for clarity. The SO_2 molecules and SbF_6 anions fill up the space between layers of the complex cations.

S distances (averaged 3.277 Å) within the three complexed TA molecules compared to the uncoordinated state (3.193 Å).[6] Additionally, weak coordinative bonds of F atoms of the $[SbF_6]^-$ anions and of the O atoms of SO_2 molecules to the Ag^+ ions are present. Each Ag^+ ion has contacts to one F atom of a neighboring $[SbF_6]^-$ ion and to two O atoms of two neighboring SO_2 molecules. The respective distances are shorter for Ag1 than for Ag2 (Ag1$\cdots$F7–SbF_5 = 2.862(4), Ag2$\cdots$F4–SbF_5 = 3.010(4) Å). Selected bond lengths and angles in **2** are listed in Table 2.5 and Table 2.6, respectively.

The arrangement of the molecules in the unit cell shows a clear separation in an organic, positively charged part, made up of the $[Ag_2(TA)_3]^{2+}$ complexes, and an inorganic, negatively charged part, made up of $[SbF_6]^-$ ions and SO_2 molecules. All $[Ag_2(TA)_3]^{2+}$ complexes are arranged in layers parallel to the *ab*-plane of the crystal structure (Fig. 2.7). The packing of the phenyl rings determines this arrangement. Between these layers, the $[SbF_6]^-$ anions and the SO_2 molecules are located. The SO_2 solvate molecules are directing their O atoms toward the organic moiety.

Table 2.4: Details of structure determination for $[Ag_2(TA)_3][SbF_6]_2 \cdot 5\,SO_2$.

Formula	$C_{36}H_{24}Ag_2F_{12}O_{10}S_{11}Sb_2$
Cell lengths	a = 21.644(3) Å, b = 12.4216(4) Å, c = 21.934(3) Å
Cell angles	$\beta = 115.038(10)^\circ$
Volume of unit cell	5342.86(11) Å^3
Crystal system, space group	monoclinic, $P2_1/c$ (No. 14)
Number of formula units, Z	4
Density (calc.), ρ	2.059 g cm^{-3}
Absorption coefficient, μ	2.245 mm^{-1}
Absorption correction	Multiscan[56] (empirical correction)
Diffractometer	KappaCCD
Radiation, wave length (λ)	Mo–Kα, 0.71073 Å
Temp. of measurement, T	123 K
Range of data collection	$3.12^\circ < \theta < 27.53^\circ$
hkl range	$-28 \leqslant h \leqslant 28$; $-16 \leqslant k \leqslant 15$; $-28 \leqslant l \leqslant 28$
Number of data collected	191011
Number of ind. refl., R_{merge}	12277, 0.126
Number of refined parameters	658
Ratio reflections/parameters	18.66
R values	$wR(F^2) = 0.0947$
	$R(\lvert F\rvert) = 0.0995$ for all 12277 refl.
	$R(\lvert F\rvert) = 0.0455$ for 7931 refl. with $F_0 > 4sig(F_0)$
GooF	1.076
Largest electron density difference peak and hole	+1.076/-1.127 eÅ^{-3}

Table 2.5: List of selected bond lengths/Å in $[Ag_2(TA)_3][SbF_6]_2 \cdot 5\,SO_2$.

Sb1–F1	1.857(4)	S4–C14	1.797(6)	C11–C12	1.381(8)
Sb1–F5	1.862(4)	S5–C25	1.782(5)	C13–C14	1.394(9)
Sb1–F3	1.869(4)	S5–C32	1.787(5)	C13–C18	1.413(9)
Sb1–F4	1.877(4)	S6–C31	1.791(5)	C14–C15	1.408(9)
Sb1–F2	1.877(4)	S6–C26	1.792(6)	C15–C16	1.414(11)
Sb1–F6	1.880(4)	S7–O2	1.408(6)	C16–C17	1.383(12)
Sb2–F12	1.857(4)	S7–O1	1.408(6)	C17–C18	1.387(11)
Sb2–F8	1.865(3)	S8–O7	1.389(6)	C19–C20	1.395(8)
Sb2–F9	1.873(4)	S8–O8	1.407(5)	C19–C24	1.408(8)
Sb2–F7	1.874(4)	S9–O6	1.409(5)	C20–C21	1.407(8)
Sb2–F10	1.881(4)	S9–O5	1.445(8)	C21–C22	1.396(9)
Sb2–F11	1.891(4)	S10–O4	1.401(6)	C22–C23	1.383(9)
Ag1–S1	2.5284(14)	S10–O3	1.410(5)	C23–C24	1.397(8)
Ag1–S3	2.5349(16)	S11–O10	1.313(8)	C25–C26	1.387(8)
Ag1–S5	2.5406(15)	S11–O9	1.354(7)	C25–C30	1.419(8)
Ag1–Ag2	2.9113(7)	C1–C6	1.386(8)	C26–C27	1.402(7)
Ag2–S2	2.5202(14)	C1–C2	1.405(8)	C27–C28	1.390(8)
Ag2–S4	2.5334(15)	C2–C3	1.389(8)	C28–C29	1.378(8)
Ag2–S6	2.5426(15)	C3–C4	1.385(8)	C29–C30	1.379(8)
S1–C8	1.786(6)	C4–C5	1.382(8)	C31–C36	1.395(8)
S1–C1	1.793(5)	C5–C6	1.401(8)	C31–C32	1.399(8)
S2–C2	1.785(6)	C7–C12	1.392(8)	C32–C33	1.397(7)
S2–C7	1.789(6)	C7–C8	1.400(7)	C33–C34	1.387(8)
S3–C20	1.780(6)	C8–C9	1.409(8)	C34–C35	1.388(9)

S3–C13	1.782(7)	C9–C10	1.397(8)	C35–C36	1.406(8)
S4–C19	1.777(6)	C10–C11	1.390(8)		

Table 2.6: List of selected bond angles/° in $[Ag_2(TA)_3][SbF_6]_2 \cdot 5\,SO_2$.

F1–Sb1–F5	92.0(2)	C8–S1–C1	101.5(3)	C11–C12–C7	120.0(5)
F1–Sb1–F3	90.9(2)	C8–S1–Ag1	105.84(17)	C14–C13–C18	120.1(6)
F5–Sb1–F3	91.5(2)	C1–S1–Ag1	108.43(18)	C14–C13–S3	123.2(5)
F1–Sb1–F4	89.64(19)	C2–S2–C7	102.0(3)	C18–C13–S3	116.7(6)
F5–Sb1–F4	91.8(2)	C2–S2–Ag2	107.80(18)	C13–C14–C15	120.9(6)
F3–Sb1–F4	176.7(2)	C7–S2–Ag2	110.88(18)	C13–C14–S4	120.3(5)
F1–Sb1–F2	179.2(2)	C20–S3–C13	102.1(3)	C15–C14–S4	118.8(6)
F5–Sb1–F2	88.1(2)	C20–S3–Ag1	114.75(19)	C14–C15–C16	117.9(8)
F3–Sb1–F2	89.9(2)	C13–S3–Ag1	109.4(2)	C17–C16–C15	121.0(7)
F4–Sb1–F2	89.60(19)	C19–S4–C14	101.6(3)	C16–C17–C18	121.0(7)
F1–Sb1–F6	89.4(2)	C19–S4–Ag2	104.11(18)	C17–C18–C13	119.1(8)
F5–Sb1–F6	178.5(2)	C14–S4–Ag2	102.02(19)	C20–C19–C24	120.2(5)
F3–Sb1–F6	89.0(2)	C25–S5–C32	101.2(2)	C20–C19–S4	121.8(4)
F4–Sb1–F6	87.7(2)	C25–S5–Ag1	106.03(18)	C24–C19–S4	118.0(4)
F2–Sb1–F6	90.5(2)	C32–S5–Ag1	104.23(18)	C19–C20–C21	119.8(5)
F12–Sb2–F8	91.3(2)	C31–S6–C26	101.7(3)	C19–C20–S3	122.1(4)
F12–Sb2–F9	92.1(3)	C31–S6–Ag2	109.72(19)	C21–C20–S3	118.0(5)
F8–Sb2–F9	90.09(19)	C26–S6–Ag2	112.15(18)	C22–C21–C20	119.3(6)
F12–Sb2–F7	90.4(2)	O2–S7–O1	118.7(4)	C23–C22–C21	120.9(6)
F8–Sb2–F7	178.20(19)	O7–S8–O8	120.5(4)	C22–C23–C24	120.3(6)
F9–Sb2–F7	90.3(2)	O6–S9–O5	115.8(5)	C23–C24–C19	119.4(6)

F12–Sb2–F10	90.3(3)	O4–S10–O3	120.1(4)	C26–C25–C30	119.7(5)
F8–Sb2–F10	88.70(18)	O10–S11–O9	121.9(7)	C26–C25–S5	122.2(4)
F9–Sb2–F10	177.3(2)	C6–C1–C2	120.4(5)	C30–C25–S5	118.1(4)
F7–Sb2–F10	90.8(2)	C6–C1–S1	118.7(4)	C25–C26–C27	120.2(5)
F12–Sb2–F11	177.9(2)	C2–C1–S1	120.9(4)	C25–C26–S6	121.7(4)
F8–Sb2–F11	89.48(18)	C3–C2–C1	119.4(5)	C27–C26–S6	118.1(4)
F9–Sb2–F11	89.9(2)	C3–C2–S2	118.5(4)	C28–C27–C26	119.6(5)
F7–Sb2–F11	88.78(18)	C1–C2–S2	122.1(4)	C29–C28–C27	120.0(5)
F10–Sb2–F11	87.8(2)	C4–C3–C2	120.2(5)	C28–C29–C30	121.6(5)
S1–Ag1–S3	123.09(5)	C5–C4–C3	120.2(6)	C29–C30–C25	118.8(5)
S1–Ag1–S5	117.55(5)	C4–C5–C6	120.4(5)	C36–C31–C32	120.5(5)
S3–Ag1–S5	118.19(5)	C1–C6–C5	119.2(5)	C36–C31–S6	117.8(4)
S1–Ag1–Ag2	96.40(3)	C12–C7–C8	120.1(5)	C32–C31–S6	121.7(4)
S3–Ag1–Ag2	84.32(4)	C12–C7–S2	118.7(4)	C33–C32–C31	119.9(5)
S5–Ag1–Ag2	100.34(3)	C8–C7–S2	121.2(4)	C33–C32–S5	118.4(4)
S2–Ag2–S4	115.36(5)	C7–C8–C9	119.4(5)	C31–C32–S5	121.7(4)
S2–Ag2–S6	124.39(5)	C7–C8–S1	122.0(4)	C34–C33–C32	119.6(5)
S4–Ag2–S6	118.53(5)	C9–C8–S1	118.5(4)	C33–C34–C35	120.9(6)
S2–Ag2–Ag1	91.72(4)	C10–C9–C8	119.9(5)	C34–C35–C36	119.9(6)
S4–Ag2–Ag1	104.07(4)	C11–C10–C9	119.6(6)	C31–C36–C35	119.2(6)
S6–Ag2–Ag1	88.00(3)	C12–C11–C10	121.0(6)		

2.1.3 Dichloridobis(thianthrene)gold(1+) tetrachloridoaurate(1–)

Preparation

Thianthrene (142.3 mg, 0.658 mmol) and gold(III) chloride (199 mg, 0.656 mmol) were weighed under dry argon atmosphere and put into two separate branches of an H-shaped vessel equipped with teflon screw cocks (Young). As about 20 mL liquid SO_2 was condensed into both sides, the largest part of $AuCl_3$ remained undissoleved. Thianthrene dissolved completely forming a bright yellow solution. This solution was then poured into the other branch, so that finally all solution was collected in the branch where the $AuCl_3$ was placed. The tube was shaken thoroughly from time to time within the first 15 minutes, and on standing the color of the solution mixture turned red within some hours. Small black crystals were already observable after one day. After two months all of $AuCl_3$ was converted to black crystals of $[AuCl_2(TA)_2][AuCl_4]$. Single crystal selection was done under inert conditions with the cold oil method (see A.4.1, p. 124). The crystal structure solution was done using the direct method[54] and H atoms were added in calculated positions and fixed on the C atoms of the benzene rings during the refinement process. Elemental analysis (*vs.* calculated value): Au 37.55 (37.90); C 27.33 (27.74); Cl 20.2 (20.47); H 1.78 (1.55); S 12.79 (12.34).

Structure

From the reaction of $AuCl_3$ and TA in liquid SO_2, black crystals of dichloridobis(thianthrene)gold(1+) tetrachloridoaurate(1-), $[AuCl_2(TA)_2][AuCl_4]$ (**3**), precipitated as the only product. Data collection on the diffractometer was performed at 110 K. Thereafter it was found that the crystal, when covered by a thin layer of inert oil, was actually stable in open air for weeks. The crystal structure determination

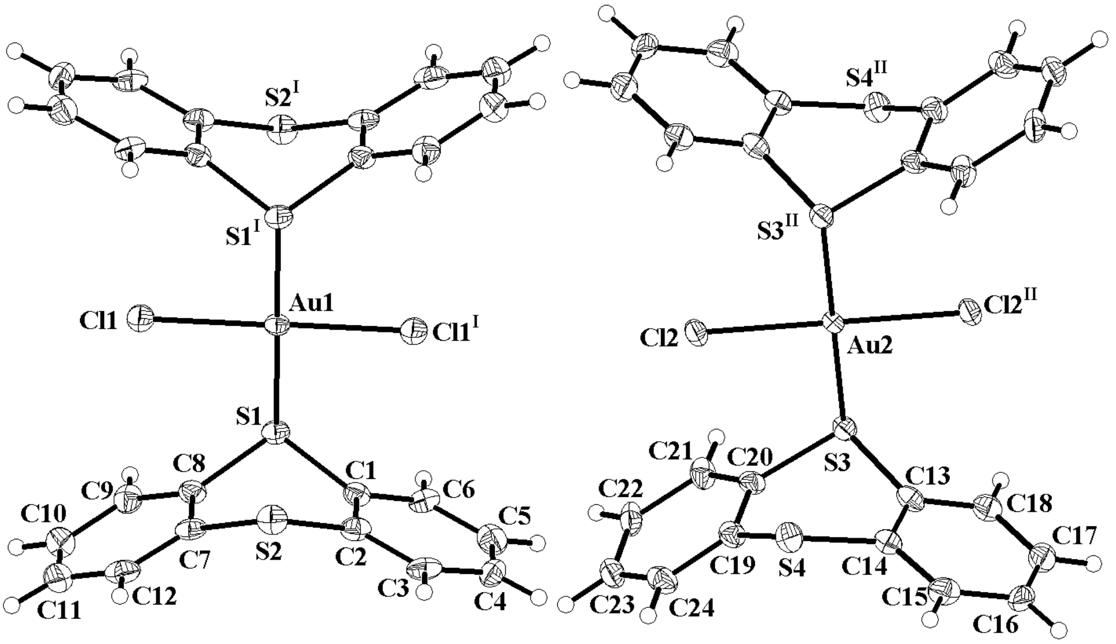
S2$^{\mathrm{I}}$
S1$^{\mathrm{I}}$
Cl1
Au1
Cl1$^{\mathrm{I}}$
S1
C8
C1
C9
C6
C10
C5
C7
S2
C2
C3
C4
C11
C12
S4$^{\mathrm{II}}$
S3$^{\mathrm{II}}$
Cl2
Au2
Cl2$^{\mathrm{II}}$
C21
C20
S3
C13
C22
C18
C17
C19
S4
C14
C15
C16
C23
C24

Figure 2.8: The two independent $[\mathrm{AuCl_2(TA)_2}]^+$ complex cation in the structure of $[\mathrm{AuCl_2(TA)_2}][\mathrm{AuCl_4}]$. Thermal displacement ellipsoids are scaled to include 50% probability. H atoms are drawn with arbitrary radius. Symmetry operation I = 1-x, 2-y, 2-z; II = 2-x, 1-y, 1-z

shows the structure to consist of $[\mathrm{AuCl_2(TA)_2}]^+$ and $[\mathrm{AuCl_4}]^-$ ions. The asymmetric unit contains two independent cations and anions. Both are located with their gold atoms on special positions on inversion centers giving them crystallographic C_i symmentry. Fig. 2.8 shows the cations whereas Fig. 2.9 shows the anions. Table 2.7 lists the details of structure determination for **3**.

In the cation, two thianthrene molecules are coordinated to the metal center each via one sulfur atom in trans position of the square planar coordination environment, typical for Au(III). The two different Au complex cations in the structure **3** do not fully fulfill the ideal D_{2h} symmetry. In cation 1 the Au–Cl bonds are almost orthogonal to the S$\cdots$S axes, while in cation 2 the Au–Cl bond are inclined toward the uncoordinated S atoms of thianthrene. The two independent complexes show significant differences in the structural parameters: the S2–S1–Au1 angle is 74.4°, but the S4–S3–Au2 angle is wider with 81.5°. The torsion angle along S2–S1–Au1–Cl1 is sig-

Cl4
Cl3^III
Au3
Cl3
Cl4^III
Cl6
Cl5^IV
Au4
Cl5
Cl6^IV

Figure 2.9: Two independent $[AuCl_4]^-$ units in the structure of $[AuCl_2(TA)_2][AuCl_4]$. Thermal displacement ellipsoids are scaled to include 50% probability. Symmetry operations: III = 1-x, 1-y, 2-z; IV = 1-x, 1-y, 1-z

nificantly bigger than that of S4–S3–Au2–Cl2, they are 85.6° and 67.7° respectively. The shape of the coordinated TA molecules is not substantially altered in comparison to the uncoordinated state. The interplanar angle of the folded TA ligands amounts 131.32° in cation 1 and 133.74° in cation 2. These values as well as the bond lengths in the molecule are equivalent to free thianthrene. Selected bond lengths and angles in **3** are listed in Table 2.8 and Table 2.9, respectively.

The two independent anions are almost identical. The Au atoms are coordinated by four Cl atoms in an undistorted square planar fashion. Despite only C_{2h} is present as crystallographic symmetry, the ideal symmetry D_{4h} is nearly fulfilled. The Au–Cl bonds amount in average 2.28 Å and the Cl–Au–Cl angles deviate less than 1° from rectangularity. The centro-symmetry of all ions in the structure causes all trans-positioned ligand atoms to be in linear coordination with the respective Cl–Au–Cl and S–Au–S angles being 180.0° (Fig. 2.9).

In the unit cell each thianthrene ligand of one cation is facing another thianthrene of the neighbouring cation. The benzene ring of one cationic complex is in front of the dithiin ring of the TA ligand of the neighboring complex, resulting in a chain of cations running along the −111 direction (Fig. 2.10). The S$\cdots$S axes between the adjacent complexes are almost orthogonal one another at 82.6° and the shortest intermolecular C$\cdots$C distance amounts 3.42 Å, present between C21 and C7.

The reaction of thianthrene and $AuCl_3$ results in two different compounds so far,

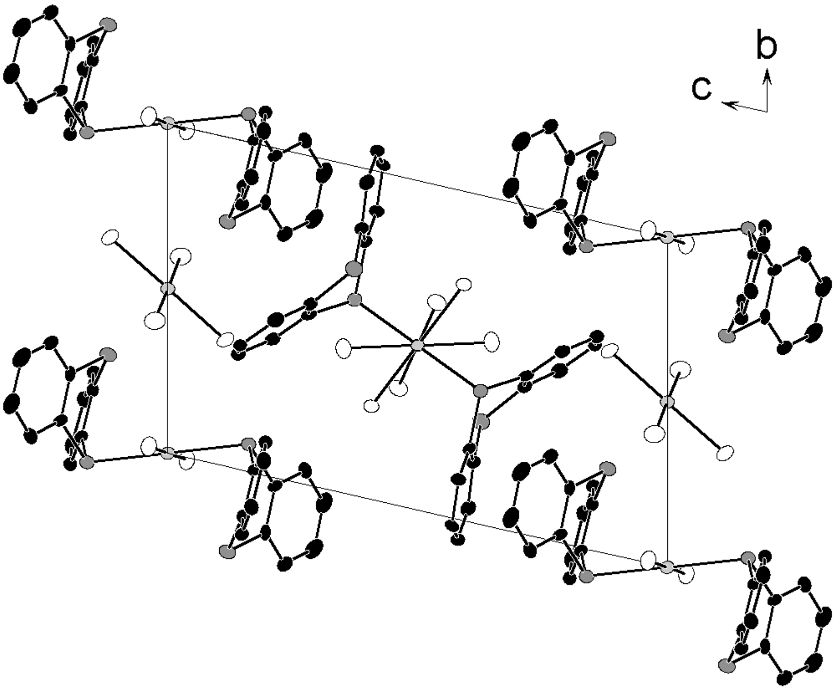

Figure 2.10: The cationic complexes in the structure of $[AuCl_2(TA)_2][AuCl_4]$ make up a chain-like arrangement along the −111 direction and the cations are located on special positions on the center of the unit cell, four edges and four faces of the unit cell. H atoms are omitted for clarity.

the already known mononuclear, uncharged complex $[AuCl_3(TA)]$[17] and the ionic salt $[AuCl_2(TA)][AuCl_4]$ from this work. If $[AuCl_2(TA)][AuCl_4]$ is mixed with chloroform, which is a much less polar solvent than liquid SO_2, the complex salt is, in fact, converted to the other form accompanied by decomposition of the salt into fine metallic gold powder. Though the black crystals of $[AuCl_2(TA)][AuCl_4]$ dissolve sparingly in $CHCl_3$, after one weak the largest part of them was converted into dark red, transparent, needle shaped crystals. The determination of the lattice constants via selected single crystals (a = 12.99 Å, b = 14.37 Å, c = 5.40 Å, β = 103.1°, V = 983.4 Å^3 at 296 K) showed that **3** underwent transformation to $[AuCl_3(TA)]$ (a = 12.88 Å, b = 14.27 Å, c = 5.33 Å, β = 103.2°, V = 955.4 Å^3 at 203 K).[17]

Table 2.7: Details of structure determination for $[AuCl_2(TA)_2][AuCl_4]$.

Formula	$C_{24}H_{16}Au_2Cl_6S_4$
Cell lengths	$a = 9.9832(2)$ Å, $b = 10.3404(2)$ Å, $c = 15.0798(4)$ Å
Cell angles	$\alpha = 75.038(1)°$, $\beta = 81.610(1)°$, $\gamma = 68.409(1)°$
Volume of unit cell	1396.15(5) Å^3
Crystal system, space group	triclinic, $P\bar{1}$ (No. 2)
Number of formula units, Z	2
Density (calc.), ρ	2.472 g cm^{-3}
Absorption coefficient, μ	11.39 mm^{-1}
Absorption correction	Multiscan[56] (empirical correction)
Diffractometer	KappaCCD
Radiation, wave length (λ)	Mo–Kα, 0.71073 Å
Temp. of measurement, T	110 K
Range of data collection	$3.14° < \theta < 27.55°$
hkl range	$-12 \leqslant h \leqslant 12$; $-13 \leqslant k \leqslant 13$; $-19 \leqslant l \leqslant 19$
Number of data collected	51960
Number of ind. refl., R_{merge}	6392, 0.0514
Number of refined parameters	331
Ratio reflections/parameters	19.31
R values	$wR(F^2) = 0.0900$
	$R(\|F\|) = 0.0516$ for 6392 all refl.
	$R(\|F\|) = 0.0365$ for 5195 refl. with $F_0 > 4sig(F_0)$
GooF	1.103
Largest electron density difference peak and hole	+1.75/-2.27 eÅ^{-3}

Table 2.8: List of selected bond lengths/Å in $[\mathrm{AuCl_2(TA)_2}][\mathrm{AuCl_4}]$.

Au1–Cl1	2.2765(18)	S4–C14	1.767(7)	C11–C12	1.379(12)
Au1–S1	2.4124(17)	S4–C19	1.771(7)	C13–C18	1.385(10)
Au2–Cl2	2.2797(16)	C1–C6	1.386(10)	C13–C14	1.412(10)
Au2–S3	2.3993(17)	C1–C2	1.405(10)	C14–C15	1.376(10)
Au3–Cl3	2.2754(18)	C2–C3	1.386(10)	C15–C16	1.386(11)
Au3–Cl4	2.2755(18)	C3–C4	1.381(11)	C16–C17	1.389(12)
Au4–Cl6	2.2803(19)	C4–C5	1.399(11)	C17–C18	1.374(11)
Au4–Cl5	2.2808(17)	C5–C6	1.375(11)	C19–C24	1.383(10)
S1–C8	1.767(7)	C7–C12	1.384(11)	C19–C20	1.388(10)
S1–C1	1.768(7)	C7–C8	1.391(10)	C20–C21	1.384(10)
S2–C2	1.760(8)	C8–C9	1.400(10)	C21–C22	1.403(10)
S2–C7	1.769(8)	C9–C10	1.386(11)	C22–C23	1.396(11)
S3–C13	1.764(8)	C10–C11	1.375(12)	C23–C24	1.365(11)
S3–C20	1.780(7)				

Table 2.9: List of selected bond angles/° in $[\mathrm{AuCl_2(TA)_2}][\mathrm{AuCl_4}]$.

Cl1–Au1–S1	87.99(6)	C4–C3–C2	120.6(7)	C15–C14–C13	119.2(7)
Cl2–Au2–S3	94.47(6)	C3–C4–C5	119.9(7)	C15–C14–S4	119.3(6)
Cl3–Au3–Cl4	90.48(7)	C6–C5–C4	120.6(7)	C13–C14–S4	121.5(6)
Cl6–Au4–Cl5	90.66(7)	C5–C6–C1	119.1(7)	C14–C15–C16	119.8(7)
C8–S1–C1	101.1(3)	C12–C7–C8	119.0(7)	C15–C16–C17	120.6(7)
C8–S1–Au1	103.5(2)	C12–C7–S2	119.5(6)	C18–C17–C16	120.4(7)

C1–S1–Au1	103.1(2)	C8–C7–S2	121.5(6)	C17–C18–C13	119.3(7)
C2–S2–C7	101.6(3)	C7–C8–C9	121.9(7)	C24–C19–C20	118.1(7)
C13–S3–C20	101.7(3)	C7–C8–S1	120.6(6)	C24–C19–S4	119.9(6)
C13–S3–Au2	104.2(2)	C9–C8–S1	117.5(5)	C20–C19–S4	121.8(5)
C20–S3–Au2	107.3(2)	C10–C9–C8	117.5(7)	C21–C20–C19	122.3(7)
C14–S4–C19	101.0(3)	C11–C10–C9	120.8(8)	C21–C20–S3	116.6(5)
C6–C1–C2	121.4(7)	C10–C11–C12	121.4(8)	C19–C20–S3	121.1(5)
C6–C1–S1	119.0(5)	C11–C12–C7	119.4(8)	C20–C21–C22	118.3(7)
C2–C1–S1	119.2(5)	C18–C13–C14	120.6(7)	C23–C22–C21	119.6(7)
C3–C2–C1	118.4(7)	C18–C13–S3	118.2(6)	C24–C23–C22	120.3(7)
C3–C2–S2	119.1(6)	C14–C13–S3	121.1(6)	C23–C24–C19	121.4(7)
C1–C2–S2	122.4(6)				

Due to its stability against ambient pressure and high temperature, it was possible to conduct further characterization of physical properties of the crystals, such as elemental analysis, UV-Vis, and IR spectroscopy, differential scanning calorimetry and electrical conductivity measurements. Because of the black color of the compound it was not possible to record a Raman spectrum. Even at low laser power only strong fluorescence was observed.

IR Spectroscopy

The IR spectrum of the complex salt differs considerably from that of free thianthrene showing some additional bands and shift of bands. The IR vibrational spectrum of thianthrene has been thoroughly studied.[61,62] The obvious differences in the spectra appear predominantly for C–S vibrations but are also present for C–C and C–H modes. For example, the stretching out of plane deformation modes, observed for thianthrene at 476, 1086 and 1101 cm^{-1} are observed for **3** at 470, 1077 and 1116 cm^{-1}. Several other absorption bands, attributed to C–H deformation and C–C stretching modes are also shifted up to 10 cm^{-1} to higher and to lower energies. Table 2.10 lists the wave numbers of the IR absorptions and the assignments for the thianthrene from two references and the observed bands of this work.

Thermal Properties

$[AuCl_2(TA)_2][AuCl_4]$ has a remarkable high thermal stability. The visual decomposition point was found at 438 K. In the DSC measurement a very small and broad endothermic effect around 350 K appeared which, however, did not appear again on the subsequent heating-cooling cycles (Fig. 2.11). The compound can be heated up to 425 K without decomposition or alteration and no sign for solid state phase transitions were detected.

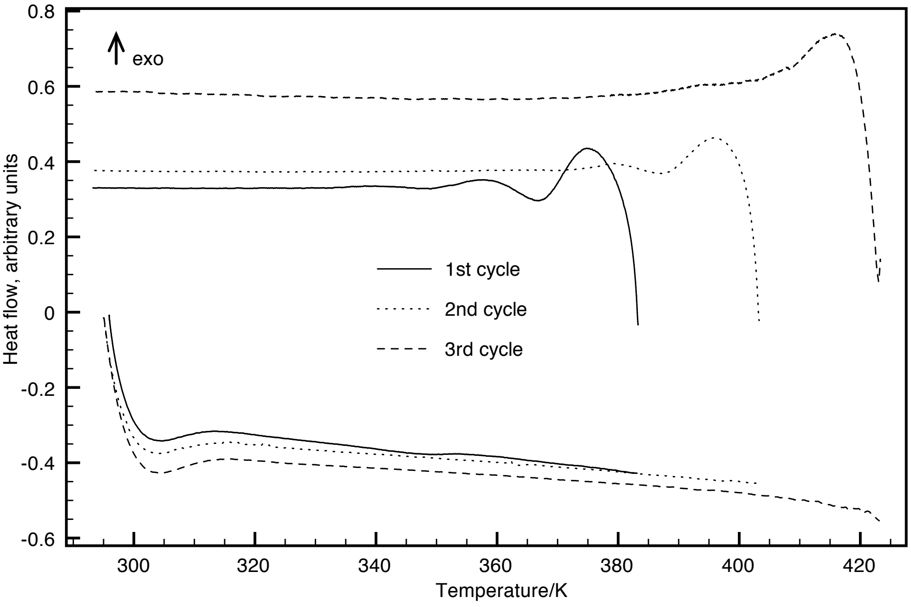

Figure 2.11: DSC measurement of $[AuCl_2(TA)_2][AuCl_4]$ was done in 3 cycles. Each cycle started from room temperature to a certain value and back to the initial temperature at rate of 10 K per minute, up and down as well. The highest temperatures were 383 K, 403 K and 423 K at the top of 1st, 2nd and 3rd cycle, respectively.

Table 2.10: A comparison of IR absorption bands of pure thianthrene according to literature and the spectrum of [AuCl$_2$(TA)$_2$][AuCl$_4$].

Bertinelli *et al.*[61] (in cm^{-1})	Kinugasa *et al.*[62,a] (in cm^{-1})	[AuCl$_2$(TA)$_2$][AuCl$_4$] (in cm^{-1})	Assignment[b]
3061 (vw)[c]	3063 81[d]	3073 (vvw)	ν(CH)
3058 (w)	3050 77	3056 (vw)	ν(CH)
1565 (vw)	1564 81	1563 (mw)	ν(CC)
1553 (w)	1554 60	1553 (w)	ν(CC)
1452 (w)	1452 72	1452 (w)	ν(CC)
1440 (vs)	1439 10	1441 (m)	ν(CC)
1432 (vs)	1432 20	1432 (mw)	ν(CC)
1422 (m)	1421 68	1 420 (sh)	ν(CC)
1282 (vw)		1288.5 (w)	ν(CC)
1262 (vvw)		1260 (w)	β(CH)
1252 (s)	1250 48	1250 (sh)	β(CH)
1160 (w)	1159 79	1159 (w)	β(CH)
1128 (vw)	1120 81	1126 (vw)	β(CH)
1101 (s)	1101 44	1116 (m)	ν(CS)
1086 (w)	1087 79	1077 (vw)	ν(CS)
	1051 77	1055 (w)	
1032 (vw)	1026 70	1030 (w)	β(CH)[e]
985 (w)	985 81	985.5 (vw)	
	948 79	951 (w)	
947 (w)	942 81	945 (mw)	γ(CH)
874 (w)	875 70	870 (w)	γ(CH)
870 (w)	871 70	869 (mw)	γ(CH)
764 (vs)	762 4	767 (vs)	γ(CH)
752 (vs)	753 10	753 (vs)	γ(CH)
659 (m)	660 70	660 (w)	ν(CC)
	549 74	542 (s)	
		496.5 (m)	
484 (w)	482 74	484 (w)	
476 (m)	473 46	470 (vs)	γ(CS)
421 (w)		421 (m)	β(CS)
		416 (m)	

[a] values are not assigned to any specific vibration mode

[b] taken from Bertinelli *et al.*, ν, stretching mode; β, in-plane deformation mode; γ, out-of-plane deformation mode

[c] s, strong; m, medium; w, weak; sh, shoulder; v, very

[d] the second values are the respective transmittances (%)

[e] taken from Munakata *et al.*[23]

Remission spectroscopy

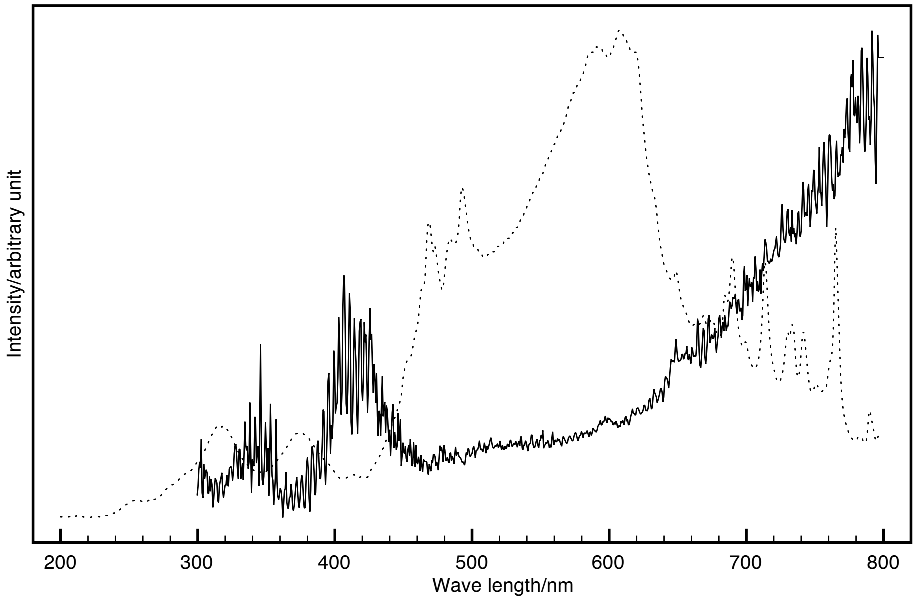

Figure 2.12: The remission profile of $[AuCl_2(TA)_2][AuCl_4]$ (continuous line) evaluated with Kubelka-Munk function. In the background the intensity profile of the Xe-lamp is given (dotted line). The dotted and the continuous lines are scaled differently with respect to the y-axis.

The UV–vis absorption profile of the complex was measured with remission spectroscopy. The complex was first mixed with $BaSO_4$ powder and formed to obtain a flat surface with area of about 25 mm^2. The exposure as well as the detection of scattered reflection were done in a special enclosure called Ulbricht sphere. The measured intensity scattered from the sample was compared with that of from pure $BaSO_4$. The representation of the absorption is a result of an evaluation according to Kubelka–Munk function, $F(R) = (1\text{-}R)^2/2R$; $R = I/I_0$, I = intensity of reflection from the mixture, I_0 = intensity of reflection from $BaSO_4$.

The black appearance of the salt became grey on high dilution with $BaSO_4$ as the sample was prepared for the remission measurement. The resulting grey-coloured mixture, in fact, absorbs light apparently starting from about 370 nm. After a noisy peak centered at 415 nm the absorption increases gradually until the highest wave-length measured, 800 nm, with a fairly steeper increment from about 650 nm. There is no dicernible peak or notch observed between 470 and 800 nm (Fig. 2.12, continuous line).

The noise in the scattering curve in the shorter wave length region could be caused by the weaker intensity of the Xe lamp at that region (Fig. 2.12, dotted line). In the region where the intensity of the source is high, the measured values are more reliable.

Conductivity measurement

Conductivity measurements were done under dry and inert atmosphere. Temperature change rate during the measurement was 30 Kh^{-1} up- and downward, programmed between 303 and 390 K.

At room temperature the electrical conductivity of $[\mathrm{AuCl_2(TA)_2}][\mathrm{AuCl_4}]$, determined via two probe technique, is very low. But on heating, a substantial conductivity is observed. The conductivity at the maximum temperature reaches 25 mS/m with semiconducting thermal behavior (Fig. 2.13). According to the DSC measurement result, **3** does not undergo any significant change in the applied temperature range. The conductivity curves show some inconsistencies. The first heating curve with a perturbation around 350–360 K indicates higher conductivity than the subsequent scan, on cooling as well as the second heating. During cooling, even a jump of conductivity is observed. During the second cooling scan it was seen that the sample decomposed just at the jump temperature of the first cooling while the conductivity rose up to the value for that of gold metal. After the measurement a gold metal layer on the electrode was observed.

The activation energy for the conductivity process of **3** can be obtained by applying the Arrhenius law. The function allows for a linear fit with good correlation between data and the linear regression line. Activation energy is calculated from the second heating curve (see A.4.2, p. 126). The value found is 0.43 eV. This low activa-

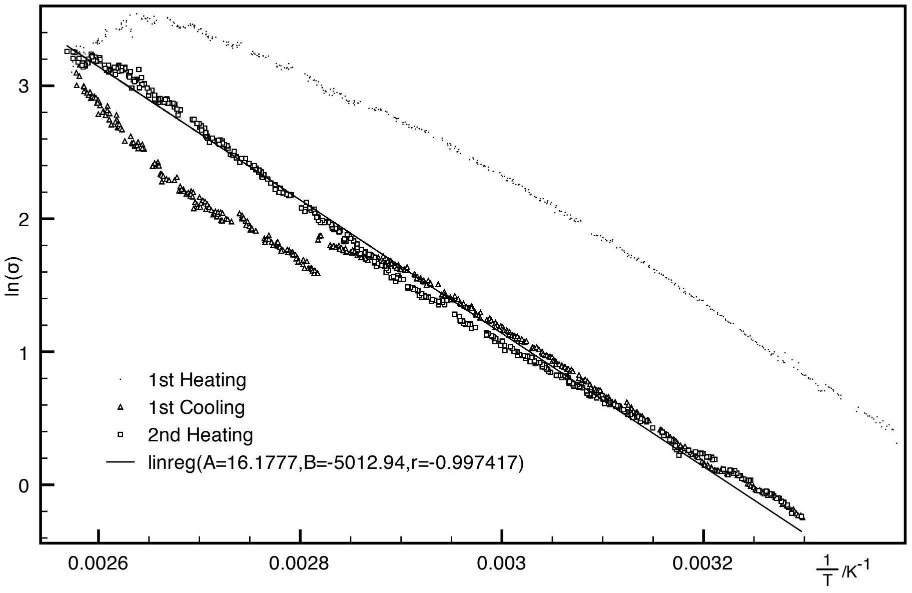

Figure 2.13: Specific conducitivity of $[AuCl_2(TA)_2][AuCl_4]$ as a function of temperature, $ln(\sigma) = f(T^{-1})$. Applied potential was 1 V.

tion energy and the relatively high conductivity of $[AuCl_2(TA)_2][AuCl_4]$ is surprising, since at first glance the salt-like character does not imply such behavior. The black color of the compound, however, is in line with the low thermal barrier.

2.1.4 Trichlorido(thianthrene)aluminium(III)

Preparation

Thianthrene (160 mg, 0.74 mmol) and aluminum chloride (100 mg, 0.75 mmol) were placed in an ampoule under inert environment. The ampoule was carefully closed by melting the tube under vacuum using a blowtorch. The closed ampoule was first heated at 100 °C for 12 hours and then aged at 40 °C for three weeks. After this time, in the ampoule purple prismatic crystals, turbid colorless hexagonal crystals of unreacted aluminum chloride or non-parallel shaped crystals of unreacted TA, depending on which compound was stoichiometrically weighed in excess, clear colorless light dispersing crystals, thin yellow polygonal crystal of unknown composition, and a

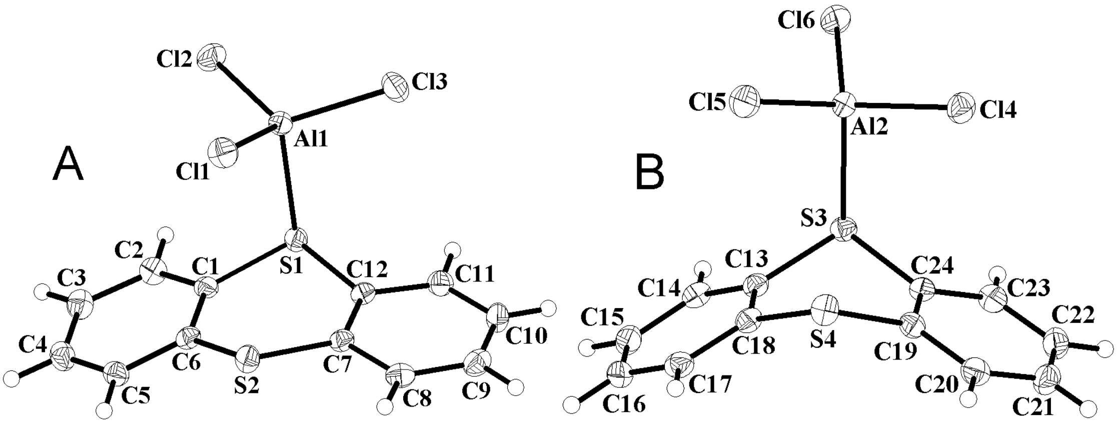

Figure 2.14: The two crystallographically independent complexes in [$AlCl_3$TA]. Thermal displacement ellipsoids are scaled to include 50% probability. H atoms were drawn with arbitrary radii.

very small amount of tiny metallic bronze luster crystals of assumed composition thianthrene radical cation tetrachloridoaluminate,[9] besides scattered colorless to violet liquid-like drops had formed.

The emerged crystals were handled under inert gas atmosphere. For single crystal X–ray investigation, the ampoule was cut under argon gas stream, filled with inert oil and a small part of the oil was then taken to a petri dish for single crystal selection. The crystal structure solution was done using the direct method[54] and H atoms were added in calculated positions and fixed on the C atoms of the benzene rings during the refinement process.

Structure

The diffraction data of a colorless crystal of trichlorido(thianthrene)aluminium(III), [$AlCl_3$TA] (**4**) were measured under inert conditions. The asymmetric unit of the structure consists of two independent molecules with little differences in their structural parameters and both without internal symmetry. The thianthrene molecule in each complex is coordinated to aluminum atoms via one S atom, thus acting as a monodentate ligand. Both aluminum atoms gain a distorted tetrahedral coordination as a result of one longer coordination Al–S and three small Cl–Al–S angles in comparison with the Cl–Al–Cl angles. The dihedral angle of thianthrene at Al1 is noticeably wider in comparison with that of the complex at Al2. The overall arrangement of the molecular structures of **4** is similar to that of [$AuCl_3$TA][17] (Fig. 1.2) but in the case of the gold complex, the metal ion has a square planar coordination, typical for gold(III).

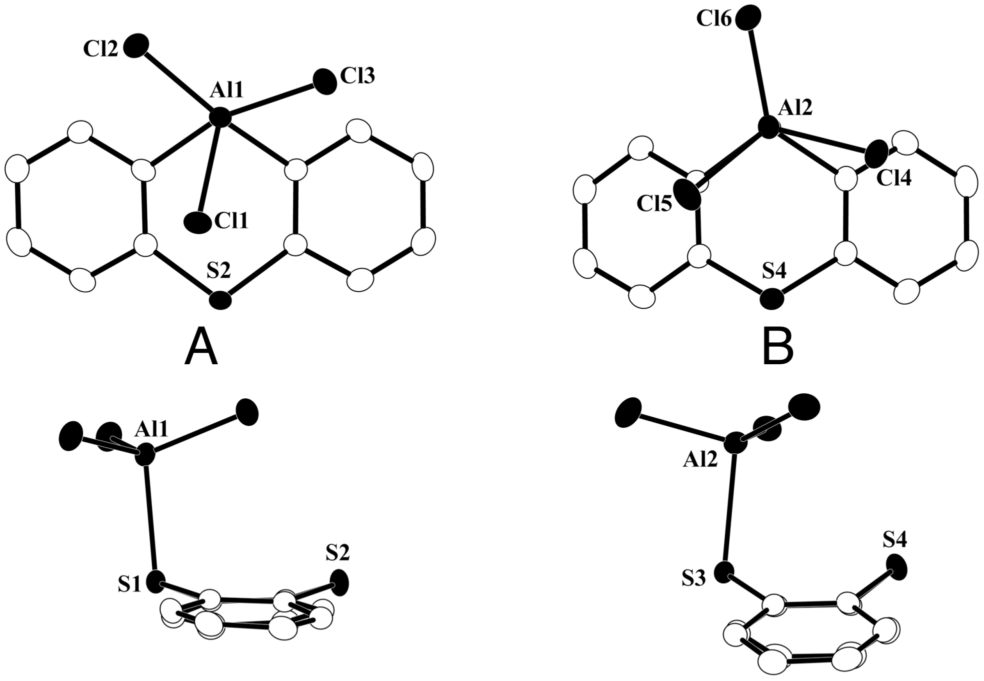

Figure 2.15: The configuration of two independent complexes in the structure of [$AlCl_3$TA] shown in different views: along Al–S bonds (top) and along the plane of the TA ligands (bottom). H atoms are omitted for clarity.

The key difference between the two independent complexes is the dihedral angle of TA. In the complex A the angle is 156°, while in the complex B it is 130°, about the same value for a free ligand (Fig. 2.14). The position of one chlorine atom in complex A seems to encounter steric hindrance with the uncoordinated S atom of its TA moiety, forcing a wider S2–S1–Al1 angle at 95°, whereas in complex B all chlorine atom are positioned at maximum distance from the uncoordinated S atom and thus the S4–S3–Al2 angle is only 83.2° (Fig. 2.15). In this conformation the distance between S2 and Cl1 is 3.63 Å, only slightly longer than the sum of van der Waals radii of S and Cl atoms, which amount to 3.56 Å. For making a clear comparison, the torsion angle S2–S1–Al1–Cl1 in molecule A is 12.6° whereas that of S4–S3–Al2–Cl5 in molecule B is much wider at 51.2°.

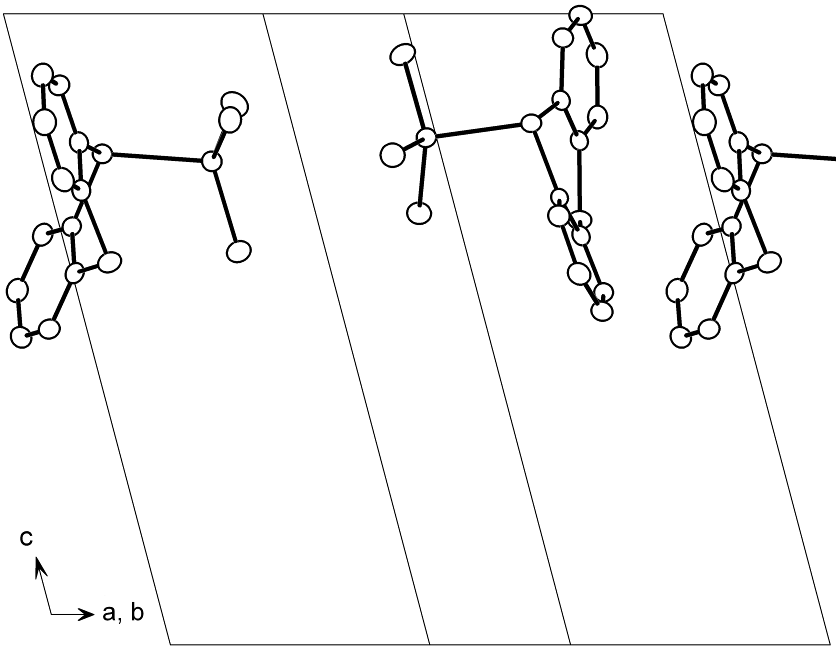

Figure 2.16: The arrangement of complexes in the structure of [$AlCl_3$TA]. H atoms are omitted for clarity.

The TA moiety of molecule A is quite close to the TA moiety of molecule B with the shortest C22· · · C12 distance of 3.49 Å. The flattened dithiin ring of S1, C1, C6, S2, C7, C12 is exactly in front of the benzene ring of C19 – C24 while the torsion angle between the S1· · · S2 and S3· · · S4 axes is 96° or near to orthogonality (Fig. 2.16). Additionally, the arrangement of a best plane through C1, C6, C7, C12 and a best plane through C19 – C24 differ from a perfect parallel alignment only 2.2°. Besides the close TA· · · TA arrangement, the structure **4** also features close Cl· · · Cl distances of neighboring molecules of 3.7 Å. Table 2.11 lists the details of structure determination for **4** and selected bond lengths and angles in **4** are listed in Table 2.12 and Table 2.13, respectively.

Table 2.11: Details of structure determination for [$AlCl_3$TA].

Formula	$C_{12}H_8AlCl_3S_2$
Cell lengths	$a = 8.1043(2)$ Å, $b = 12.8221(2)$ Å, $c = 14.6312(3)$ Å
Cell angles	$\alpha = 107.234(1)^\circ$, $\beta = 93.378(1)^\circ$, $\gamma = 91.431(1)^\circ$
Volume of unit cell	1448.17(5) Å^3
Crystal system, space group	triclinic, $P\bar{1}$ (No. 2)
Number of formula units, Z	4
Density (calc.), ρ	1.604 g cm^{-3}
Absorption coefficient, μ	0.958 mm^{-1}
Absorption correction	Multiscan[56] (empirical correction)
Diffractometer	KappaCCD
Radiation, wave length (λ)	Mo–Kα, 0.71073 Å
Temp. of measurement, T	110 K
Range of data collection	$3.29^\circ < \theta < 27.55^\circ$
hkl range	$-10 \leqslant h \leqslant 10$; $-16 \leqslant k \leqslant 16$; $-18 \leqslant l \leqslant 18$
Number of data collected	44591
Number of ind. refl., R_{merge}	6656, 0.0819
Number of refined parameters	389
Ratio reflections/parameters	17.11
R values	$wR(F^2) = 0.0786$
	$R(\|F\|) = 0.0621$ for 6656 all refl.
	$R(\|F\|) = 0.0362$ for 5009 refl. with $F_0 > 4sig(F_0)$
GooF	1.051
Largest electron density difference peak and hole	+0.32/-0.41 eÅ^{-3}

Table 2.12: List of bond lengths in [$AlCl_3$TA].

S1–C1	1.779(2)	Cl5–Al2	2.1008(10)	C11–C12	1.393(3)
S1–C12	1.782(2)	Cl6–Al2	2.1050(9)	C13–C14	1.393(3)
S1–Al1	2.3802(9)	C1–C2	1.390(3)	C13–C18	1.396(3)
S2–C7	1.757(2)	C1–C6	1.397(3)	C14–C15	1.388(4)
S2–C6	1.761(2)	C2–C3	1.393(4)	C15–C16	1.386(4)
S3–C13	1.781(2)	C3–C4	1.381(4)	C16–C17	1.385(4)
S3–C24	1.786(2)	C4–C5	1.387(3)	C17–C18	1.398(3)
S3–Al2	2.4218(9)	C5–C6	1.397(3)	C19–C20	1.396(3)
S4–C19	1.766(2)	C7–C8	1.398(3)	C19–C24	1.395(3)
S4–C18	1.769(2)	C7–C12	1.396(3)	C20–C21	1.385(4)
Cl1–Al1	2.1034(9)	C8–C9	1.384(4)	C21–C22	1.385(4)
Cl2–Al1	2.1057(9)	C9–C10	1.388(4)	C22–C23	1.392(4)
Cl3–Al1	2.1008(9)	C10–C11	1.387(3)	C23–C24	1.386(3)
Cl4–Al2	2.1112(9)				

Table 2.13: List of selected bond angles/° in [$AlCl_3$TA].

C1–S1–C12	106.12(11)	C2–C1–C6	121.4(2)	C14–C13–C18	121.5(2)
C1–S1–Al1	104.38(8)	C2–C1–S1	114.94(18)	C14–C13–S3	118.21(18)
C12–S1–Al1	103.61(8)	C6–C1–S1	123.68(18)	C18–C13–S3	120.23(18)
C7–S2–C6	105.34(11)	C1–C2–C3	119.3(2)	C15–C14–C13	119.1(2)
C13–S3–C24	102.36(11)	C4–C3–C2	119.7(2)	C16–C15–C14	119.9(2)
C13–S3–Al2	108.86(8)	C3–C4–C5	120.9(2)	C15–C16–C17	120.9(2)
C24–S3–Al2	105.82(8)	C4–C5–C6	120.3(2)	C16–C17–C18	120.1(2)

C19–S4–C18	101.19(11)	C5–C6–C1	118.3(2)	C17–C18–C13	118.4(2)
Cl3–Al1–Cl1	115.06(4)	C5–C6–S2	115.70(18)	C17–C18–S4	120.00(18)
Cl3–Al1–Cl2	116.87(4)	C1–C6–S2	125.96(18)	C13–C18–S4	121.60(18)
Cl1–Al1–Cl2	112.42(4)	C8–C7–C12	118.3(2)	C20–C19–C24	118.3(2)
Cl3–Al1–S1	101.72(4)	C8–C7–S2	115.67(18)	C20–C19–S4	119.81(19)
Cl1–Al1–S1	106.99(4)	C12–C7–S2	126.01(17)	C24–C19–S4	121.87(18)
Cl2–Al1–S1	101.62(4)	C9–C8–C7	120.5(2)	C21–C20–C19	120.3(2)
Cl5–Al2–Cl6	112.94(4)	C8–C9–C10	120.6(2)	C20–C21–C22	120.8(2)
Cl5–Al2–Cl4	118.76(4)	C11–C10–C9	119.8(2)	C21–C22–C23	119.7(2)
Cl6–Al2–Cl4	111.71(4)	C10–C11–C12	119.5(2)	C24–C23–C22	119.3(2)
Cl5–Al2–S3	110.11(4)	C11–C12–C7	121.2(2)	C23–C24–C19	121.7(2)
Cl6–Al2–S3	100.19(4)	C11–C12–S1	114.99(18)	C23–C24–S3	118.38(18)
Cl4–Al2–S3	100.72(4)	C7–C12–S1	123.76(17)	C19–C24–S3	119.96(18)

Since the crystals of $\mathrm{AlCl_3}$TA are stable in inert atmosphere and ambient pressure, it was possible to carry out further characterizations of the colorless crystals of **4**. The determination of electrical conductivity was performed in a glove box and also the preparation for DSC measurement. Raman spectrometry was done directly on the crystals in a closed ampoule.

Thermal properties

In inert atmosphere, [$\mathrm{AlCl_3}$TA] is stable up to 367 K when it was heated in the first cycle of DSC measurement. Thereafter, a small endothermic effect appears continued by a decomposition starting at 378 K, which do not appear at the second cycle anymore. This result was the base for temperature range selection in the electrical conductivity measurement (Fig. 2.17).

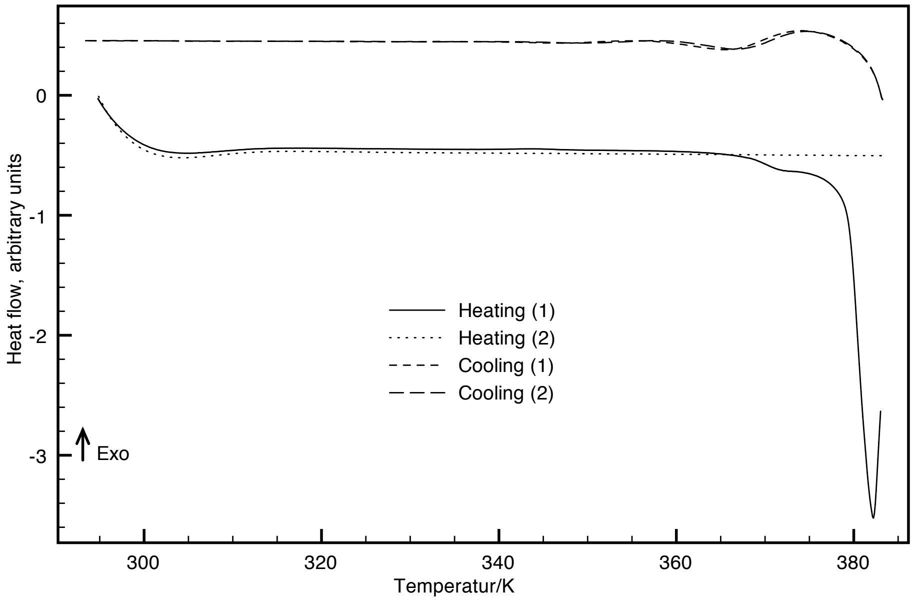

Figure 2.17: The thermal behavior of colorless [$AlCl_3$TA] crystals. The DSC measurement was done in two cycles of heating and cooling each between 303 – 383 K.

Electrical conductivity

Concerning the structure of **4**, the close TA$\cdots$TA distance is quite similar to that of the gold complexes in **3**. Based on this consideration, the colorless crystal was measured for its electrical properties. The measured values up to 380 K unexpectedly show a semiconducting feature. However, the large variation and the reliability of these values, especially in lower temperature, is questionable (Fig. 2.18). By calculating only the most reliable parts it was possible to plot the specific conductivity of the sample versus the reciprocal temperature and the resulting graph enables the prediction of the activation energy by means of the Arrhenius relation (Fig. 2.19). The first heating values included in the graph are only those starting from 340 K and for the second heating those from 320 K. The first cooling values included in the graph are limited only up to 313 K and for the second cooling up to 323 K.

The function of the specific conductivity with the temperature in a logarithmic ordinate shows a gradual increase start from the initial temperature and a steep

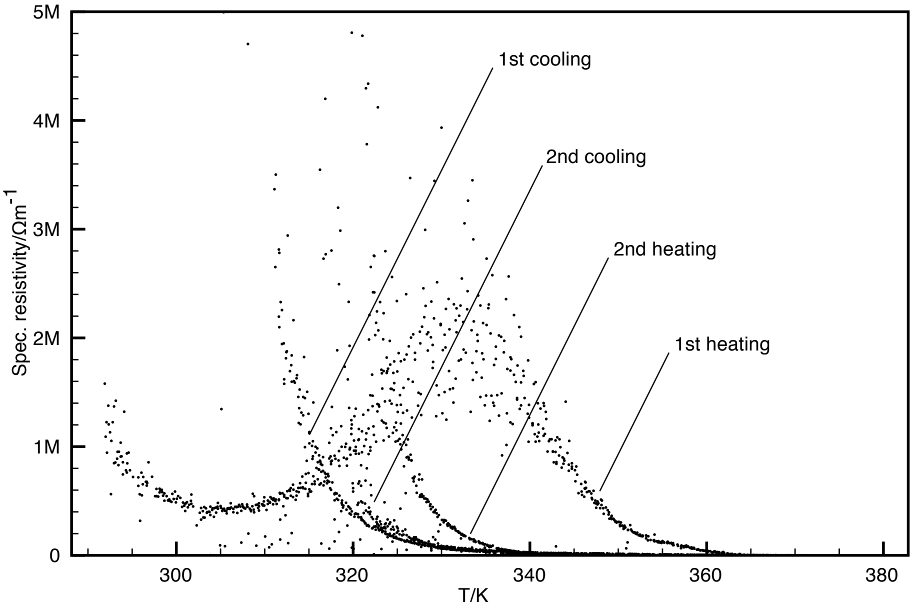

Figure 2.18: The conductivity measurement of the colorless [$AlCl_3TA$] crystals. The measured values are plotted as the function of *specific resistivity = f(temperature)*. Applied potential was 1 V.

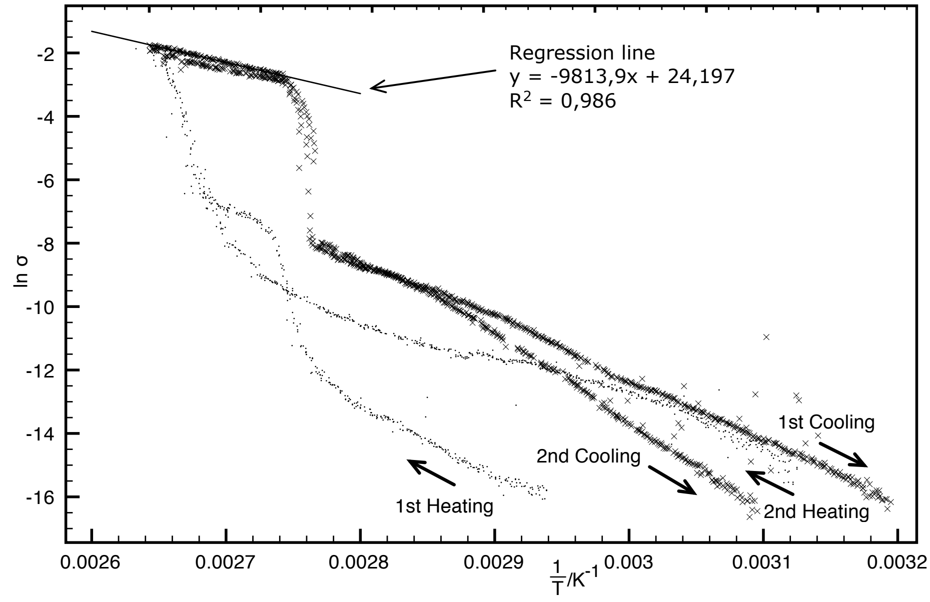

Figure 2.19: The Arrhenius plot of the conductivity function of [$AlCl_3TA$] according to $ln(\sigma) = f(T^{-1})$.

rise close to the maximum (Fig. 2.19, from the right side of the curve to the left). On cooling the decrease in conductivity is much more gradual and linear, with an activation energy of 0.845 eV, before an abrupt decrease to a certain value. It is an interesting feature that the compound maintains its high electrical conductivity once it reached the maximum measured temperature down to about 361 K before a sudden change to a less conductive material when the optimum region of temperature is passed. Due to the less reliable values at the lower temperature, that is in the temperature range lower than 361 K, the calculations of activation energy at these regions are much less valid. The activation energy is calculated from the first cooling curve using the Arrhenius Law (see A.4.2, p. 126).

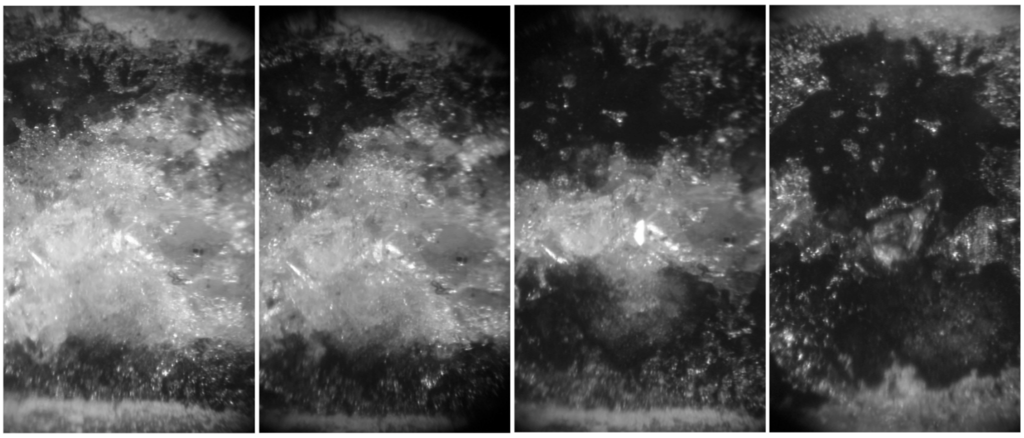

Figure 2.20: The color change of the colorless crystalline sample of [$AlCl_3$TA] in quartz tube in open air at ambient temperature after the conductivity measurement. The dark area is referred to violet color.

After the conductivity measurement there was no visual change on the colorless crystalline sample. But placing the quartz tube with the sample to the open atmosphere initiated a decay process starting from the part that had direct contact to the air. Figure 2.20 shows how the sample became darker and reached a violet color, stepwise until the whole sample completely turned almost black within about 15 minutes. In the case of TA violet color is associated to radical fomation. However, within one day no more violet color could be observed, but a white appearance of a wet, rough aggregate.

Raman spectroscopy

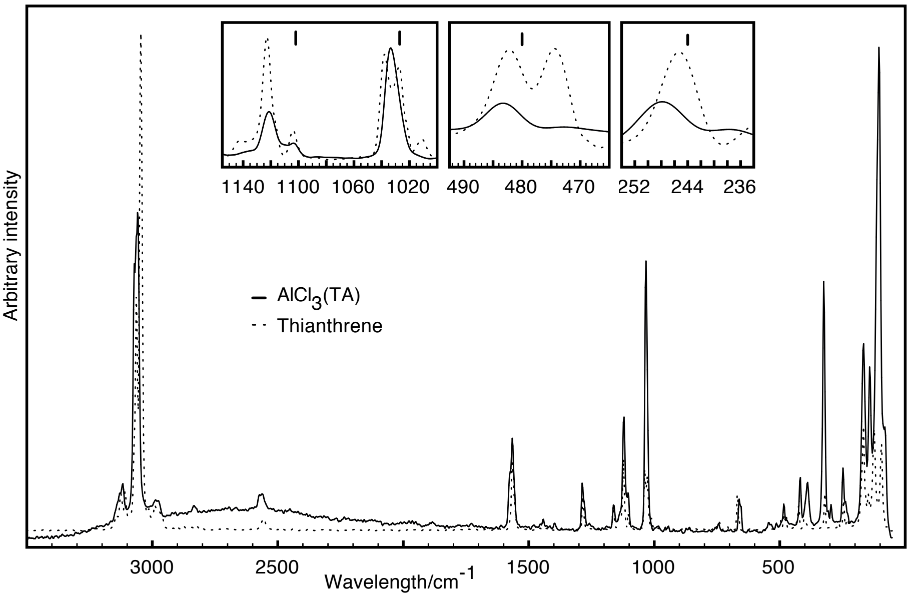

Figure 2.21: The Raman spectra of [$AlCl_3$TA] crystals and pure thianthrene. The insets show enlarged ranges of the spectra containing vibrations of C–S bonds of thianthrene, ticked with black marks.

The preserved configuration of thianthrene in the structure of **4** in comparison with that of the uncoordinated thianthrene is in agreement with the Raman measurement results. The sample of **4** was measured directly in the closed ampoule whereas the uncoordinated molecule was the crystalline powder of the purified thianthrene. The measurements were taken at a resolution of 4 cm^{-1}. Small differences appear at bands corresponding to C–S vibration, they are at 1102 cm^{-1} for ν(CS), 1027 cm^{-1} for γ(CS), 480 cm^{-1} for δ(CSC) and at 244 cm^{-1} for δ(CSC) as well (Fig. 2.21).

2.2 Thianthrene radical cation salts

The literature provides reports with flattened and flat thianthrene radical cations. No dication of thianthrene has so far been crystallized. Additionally, the radical tends to pair, forming dimers as well as trimers. Laboratory work conducted in liquid SO_2 confirms those findings with two new structures, $(TA^{\cdot})(HSO_4) \cdot H_2SO_4$ (**5**) and $(TA^{\cdot})[FeCl_4]$ (**6**). The known thianthrene radical cation tetrachloridoaluminate[9] could also be synthesized in liquid SO_2. In the reaction without solvent a new trimer variant was found, $(TA_3)[Al_2Cl_7]_2$ (**7**). Due to the very low yield of these compounds, no further characterization has been performed.

2.2.1 Thianthreniumyl hydrosulfate

Preparation

Under inert atmosphere of the glove box, thianthrene (50 mg, 0.23 mmol) and silver nitrate (39 mg, 0.23 mmol) were placed in different branches of an H-vessel. Liquid SO_2 was condensed into the branch filled with thianthrene resulting in a bright yellow solution. The solution turned slowly orange as it was poured into the other side through the glass filter. After about a week, dark crystals with a golden metallic luster precipitated on the wall of the H-tube out of a red SO_2 solution. Crystals also developed on the surface of the undissolved silver nitrate particles. When the liquid SO_2 was removed via evaporation the red solution leaves behind a mixture of colorless, dark blue and metallic crystals forming a layer on the tube's wall. *This reaction was not reproducible in the liquid SO_2 purchased from Praxair* (see Tab. A.1, Fig. A.1 and Fig. A.2). Single crystal selection was done under inert conditions with the cold oil method (see A.4.1, p. 124). The crystal structure solution was done using the direct method[54] and H atoms in the benzene rings were added in calculated position during the refinement process. The H atoms for the HSO_4 units were added and refined, according to the assumption that the very close distances between two O atoms are bridged by hydrogen bonds.

Structure

The crystal structure refinement reveals $(\mathrm{TA}^{\bullet})(\mathrm{HSO_4})\cdot\mathrm{H_2SO_4}$ (**5**) in the triclinic system with inversion centers, space group $P\bar{1}$. The asymmetric unit of the crystal structure consists of an almost flat thianthrene unit and two tetrahedral $\mathrm{SO_4}$ units (Fig. 2.22). The dihedral angle in the TA unit between the planes made up of a benzene ring and two sulfur atoms is 172.87°. Because of small differences in bond lengths and angles between both sides, the ideal C_{2v} point group is not fulfilled. The structure contains pairs of thianthrenium ions with a close $\mathrm{S}\cdots\mathrm{S}$ intermolecular distance of 3.054 Å (Fig. 2.23). Two identical molecules with C_1 point group consequently give a radical pair with only C_i point group, though its symmetry is actually very close to D_{2h}. The positions of the H atoms in the thianthrene molecule were calculated and fixed to C atoms and included in the refinement. H atoms at the $\mathrm{SO_4}$ unit were also added, at special positions due to $\mathrm{O}\cdots\mathrm{O}$ short distances. The whole arrangement of the molecular entities of **5** is shown in Figure 2.24.

The thianthrene molecule has apparently been oxidized into its radical cation (1+) confirmed by the large dihedral angle. It is unlikely to be oxidized to the +2 state since a pair of two 2+ charged thianthrenium ions was not observed in a fast cyclic voltammetry experiment.[33] Each thianthreniumyl unit is accompanied by two $\mathrm{SO_4}$ units. These units must carry one negative charge to neutralize the charge of the thianthrene radical cation. Nevertheless, there are three possibilities to assign the charges. The difference is originated from the different amount of H atoms added into the structure.

The first way is based on the structural consideration. Each of seven oxygen atoms out of eight from both $\mathrm{SO_4}$ units are very close to another oxygen atoms from

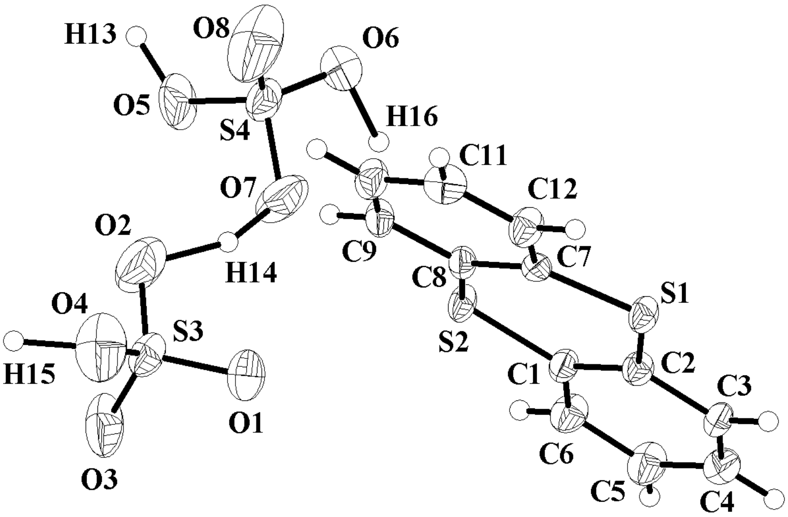
H13
O8
O6
O5
S4
H16
C11
O7
C12
O2
C9
C7
H14
C8
S1
O4
S3
S2
H15
C1
C2
C3
O1
C6
O3
C5
C4

Figure 2.22: The asymmetric unit of the structure of $(TA^{\cdot})(HSO_4) \cdot H_2SO_4$. Thermal displacement ellipsoids are scaled to include 50% probability. H atoms are drawn with arbitrary radii.

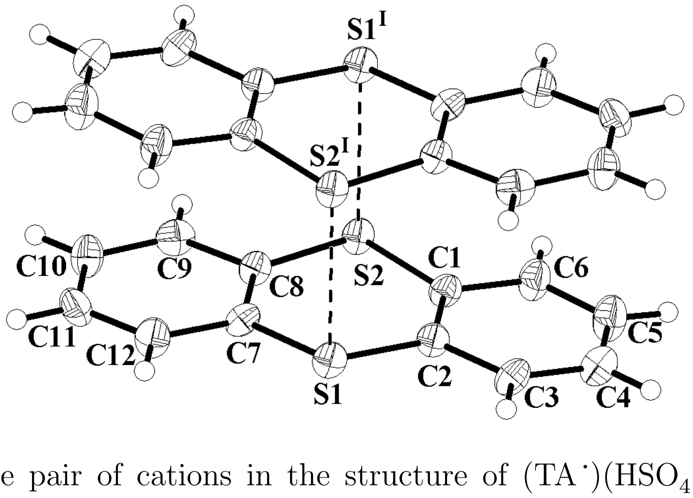
S1^I
S2^I
C10
C9
C8
S2
C1
C6
C11
C12
C7
C5
S1
C2
C3
C4

Figure 2.23: The pair of cations in the structure of $(TA^{\cdot})(HSO_4) \cdot H_2SO_4$, generated through an inversion center. The S···S distances amount 3.05 Å. Thermal displacement ellipsoids are scaled to include 50% probability. H atoms are drawn with arbitrary radii. Symmetry operation I = -x, 2-y, 2-z.

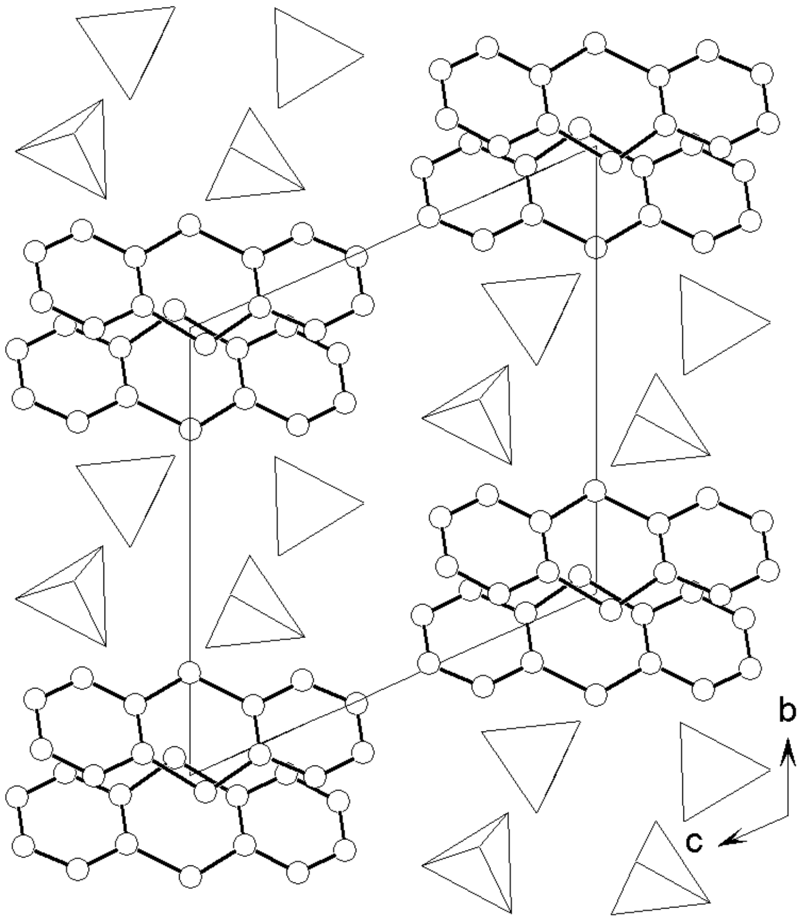

Figure 2.24: The arrangement of molecules in $(TA^{\cdot})(HSO_4) \cdot H_2SO_4$. The SO_4 units are shown as polyhedra, hydrogen atoms are omitted for clarity.

neighboring units with O···O distances in the range of strong O···H–O hydrogen bonds, 2.7 Å.[63] H atoms were therefore added into the gaps between the oxygen atoms. The eighth oxygen atom (O8) is considered as terminal; its thermal ellipsoid is comparably larger than those of the other oxygen atoms (Figure 2.25). There must be 3/2 hydrogen atoms for the SO_4 with one terminal oxygen and 4/2 hydrogen atoms for the other SO_4 unit. This gives an overall charge for both SO_4 units of –0.5. Since the cations exist in pairs, each pair must carry only one positive charge because every one pair of thianthrene molecules coexists with three sulfuric acid and one hydrosulfate anion. The phenomenon of a pair with one positive charge has already been observed and attributed to intermolecular charge–resonance complex, where one neutral thianthrene is paired with its radical, $[(\mathrm{TA})_2^{\cdot}]^+$.[32]

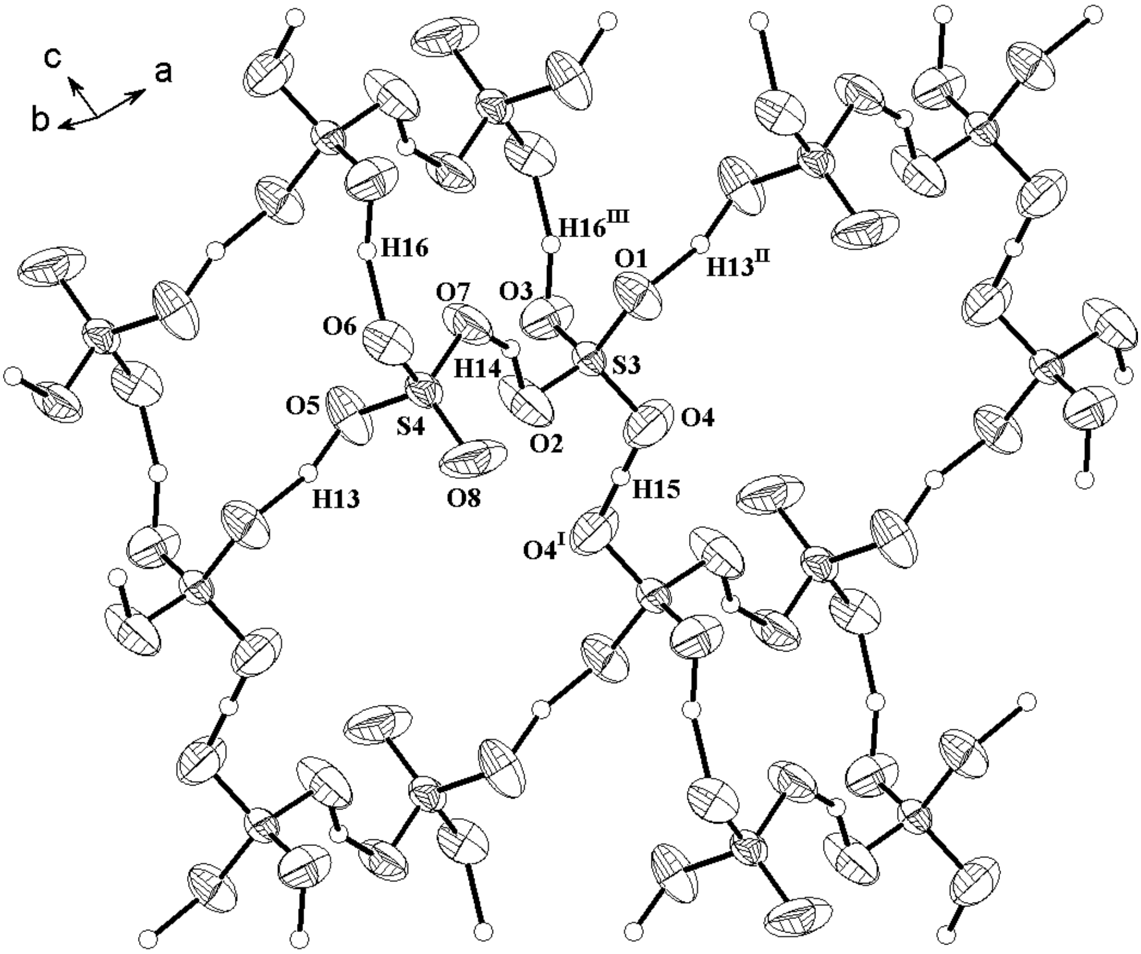

Figure 2.25: The $\mathrm{HSO_4^-} \cdot \mathrm{H_2SO_4}$ hydrogen bridged network in the structure of $(\mathrm{TA}^{\cdot})$ $(\mathrm{HSO_4}) \cdot \mathrm{H_2SO_4}$. The hydrogen bonds are drawn in the same way as the other bonds. Thermal displacement ellipsoids are scaled to include 50% probability. H atoms are drawn with arbitrary radii. Symmetry operation I = -x, 3-y, 1-z; II = 1+x, y, z; III = -x, 3-y, 2-z.

The second way is based on the preference for a pair of two radical ions $(\mathrm{TA}^{\cdot+})_2$, which is already known. To compensate the charges of the pair, which is now charged 2+, one hydrogen atom needs to be removed from the four $\mathrm{SO_4}$ units. Since all H atoms were added into the special positions in the unit cell, the only choice for removing one H atom is the atom H15 which is bridging between two O4 atoms though these atoms have the shortest O$\cdots$O distance of 2.533 Å. Any other H atoms are bridging two different O atoms, making the removal of only one H atom impossible. In this case, the bond length and angle parameters of the thianthreniumyl molecule are in agreement with those in the literature except for the dihedral angle.[9] On the other hand, very short O$\cdots$O distances will destabilize the $HSO_4^- \cdot H_2SO_4$ hydrogen bridged network.

The third way is based on the opposite preference of that of the second, it is by removing an H atom from between the longest O$\cdots$O distance which is actually short enough, O2$\cdots$O7, 2.689 Å. This would result in not only two additional terminal O atoms, O2 and O7, but also the concomitant additional two negative charge to the four SO_4 units. In this case, each oxidized thianthrene pair must have three positive charge which is unlikely to be true.

The third way is the most less possible one since no supporting data available in the literature for such thianthrene pair structure. The second way results in an acceptable $(TA^{\cdot +})_2$ structure, but accompanied by an unreliable $HSO_4^- \cdot H_2SO_4$ hydrogen bridged network. The first way is the most preferable one, resulting in a new crystallographically supported structure of $[(TA)_2^{\cdot}]^+$, which was previously inferred in the literature,[32] accompanied by a reliable $HSO_4^- \cdot H_2SO_4$ hydrogen bridged network. Table 2.14 lists the details of structure determination for **5**. Table 2.15 and 2.16 list the selected bond lengths and angles in the structure, respectively.

Table 2.14: Details of structure determination for $(TA^{\bullet})(HSO_4) \cdot H_2SO_4$.

Formula	$C_{12}H_8S_4O_8$
Cell lengths	a = 7.758(3) Å, b = 10.862(6) Å, c = 10.931(9) Å
Cell angles	α = 107.00(4)°, β = 108.08(7)°, γ = 105.45(5)°
Volume of unit cell	770.1(8) $Å^3$
Crystal system, space group	triclinic, $P\bar{1}$ (No. 2)
Number of formula units, Z	2
Density (calc.), ρ	1.761 g cm^{-3}
Absorption coefficient, μ	0.657 mm^{-1}
Absorption correction	Multiscan[56] (empirical correction)
Diffractometer	KappaCCD
Radiation, wave length (λ)	Mo–Kα, 0.71073 Å
Temp. of measurement, T	173 K
Range of data collection	$3.00° < \theta < 25.00°$
hkl range	$-9 \leqslant h \leqslant 9$; $-12 \leqslant k \leqslant 12$; $-12 \leqslant l \leqslant 12$
Number of data collected	10279
Number of ind. refl., R_{merge}	2706, 0.107
Number of refined parameters	217
Ratio reflections/parameters	12.47
R values	$wR(F^2)= 0.1594$ $R(\|F\|) = 0.1088$ for all 2706 refl. $R(\|F\|) = 0.0658$ for 1865 refl. with $F_0 > 4sig(F_0)$
GooF	1.065
Largest electron density difference peak and hole	+1.044/-0.477 $eÅ^{-3}$

Table 2.15: List of selected bond lengths/Å in $(\mathrm{TA}^{\cdot})(\mathrm{HSO}_4)\cdot\mathrm{H}_2\mathrm{SO}_4$.

S1–C7	1.724(6)	S4–O8	1.386(6)	C4–C5	1.399(9)
S1–C2	1.728(6)	S4–O7	1.474(6)	C5–C6	1.375(9)
S2–C8	1.722(6)	S4–O6	1.493(6)	C7–C12	1.407(8)
S2–C1	1.734(6)	S4–O5	1.499(5)	C7–C8	1.421(8)
S3–O3	1.438(6)	C1–C6	1.408(8)	C8–C9	1.420(8)
S3–O4	1.461(6)	C1–C2	1.416(8)	C9–C10	1.395(9)
S3–O2	1.472(6)	C2–C3	1.421(8)	C10–C11	1.410(9)
S3–O1	1.477(5)	C3–C4	1.382(9)	C11–C12	1.378(9)

Table 2.16: List of selected bond angles/° in $(\mathrm{TA}^{\cdot})(\mathrm{HSO}_4)\cdot\mathrm{H}_2\mathrm{SO}_4$.

C7–S1–C2	107.4(3)	O7–S4–O5	102.9(4)	C5–C6–C1	119.8(6)
C8–S2–C1	107.4(3)	O6–S4–O5	107.4(3)	C12–C7–C8	119.7(5)
O3–S3–O4	110.5(4)	C6–C1–C2	120.6(5)	C12–C7–S1	114.9(4)
O3–S3–O2	110.1(4)	C6–C1–S2	114.4(4)	C8–C7–S1	125.3(5)
O4–S3–O2	108.5(4)	C2–C1–S2	125.0(5)	C9–C8–C7	118.6(5)
O3–S3–O1	111.4(4)	C1–C2–C3	118.2(5)	C9–C8–S2	114.4(4)
O4–S3–O1	108.0(4)	C1–C2–S1	126.9(4)	C7–C8–S2	126.9(4)
O2–S3–O1	108.3(4)	C3–C2–S1	114.8(4)	C10–C9–C8	120.4(5)
O8–S4–O7	116.4(5)	C4–C3–C2	120.1(6)	C9–C10–C11	120.2(6)
O8–S4–O6	111.2(5)	C3–C4–C5	120.8(6)	C12–C11–C10	119.9(6)
O7–S4–O6	105.1(3)	C6–C5–C4	120.4(6)	C11–C12–C7	121.0(6)
O8–S4–O5	113.0(4)				

2.2.2 Thianthreniumyl tetrachloridoferrate(III)

Preparation

Thianthrene (60 mg, 0.277 mmol) and iron(III) chloride (45 mg, 0.277 mmol) were placed in two different branches of an H-shaped vessel, under inert atmosphere in a glove box. Liquid SO_2 was then condensed into both branches of the vessel, giving yellow colored solutions for thianthrene as well as for iron(III) chloride. Most of the iron salt was insoluble. When the thianthrene solution was transferred into the other side through the glass fritt, the color turned dark violet immediately. The tube was shaken thoroughly for about ten seconds and aged at room temperature. Crystals precipitated in less than five minutes, dispersed among the major white powder solid. Single crystal selection was done under inert conditions with the cold oil method (see A.4.1, p. 124). The crystal structure solution was done using the direct method[54] and H atoms were added in calculated positions and fixed on the C atoms of the benzene rings during the refinement process.

Structure

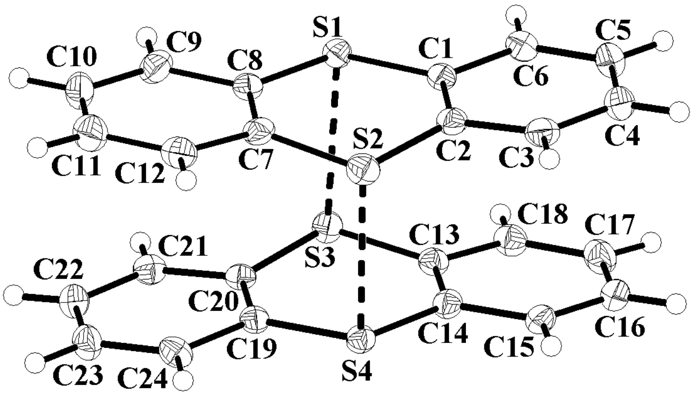

Figure 2.26: The thianthrene radical cations pair in $(TA^{\bullet})[FeCl_4]$. Thermal displacement ellipsoids are scaled to include 50% probability. H atoms are drawn with arbitrary radii.

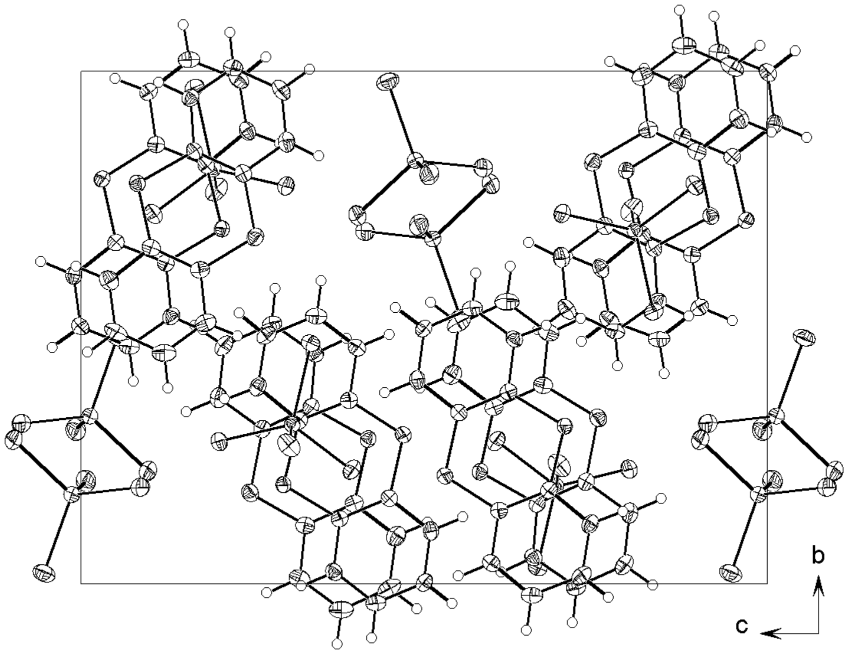

Figure 2.27: The arrangement of the ions in the unit cell of $(TA^{\bullet})[FeCl_4]$.

In the structure of thianthreniumyl tetrachloridoferrate(III), $(TA^{\bullet})[FeCl_4]$ (**6**) screw axes are present in a, b, and c directions defining the space group $P2_12_12_1$. The structure is isotypical to that of thianthrene radical cation tetrachloridoaluminate[9] (Fig. 2.27). The thianthrene is present in oxidized form as its radical cation and the dihedral angle amounts 172°. The radicals are paired at close $S\cdots S$ distances of 3.074 Å in average. Slippage is present in the pair so that the $S\cdots S$ axes do not from a rectangular arrangement and slight differences among the C–C bond lengths

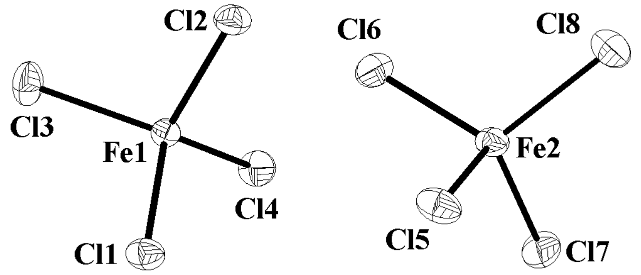

Figure 2.28: The $[FeCl_4]^-$ anions in the structure of $(TA^{\bullet})[FeCl_4]$. Thermal displacement ellipsoids are scaled to include 50% probability.

prevent the $(TA^{\cdot+})_2$ from the ideal D_{2h} point group symmetry. There is actually no crystallographic symmetry present in the ion pair (Fig. 2.26). The angles and the bond lengths in the tetrahedral $[FeCl_4]^-$ anions are not uniform, giving the anions also the lowest symmetry C_1 (Fig. 2.28).

It is obvious that the size of the unit cell of $(TA^{\cdot})[FeCl_4]$ (3069.2 Å^3 at 110 K), which is slightly smaller than that of the known thianthrene radical cation tetrachloridoaluminate (3073.8 Å^3 at 90 K), is contradicting the fact that ionic radius of iron(III) is larger than that of aluminum(III) (0.63 Å *vs.* 0.53 Å).[64] Furthermore, in general, higher temperature of measurement should lead to larger cell parameters and hence the larger volume of unit cell. The bond lengths of Fe–Cl in the structure of **6** is 2.195 Å in average, longer than those of Al–Cl in the structure of the known thianthreniumyl dimer (2.138 Å).[9] However, the volume of $FeCl_4^-$ is, actually, slightly smaller than that of $AlCl_4^-$ according to anion volumes obtained from alkali and alkaline earth metal salts (155 Å^3 *vs.* 156 Å^3). The cation volumes, calculated based on Goldschmidt radii, were subtracted from the total volume to give the the anion volumes.[65] Elsewhere, derived from ionic volumes, the estimated anion radius for $FeCl_4^-$ is also smaller than that of $AlCl_4^-$ (3.02 Å *vs.* 3.33 Å).[66] The smaller cell volume of $(TA^{\cdot})[FeCl_4]$ (**6**) in comparison to the $(TA^{\cdot})[AlCl_4]$[9] is, therefore, in agreement with the previous finding of anion volumes.

Table 2.18 and 2.19 list the bond lengths and angles in the molecule, respectively. Details of the structure refinement are listed in Table 2.17. However, as a result of the very small yield in comparison with the overwhelming amount of white powder-like solid, no further characterization has been made.

Table 2.17: Details of structure determination for (TA$^\bullet$)[FeCl$_4$].

Formula	$C_{12}H_8Cl_4FeS_2$
Cell lengths	a = 12.6256(1) Å, b = 13.4651(3) Å, c = 18.0533(4) Å
Volume of unit cell	3069.15(10) Å^3
Crystal system, space group	orthorhombic, $P2_12_12_1$ (No. 19)
Number of formula units, Z	8
Density (calc.), ρ	1.792 g cm^{-3}
Absorption coefficient, μ	1.931 mm^{-1}
Absorption correction	Multiscan[56] (empirical correction)
Diffractometer	KappaCCD
Radiation, wave length (λ)	Mo–Kα, 0.71073 Å
Temp. of measurement, T	110 K
Range of data collection	$3.03° < \theta < 27.49°$
hkl range	$-15 \leqslant h \leqslant 15$; $-17 \leqslant k \leqslant 17$; $-23 \leqslant l \leqslant 23$
Number of data collected	53123
Number of ind. refl., R_{merge}	6987, 0.0764
Number of refined parameters	343
Ratio reflections/parameters	20.37
Flack x parameter	-0.0111 with esd 0.0137
R values	wR(F^2)= 0.0634
	R(|F|) = 0.0453 for all 6987 refl.
	R(|F|) = 0.0329 for 6100 refl. with $F_0 > 4\mathrm{sig}(F_0)$
GooF	1.084
Largest electron density difference peak and hole	+0.398/-0.411 eÅ^{-3}

Table 2.18: List of selected bond lengths/Å in $(\mathrm{TA}^{\cdot})[\mathrm{FeCl}_4]$.

Cl1–Fe1	2.1739(10)	C14–C15	1.411(5)	S2–C7	1.726(4)
Cl2–Fe1	2.193(1)	C15–C16	1.379(5)	C1–C6	1.403(5)
Cl3–Fe1	2.2035(10)	C16–C17	1.405(6)	C1–C2	1.416(5)
Cl4–Fe1	2.2027(11)	C17–C18	1.369(6)	C2–C3	1.410(5)
Cl5–Fe2	2.1999(11)	C19–C24	1.406(5)	C3–C4	1.373(6)
Cl6–Fe2	2.1922(11)	C19–C20	1.419(5)	C4–C5	1.400(6)
Cl7–Fe2	2.1995(11)	C20–C21	1.401(5)	C5–C6	1.378(5)
Cl8–Fe2	2.1962(11)	C21–C22	1.371(5)	C7–C12	1.403(5)
S3–C20	1.721(4)	C22–C23	1.400(6)	C7–C8	1.415(5)
S3–C13	1.722(4)	C23–C24	1.373(6)	C8–C9	1.414(5)
S4–C14	1.728(4)	S1–C8	1.731(4)	C9–C10	1.372(6)
S4–C19	1.731(4)	S1–C1	1.731(4)	C10–C11	1.391(6)
C13–C18	1.401(5)	S2–C2	1.717(4)	C11–C12	1.378(6)
C13–C14	1.421(5)				

Table 2.19: List of selected bond angles/° in $(\mathrm{TA}^{\cdot})[\mathrm{FeCl}_4]$.

Cl1–Fe1–Cl4	110.63(4)	C16–C15–C14	120.1(4)	C3–C2–C1	119.8(3)
Cl2–Fe1–Cl4	108.68(4)	C15–C16–C17	120.7(4)	C3–C2–S2	114.5(3)
Cl1–Fe1–Cl3	109.20(4)	C18–C17–C16	120.2(4)	C1–C2–S2	125.7(3)
Cl2–Fe1–Cl3	108.89(4)	C17–C18–C13	120.3(4)	C4–C3–C2	119.6(4)
Cl4–Fe1–Cl3	110.19(4)	C24–C19–C20	118.7(3)	C3–C4–C5	121.0(4)
Cl6–Fe2–Cl8	113.37(5)	C24–C19–S4	114.9(3)	C6–C5–C4	120.0(4)

Cl6–Fe2–Cl7	106.51(5)	C20–C19–S4	126.3(3)	C5–C6–C1	120.5(4)
Cl8–Fe2–Cl7	108.05(5)	C21–C20–C19	119.7(3)	C12–C7–C8	119.7(4)
Cl6–Fe2–Cl5	107.56(5)	C21–C20–S3	115.0(3)	C12–C7–S2	114.6(3)
Cl8–Fe2–Cl5	109.99(4)	C19–C20–S3	125.3(3)	C8–C7–S2	125.6(3)
Cl7–Fe2–Cl5	111.36(5)	C22–C21–C20	120.3(4)	C9–C8–C7	118.4(3)
C20–S3–C13	107.79(17)	C21–C22–C23	120.3(4)	C9–C8–S1	115.4(3)
C14–S4–C19	107.39(17)	C24–C23–C22	120.6(4)	C7–C8–S1	126.1(3)
C18–C13–C14	120.1(3)	C23–C24–C19	120.4(4)	C10–C9–C8	120.2(4)
C18–C13–S3	114.3(3)	C8–S1–C1	107.22(18)	C9–C10–C11	121.3(4)
C14–C13–S3	125.5(3)	C2–S2–C7	107.64(18)	C12–C11–C10	119.6(4)
C15–C14–C13	118.5(3)	C6–C1–C2	119.1(3)	C11–C12–C7	120.6(4)
C15–C14–S4	115.5(3)	C6–C1–S1	114.8(3)		

2.2.3 Tris(thianthrene)(2+) bis(heptachloridodialuminate)

The preparation of this compound is the same as the previously explained synthesis of **4** (2.1.4, p. 40). From the same ampoule a red colored crystal was picked up and measured on a single crystal X-ray diffractometer.

Structure

The diffraction intensities of the mechanically very unstable, purple prismatic crystal of $(TA_3)[Al_2Cl_7]_2$, tris(thianthrene)(2+) bis(heptachloridodialuminate) (**7**) were measured and collected at room temperature. The crystal structure refinement reveals a parallel stack of three flattened TA molecules as a divalent cation $(TA_3)^{2+}$ accompanied by two heptachloridodialuminate $[Al_2Cl_7]^-$ anions. The TA in the middle of the stack is planar with C_i symmetry while the two outer TA molecules are bent at 164.4° with the lowest symmetry point group C_1. The trimer is generated by an inversion

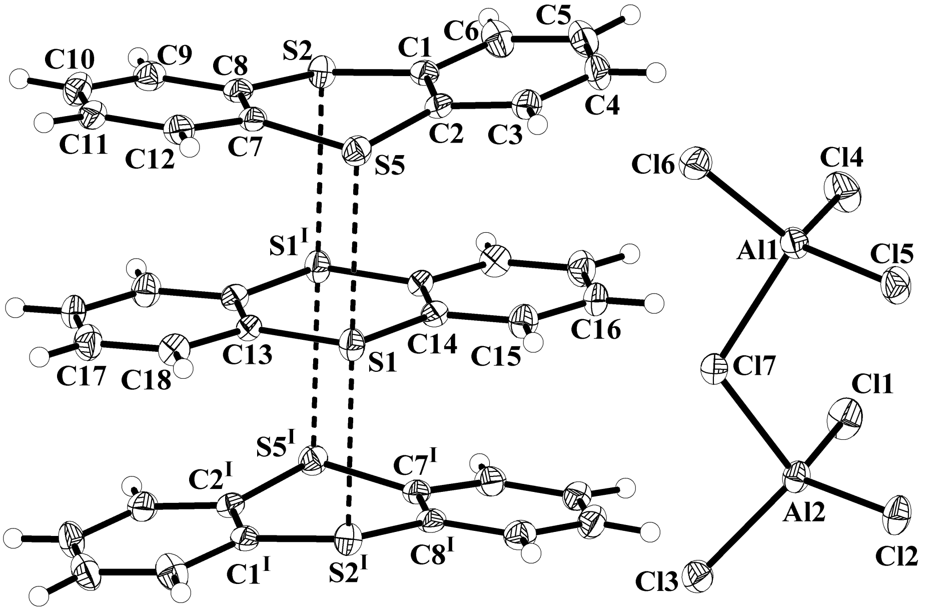

Figure 2.29: The view of cationic thianthrene trimer and the $[Al_2Cl_7]^-$ ion in the structure of $(TA_3)[Al_2Cl_7]_2$. Thermal displacement ellipsoids are scaled to include 50% probability. H atoms are drawn with arbitrary radii. Symmetry operation I = 1-x, 1-y, 1-z.

center but deviates only slightly from D_{2h} point group (Fig. 2.29). The shortest distance between two S atoms of the two outer TA molecules in this trimer is 6.288 Å, slightly longer than 6.202 Å of the previously known twisted trimer[34] (Fig. 1.5, p. 8). The average $S \cdots S$ intermolecular distance between the outer thianthrene molecule and the middle one is also observed as longer than the $S \cdots S$ intermolecular distances in the dimers. In this structure this distance is 3.144 Å, while in the dimers 3.077 Å are found in the structure of $(TA^{\cdot})[AlCl_4]$,[9] 3.054 Å in $(TA^{\cdot})(HSO_4) \cdot H_2SO_4$ (**5**) and 3.074 Å in $(TA^{\cdot})[FeCl_4]$ (**6**).

The longer distance between two adjacent thianthrenes in this trimer than those in the dimers seems to be contradicting the repulsion force of the positive–positive charge of the molecules. In the trimer two positive charges are dispersed over three molecules, whereas in the dimer, over only two molecules. However, this observation confirms the role of the radical electron in the interaction. In the dimer, there are

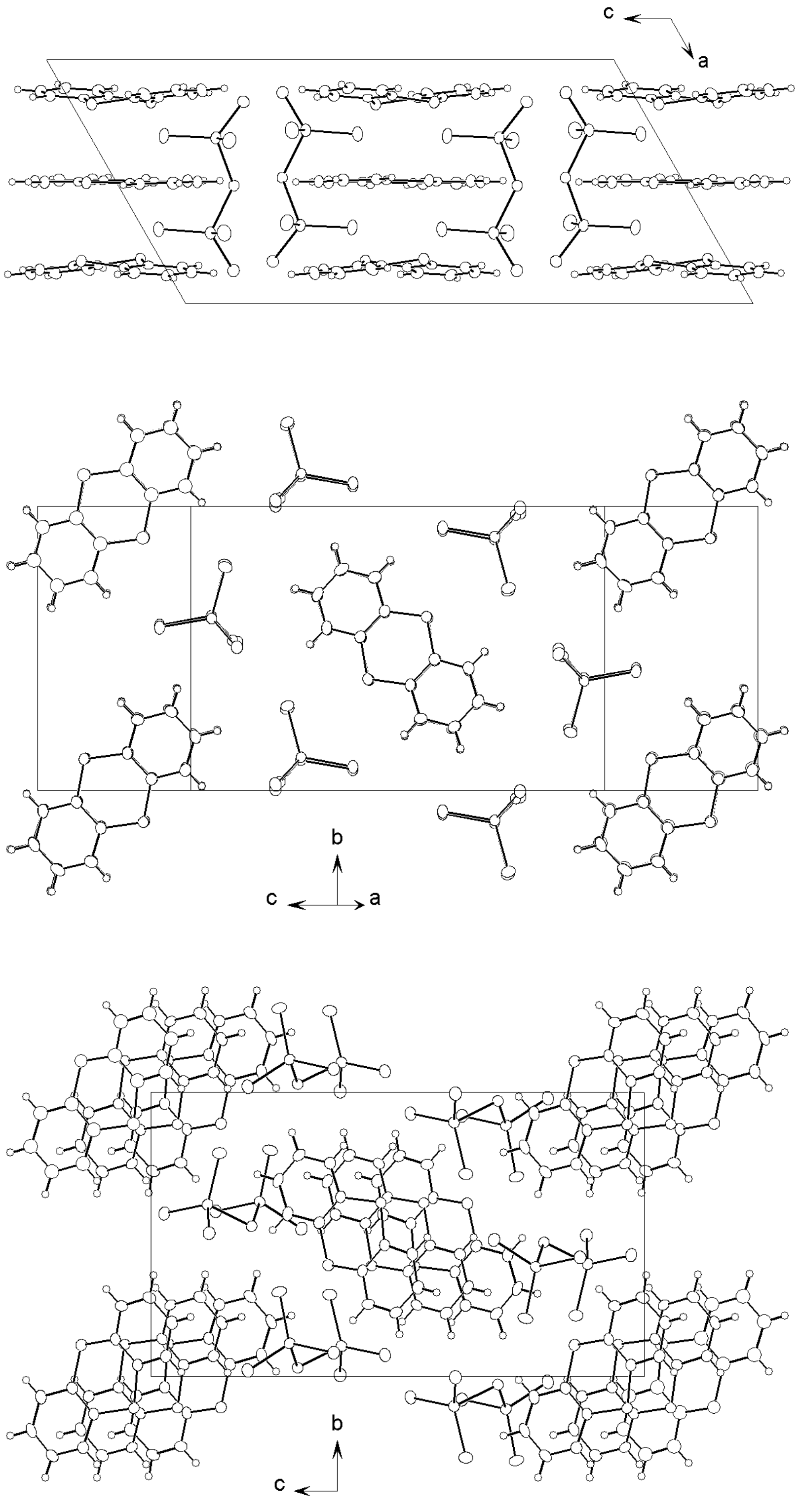

Figure 2.30: Arrangement of the ions in the structure of $(TA_3)[Al_2Cl_7]_2$ in a view along crystallographic and *b*-axis (top), along the stack of the thianthrene trimer (middle) and along crystallographic *a*-axis (bottom).

two radical electrons bonding two molecules, whereas in the trimer, there are two electrons for three molecules resulting in lower bond order.

The $S\cdots S$ distances between the adjacent molecules in the 'triple decker' of this structure is 3.14 Å, which is smaller than the sum of van der Waals radii of two S atoms (3.7 Å). On the twisted trimer, this distance is 3.98 Å.[34] Since the positive charges are localized in the S atoms, the arrangement of molecules in the twisted trimer provides weaker positive-positive centers repulsion, hence, slightly narrower stack.

The S–C bond lengths in the thianthrene molecule change depending on the oxidation state. These bonds in neutral thianthrene are averaged 1.771 Å,[6] but in the oxidized thianthrene shortened to 1.732 Å, in average, as found in the structure of $TA[AlCl_4]$.[9] The S–C bonds in the previous two compounds from this work are, in average, even shorter, 1.727 and 1.726 Å in $(TA^{\cdot})(HSO_4)\cdot H_2SO_4$ (**5**) and $(TA^{\cdot})[FeCl_4]$ (**6**), respectively. Thianthrene molecule in the middle of the 'triple decker' has an average S–C distances of 1.736 Å and the outer molecule have longer average S–C bonds of 1.750 Å. These bond lengths are longer than those in the thianthrene radical cation, but shorter than those in the neutral molecule. However, the outer thianthrene molecules are close to the form of neutral molecule whereas the central thianthrene is close to the form of the radical cation. This bond lengths characteristic indicates the distribution of the positive charge over the three molecules with the maximum found at the central molecule, which is in agreement with the twisted trimer.[34]

The dinuclear anion $[Al_2Cl_7]^-$ is known to form from $[AlCl_4]^-$ and $AlCl_3$ in the presence of big cations. There is actually no crystallographic symmetry present, but the configuration is only slightly distorted from C_{2v}. All terminal Cl atoms have shorter distances to the Al atoms in comparison with the bridging Cl atom. Additionally, the angles among them are almost uniformly bigger than the angles between the terminal Cl atoms, Al atoms and the bridging Cl atom so that the overall shape is a corner-sharing pair of two distorted tetrahedra. There are six anions surrounding each cation in a plane parallel to the TA molecules (Fig. 2.30, top and middle). The next layer is located relative to the first at a distance of 3.3 Å (C9$\cdots$C9) and 3.22 Å (H10$\cdots$S2) (Fig. 2.30, bottom). Selected details of structure determination, bond lengths and angles are listed in Table 2.20, 2.21 and 2.22, respectively.

Table 2.20: Details of structure determination for $(TA_3)[Al_2Cl_7]_2$.

Formula	$C_{18}H_{12}Al_2Cl_7S_3$
Cell lengths	$a = 11.2114(3)$ Å, $b = 11.3216(3)$ Å, $c = 22.6464(4)$ Å
Cell angles	$\beta = 119.6740(10)°$
Volume of unit cell	2497.55(10) Å^3
Crystal system, space group	monoclinic, $P2_1/c$ (No. 14)
Number of formula units, Z	4
Density (calc.), ρ	1.666 g cm^{-3}
Absorption coefficient, μ	1.12 mm^{-1}
Absorption correction	Multiscan[56] (empirical correction)
Diffractometer	KappaCCD
Radiation, wave length (λ)	Mo–Kα, 0.71073 Å
Temp. of measurement, T	293(2) K
Range of data collection	$3.29° < \theta < 27.55°$
hkl range	$-14 \leqslant h \leqslant 14$; $-14 \leqslant k \leqslant 14$; $-29 \leqslant l \leqslant 29$
Number of data collected	49327
Number of ind. refl., R_{merge}	5690, 0.0754
Number of refined parameters	283
Ratio reflections/parameters	20.11
R values	wR(F^2)= 0.0855 R(|F|) = 0.1015 for 5690 all refl. R(|F|) = 0.0478 for 3647 refl. with $F_0 > 4\mathrm{sig}(F_0)$
GooF	1.065
Largest electron density difference peak and hole	+0.453/-0.458 eÅ^{-3}

Table 2.21: List of selected bond lengths/Å in $(TA_3)[Al_2Cl_7]_2$.

S1–C13	1.724(4)	S5–C2	1.756(4)	C10–C11	1.389(5)
S1–C14	1.747(4)	C1–C6	1.409(5)	C11–C12	1.377(5)
C13–C18	1.416(5)	C1–C2	1.414(5)	Cl1–Al2	2.1226(15)
C14–C15	1.402(5)	C2–C3	1.402(5)	Cl2–Al2	2.1046(14)
C14–C13^{I}	1.409(5)	C3–C4	1.391(6)	Cl3–Al2	2.1043(15)
C15–C16	1.382(6)	C4–C5	1.384(6)	Cl4–Al1	2.1171(16)
C17–C18	1.374(5)	C5–C6	1.379(5)	Cl5–Al1	2.1052(14)
C17–C16^{I}	1.411(6)	C7–C12	1.405(5)	Cl6–Al1	2.1013(15)
S2–C1	1.741(4)	C7–C8	1.413(5)	Cl7–Al2	2.2716(14)
S2–C8	1.760(4)	C8–C9	1.401(5)	Cl7–Al1	2.2853(14)
S5–C7	1.741(4)	C9–C10	1.395(5)		

Table 2.22: List of selected bond angles/° in $(TA_3)[Al_2Cl_7]_2$.

C13–S1–C14	107.40(18)	C3–C2–C1	118.6(3)	C12–C11–C10	119.4(4)
C14^{I}–C13–C18	119.9(3)	C3–C2–S5	115.4(3)	C11–C12–C7	120.8(4)
C14^{I}–C13–S1	126.1(3)	C1–C2–S5	126.0(3)	Al2–Cl7–Al1	114.19(5)
C18–C13–S1	114.0(3)	C4–C3–C2	120.5(4)	Cl6–Al1–Cl5	112.79(6)
C15–C14–C13^{I}	118.9(3)	C5–C4–C3	120.8(4)	Cl6–Al1–Cl4	114.79(7)
C15–C14–S1	114.6(3)	C6–C5–C4	119.9(4)	Cl5–Al1–Cl4	114.64(7)
C13^{I}–C14–S1	126.5(3)	C5–C6–C1	120.5(4)	Cl6–Al1–Cl7	101.75(6)
C16–C15–C14	120.8(4)	C12–C7–C8	120.0(3)	Cl5–Al1–Cl7	106.31(6)
C15–C16–C17^{I}	120.1(4)	C12–C7–S5	115.1(3)	Cl4–Al1–Cl7	104.95(6)

C18–C17–C16^{I}	120.1(4)	C8–C7–S5	124.8(3)	Cl3–Al2–Cl2	113.43(6)
C17–C18–C13	120.2(4)	C9–C8–C7	118.4(3)	Cl3–Al2–Cl1	113.48(6)
C1–S2–C8	106.50(18)	C9–C8–S2	115.1(3)	Cl2–Al2–Cl1	115.08(7)
C7–S5–C2	106.63(18)	C7–C8–S2	126.4(3)	Cl3–Al2–Cl7	100.85(6)
C6–C1–C2	119.8(3)	C10–C9–C8	120.3(4)	Cl2–Al2–Cl7	105.55(6)
C6–C1–S2	114.8(3)	C11–C10–C9	121.0(4)	Cl1–Al2–Cl7	106.82(6)
C2–C1–S2	125.4(3)				

2.3 Other related salts

Owing similarity to the structure of thianthrene, selenanthrene (SA) and phenazine (PAz) (Fig. 1.1, p. 3) have also been used as reactants in liquid SO_2. The reaction with selenanthrene yielded the salt like compounds $(SA^{\bullet})[AlCl_4]$ (**8**), $SAO(HSO_4)_2$ (**9**) and $(SA^{\bullet})_2[SO_4(BF_3)_2]$ (**10**), whereas from phenazine the acidic salt $(H_2PAz)[HSO_4]_2$ (**11**), was obtained.

2.3.1 Selenanthreniumyl tetrachloridoaluminate

Preparation

Into an H-vessel, selenanthrene (31 mg, 0.1 mmol) and aluminum trichloride (26.66 mg, 0.2 mmol) were placed separately in the two branches. About 5 mL liquid SO_2 were condensed into each side, resulting in yellow and colorless solutions for selenanthrene and aluminum chloride, respectively. When both solutions were combined, the color of the mixture turned to dark violet immediately. After one day crystals of metallic luster appeared. After evaporation of the solvent, the solution left behind a mixture of colorless and blue crystals adhered on the wall of the tube. The precipitation of the metallic colored crystals disappeared whenever the tube was shaken during the aging process. Single crystal selection was done under inert condition with the cold oil method (see A.4.1, p. 124). The crystal structure solution was done using the direct method[54] and H atoms were added in calculated positions and fixed on the C atoms of the benzene rings during the refinement process.

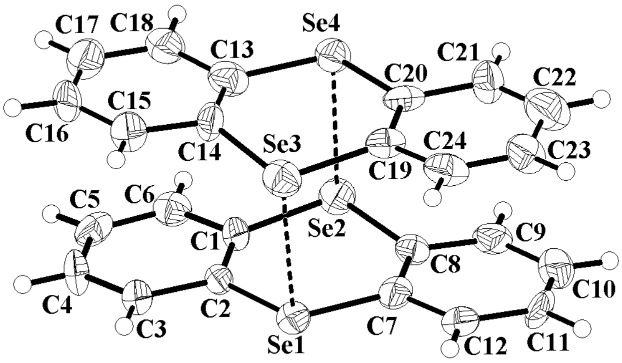
C17
C18
C13
Se4
C21
C22
C20
C15
C16
C14
Se3
C24
C23
C19
C5
C6
C1
Se2
C9
C8
C10
C4
C2
C3
Se1
C7
C12
C11

Figure 2.31: The selenanthrene radical cation pair in the structure of SA$^{\cdot}$[AlCl$_4$]. Thermal displacement ellipsoids are scaled to include 50% probability. H atoms are drawn with arbitrary radii.

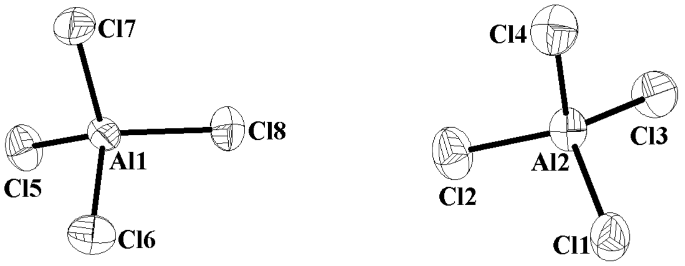
Cl7
Cl8
Cl5
Al1
Cl6
Cl4
Cl3
Cl2
Al2
Cl1

Figure 2.32: The two independent [AlCl$_4$]$^-$ anions in the structure of (SA$^{\cdot}$)[AlCl$_4$]. Thermal displacement ellipsoids are scaled to include 50% probability.

Structure

The crystal structure of selenanthreniumyl tetrachlorido aluminate, (SA$^{\cdot}$)[AlCl$_4$] (**8**), belongs to the orthorhombic crystal system and the acentric space group $P2_12_12_1$. The asymmetric unit of the crystal structure consists of two almost flat selenanthrene units forming a pair, and two AlCl$_4$ tetrahedra. In the selenanthrene cations the dihedral angle between planes each composed of a benzene ring and two selenium atoms in the selenanthrene unit is 172.95°. The close intermolecular Se$\cdots$Se distances are 3.188 Å and 3.133 Å. The selenanthreniumyl pair is slightly slipped so that the Se$\cdots$Se axes do not from a rectangular arrangement. The structure is isotypical to that of the sulfur analogue **6** (2.2.2, p. 59). Figure 2.31 and 2.32 show the radical pair and the tetrahedral anions, respectively.

Table 2.23: Details of structure determination for $(SA^{\bullet})[AlCl_4]$.

Formula	$C_{12}H_8AlCl_4Se_2$
Cell lengths	a = 12.8314(7) Å, b = 13.5237(9) Å, c = 18.3434(11) Å
Volume of unit cell	3183.1(3) Å^3
Crystal system, space group	orthorhombic, $P2_12_12_1$ (No. 19)
Number of formula units, Z	8
Density (calc.), ρ	1.999 g cm^{-3}
Absorption coefficient, μ	5.354 mm^{-1}
Absorption correction	Multiscan[56] (empirical correction)
Diffractometer	KappaCCD
Radiation, wave length (λ)	Mo–Kα, 0.71073 Å
Temp. of measurement, T	203 K
Range of data collection	$3.01° < \theta < 27.44°$
hkl range	$-16 \leqslant h \leqslant 16$; $-16 \leqslant k \leqslant 16$; $-23 \leqslant l \leqslant 23$
Number of data collected	18218
Number of ind. refl., R_{merge}	6416, 0.1045
Number of refined parameters	343
Ratio reflections/parameters	18.71
Flack x parameter	0.0022 with esd 0.0137
R values	wR(F^2)= 0.1045
	R(|F|) = 0.1104 for all 6416 refl.
	R(|F|) = 0.0543 for 3991 refl. with $F_0 > 4sig(F_0)$
GooF	0.955
Largest electron density difference peak and hole	+0.655/-0.707 eÅ^{-3}

Table 2.24: List of selected bond lengths/Å in $(\mathrm{SA}^{\bullet})[\mathrm{AlCl}_4]$.

Se1–C2	1.871(9)	C3–C4	1.365(13)	C14–C15	1.395(14)
Se1–C7	1.877(10)	C3–H3	0.9300	C15–C16	1.377(15)
Se2–C8	1.867(9)	C4–C5	1.387(13)	C15–H15	0.9300
Se2–C1	1.870(10)	C4–H4	0.9300	C16–C17	1.392(16)
Se3–C14	1.865(10)	C5–C6	1.373(14)	C16–H16	0.9300
Se3–C19	1.872(10)	C5–H5	0.9300	C17–C18	1.367(15)
Se4–C20	1.878(9)	C6–H6	0.9300	C17–H17	0.9300
Se4–C13	1.890(11)	C7–C8	1.388(12)	C18–H18	0.9300
Cl1–Al2	2.130(4)	C7–C12	1.407(13)	C19–C24	1.374(13)
Cl2–Al2	2.134(4)	C8–C9	1.393(13)	C19–C20	1.395(12)
Cl3–Al2	2.130(4)	C9–C10	1.388(14)	C20–C21	1.431(14)
Cl4–Al2	2.123(4)	C9–H9	0.9300	C21–C22	1.348(15)
Cl5–Al1	2.109(4)	C10–C11	1.376(15)	C21–H21	0.9300
Cl6–Al1	2.130(4)	C10–H10	0.9300	C22–C23	1.428(15)
Cl7–Al1	2.128(3)	C11–C12	1.382(14)	C22–H22	0.9300
Cl8–Al1	2.136(4)	C11–H11	0.9300	C23–C24	1.360(15)
C1–C2	1.392(13)	C12–H12	0.9300	C23–H23	0.9300
C1–C6	1.426(13)	C13–C14	1.384(14)	C24–H24	0.9300
C2–C3	1.408(13)	C13–C18	1.402(14)		

Table 2.25: List of selected bond angles/° in $(\mathrm{SA}^{\bullet})[\mathrm{AlCl}_4]$.

C2–Se1–C7	104.9(4)	C1–C2–C3	118.8(8)	C14–C13–Se4	126.5(8)
C8–Se2–C1	105.4(4)	C1–C2–Se1	127.1(7)	C18–C13–Se4	113.9(8)
C14–Se3–C19	105.9(4)	C3–C2–Se1	114.0(7)	C13–C14–C15	119.2(10)
C20–Se4–C13	104.6(5)	C4–C3–C2	119.9(10)	C13–C14–Se3	127.3(8)
Cl5–Al1–Cl7	109.70(16)	C3–C4–C5	121.2(10)	C15–C14–Se3	113.2(8)
Cl5–Al1–Cl6	109.79(15)	C6–C5–C4	121.0(9)	C16–C15–C14	120.7(10)
Cl7–Al1–Cl6	108.36(17)	C5–C6–C1	118.2(9)	C15–C16–C17	120.0(11)
Cl5–Al1–Cl8	110.62(17)	C8–C7–C12	118.7(9)	C18–C17–C16	119.7(12)
Cl7–Al1–Cl8	109.86(16)	C8–C7–Se1	127.7(7)	C17–C18–C13	120.7(11)
Cl6–Al1–Cl8	108.47(16)	C12–C7–Se1	113.6(7)	C24–C19–C20	120.8(10)
Cl4–Al2–Cl3	107.36(18)	C7–C8–C9	120.5(9)	C24–C19–Se3	114.2(7)
Cl4–Al2–Cl1	112.71(17)	C7–C8–Se2	126.4(7)	C20–C19–Se3	124.8(7)
Cl3–Al2–Cl1	108.99(19)	C9–C8–Se2	113.1(7)	C19–C20–C21	117.9(9)
Cl4–Al2–Cl2	107.97(18)	C10–C9–C8	120.1(9)	C19–C20–Se4	128.8(8)
Cl3–Al2–Cl2	110.90(18)	C11–C10–C9	119.8(10)	C21–C20–Se4	113.3(7)
Cl1–Al2–Cl2	108.92(18)	C10–C11–C12	120.6(10)	C22–C21–C20	121.0(11)
C2–C1–C6	120.8(9)	C11–C12–C7	120.3(10)	C21–C22–C23	119.4(12)
C2–C1–Se2	127.0(7)	C14–C13–C18	119.6(10)	C23–C24–C19	120.8(11)
C6–C1–Se2	112.3(7)				

2.3.2 μ-oxy-selenanthrene(2+) bis(hydrosulfate)

Preparation

Loading of the reaction vessel was done in a glove box. Selenanthrene (31 mg, 0.1 mmol) and silver trifluoromethansulfonate (25.7 mg, 0.1 mmol) were placed in different branches of an H-shaped vessel. The filled H-vessel was then evacuated and filled with O_2 several times before finally SO_2 was condensed into both branches at the pressure of 8×10^{-3} mbar. The bright yellow solution of selenanthrene was transferred into the other branch with the colorless solution of the silver salt, and shaken thoroughly. After a week, the color of the solution was violet and many golden shiny crystals deposited. Shaking the vessel resulted in darkening of the solution, but the dark color did not maintain. Ten days later, the golden shiny crystals disappeared and colorless crystals were obtained. *This reaction was not reproducible in the liquid SO_2 purchased from Praxair* (see Tab. A.1, Fig. A.1 and Fig. A.2). Single crystal selection was done under inert conditions with the cold oil method (see A.4.1, p. 124). The crystal structure solution was done using the direct method[54] and H atoms in the benzene rings were added in calculated position during the refinement process. The H atoms for the HSO_4 units were added and refined, according to the assumption that the very close distances between two O atoms are bridged by hydrogen bonds.

Structure

The crystal structure of μ-oxy-selenanthrene(2+) bis(hydrosulfate), $SAO(HSO_4)_2$ (**9**) reveals a new type of oxidized selenanthrene with a unique configuration. The asymmetric unit of the structure consists of an oxidized selenanthrene molecule and two HSO_4^- units. There is an oxygen atom bridging both Se atoms within a selenanthrene molecule. Though oxidized, the bridging oxygen atom brings the molecule to a stronger bent form, at 121°. It has no internal symmetry, but the configuration is only slightly deviating from the ideal C_{2v}. The bridging oxygen is obviously closer to Se1, at 1.762 Å, whereas the bond length to Se2 is 1.931 Å. Additionally, both Se atoms are close to the oxygen atoms of two different SO_4 units which are connected differently to the SA molecule (Fig. 2.33) so that each selenium atom has coordination number of 4. The oxygen atom bonded to Se1 is obviously at greater distance than that of O5 from Se2. Table 2.26 contains the details of the structure refinement, Table 2.27 and 2.28 lists selected bond lengths and angles, respectively.

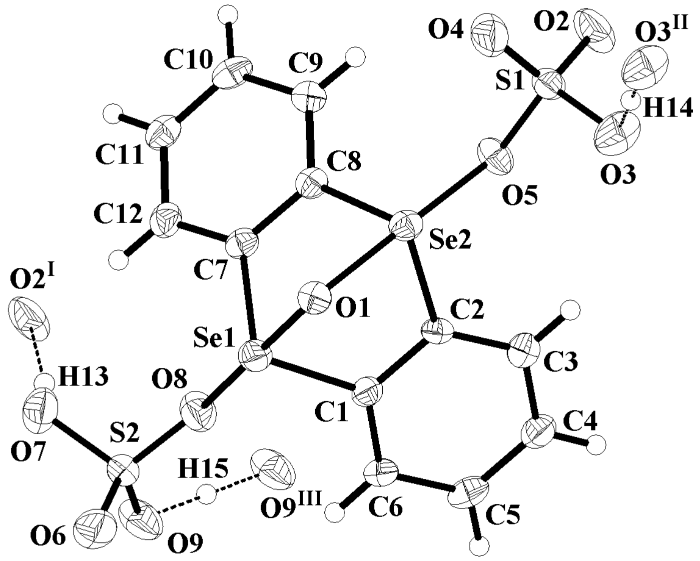

Figure 2.33: The molecular moiety in the structure of $SAO(HSO_4)_2$. Thermal displacement ellipsoids are scaled to include 50% probability. H atoms are drawn with arbitrary radii. I = 1-x, 2-y, 1-z; II = -x, 2-y, 2-z; III = 1-x, 1-y, -z.

The two SO_4 units differ considerably from each other. The longest O–S bond on the first SO_4 is at the O5 atom which is connected to the Se1 atom, whereas for the second SO_4 group at the O7 atom which is not directing to any Se atom. There are three close O$\cdots$O distances in the structure, i.e. between O7 and O2^{I}, between O3 and O3^{II} and between O9 and O9^{III}, at 2.54, 2.478 and 2.495 Å, respectively (Fig. 2.33). These distances are in the range of strong H bonds with a linear O–H$\cdots$O bridges.[63] Therefore, there must be additional H atoms added to the anionic part of the structure.

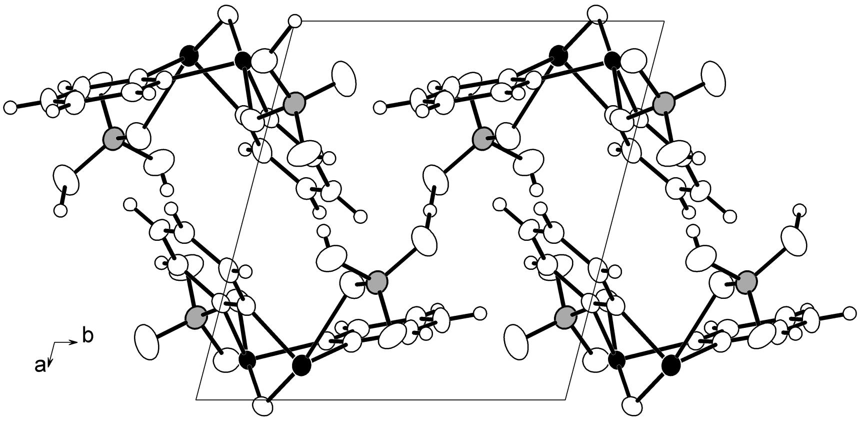

Figure 2.34: The unit cell view in the $SAO(HSO_4)_2$. Thermal displacement ellipsoids are scaled to include 50% probability. H atoms are drawn with arbitrary radii.

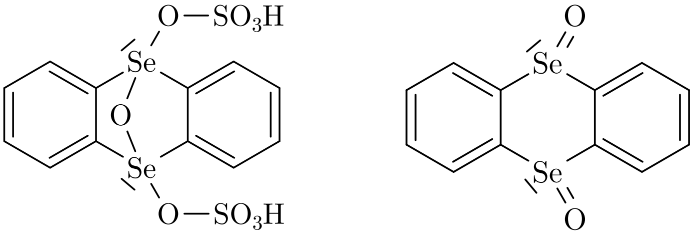

Figure 2.35: The Lewis structure of $SAO(HSO_4)_2$ (left) and selenanthrene-5,10-dioxide (right).

The three close O···O distances involving four oxygen atoms, or, from the view of the SO_4 units, four of the oxygen atoms have close distance to another O atom. Overall, there must be 4/2 H atoms for both SO_4 units. These two H atoms had been added to the atom list and included in the subsequent refinement process to give the final structure of $SAO(HSO_4)_2$. Since the μ-oxy-selenanthrene(2+) unit is accompanied by two HSO_4^-, it has two positive charges, SAO^{2+}. The electron configuration of selenanthrene in this derivate, the $SAO(HSO_4)_2$, is therefore related to the known selenanthrene-5,10-dioxide[67] (Fig. 2.35). Figure 2.34 shows the arrangement of molecules in the crystal structure. The close distances among μ-oxy-selenanthrene(2+) bis(hydrosulfate) in the structure consist of O···Se interaction and hydrogen bonds.

Table 2.26: Details of structure determination for $SAO(HSO_4)_2$.

Formula	$C_{12}H_{10}O_9S_2Se_2$
Cell lengths	$a = 9.2116(4)$ Å, $b = 9.7152(5)$ Å, $c = 10.0761(5)$ Å
Cell angles	$\alpha = 116.350(3)^\circ$, $\beta = 91.447(3)^\circ$, $\gamma = 102.485(3)^\circ$
Volume of unit cell	781.33(7) $Å^3$
Crystal system, space group	triclinic, $P\bar{1}$ (No. 2)
Number of formula units, Z	2
Density (calc.), ρ	2.211 g cm^{-3}
Absorption coefficient, μ	5.05 mm^{-1}
Absorption correction	Multiscan[56] (empirical correction)
Diffractometer	KappaCCD
Radiation, wave length (λ)	Mo–Kα, 0.71073 Å
Temp. of measurement, T	203 K
Range of data collection	$3.14^\circ < \theta < 27.44^\circ$
hkl range	$-11 \leqslant h \leqslant 11$; $-12 \leqslant k \leqslant 12$; $-13 \leqslant l \leqslant 13$
Number of data collected	21313
Number of ind. refl., R_{merge}	3539, 0.105
Number of refined parameters	230
Ratio reflections/parameters	15.39
R values	$wR(F^2) = 0.1039$
	$R(\lvert F\rvert) = 0.0805$ for all 3539 refl.
	$R(\lvert F\rvert) = 0.0447$ for 2517 refl. with $F_0 > 4sig(F_0)$
GooF	1.080
Largest electron density difference peak and hole	+0.47/-0.99 e$Å^{-3}$

Table 2.27: List of selected bond lengths/Å in SAO(HSO$_4$)$_2$.

Se1–O1	1.763(3)	S1–O3	1.484(4)	C3–C4	1.386(7)
Se1–C7	1.927(5)	S1–O5	1.528(4)	C4–C5	1.397(8)
Se1–C1	1.928(5)	S2–O6	1.424(4)	C5–C6	1.398(7)
Se1–O8	2.522(4)	S2–O8	1.452(4)	C7–C8	1.386(7)
Se2–C2	1.920(5)	S2–O9	1.486(4)	C7–C12	1.391(7)
Se2–O1	1.932(3)	S2–O7	1.545(4)	C8–C9	1.386(7)
Se2–C8	1.933(5)	C1–C6	1.373(7)	C9–C10	1.388(7)
Se2–O5	2.051(3)	C1–C2	1.404(7)	C10–C11	1.369(8)
S1–O4	1.433(4)	C2–C3	1.380(7)	C11–C12	1.400(7)
S1–O2	1.442(4)				

Table 2.28: List of selected bond angles/° in SAO(HSO$_4$)$_2$.

O1–Se1–C7	88.39(18)	O6–S2–O8	115.9(3)	C4–C5–C6	120.4(5)
O1–Se1–C1	89.83(18)	O6–S2–O9	112.3(3)	C1–C6–C5	118.0(5)
C7–Se1–C1	97.4(2)	O8–S2–O9	109.8(2)	C8–C7–C12	121.2(5)
C2–Se2–O1	86.18(17)	O6–S2–O7	105.0(2)	C8–C7–Se1	114.9(4)
C2–Se2–C8	97.7(2)	O8–S2–O7	107.4(2)	C12–C7–Se1	123.6(4)
O1–Se2–C8	85.88(17)	O9–S2–O7	105.6(2)	C9–C8–C7	121.4(5)
C2–Se2–O5	87.48(17)	C6–C1–C2	121.8(5)	C9–C8–Se2	123.8(4)
O1–Se2–O5	170.45(13)	C6–C1–Se1	124.5(4)	C7–C8–Se2	114.6(4)
C8–Se2–O5	87.90(17)	C2–C1–Se1	113.5(4)	C8–C9–C10	117.5(5)
O4–S1–O2	115.5(3)	C3–C2–C1	120.2(4)	C11–C10–C9	121.2(5)

O4–S1–O3	110.4(3)	C3–C2–Se2	124.1(4)	C10–C11–C12	122.0(5)
O2–S1–O3	108.5(3)	C1–C2–Se2	115.7(3)	C7–C12–C11	116.6(5)
O4–S1–O5	109.4(2)	C2–C3–C4	118.6(5)	Se1–O1–Se2	108.74(16)
O2–S1–O5	107.2(2)	C3–C4–C5	121.1(5)	S1–O5–Se2	114.37(19)
O3–S1–O5	105.2(2)				

2.3.3 Bis(selenanthreniumyl) bis(trifluoridoborate)(tetraoxidosulfate)(2–) mono(sulfur dioxide)

Preparation

The preparation was performed in an inert atmosphere inside a glove box. The reactants were placed in two separate branches of an H-shaped vessel. Selenanthrene (26 mg, 0.084 mmol) is soluble in SO_2 giving an intensive yellow colored solution, whereas silver tetrafluoroborate (16.32 mg, 0.084 mmol) is apparently insoluble in the solvent. The color of the mixture was similar to the selenanthrene solution, but after one day the solution over the unsoluble salt became slightly pink. After a week, the solution became darker and violet. After another week, dark metallic shiny crystals and colorless crystals appeared. *This reaction was not reproducible in the liquid* SO_2 *purchased from Praxair* (see Tab. A.1, Fig. A.1 and Fig. A.2). Crystal selection was done under inert conditions with the cold oil method (see A.4.1, p. 124). The majority of the selected crystals were twinned as confirmed by the diffraction patterns of the crystal obtained by the X-ray diffractometer. After several tries, a fairly suitable crystal was chosen for recording intensity data.

The crystal structure solution was done with direct method[54] and *Multiscan*[56] absorption correction. The twin law was applied in the refinement process. The *.hkl*

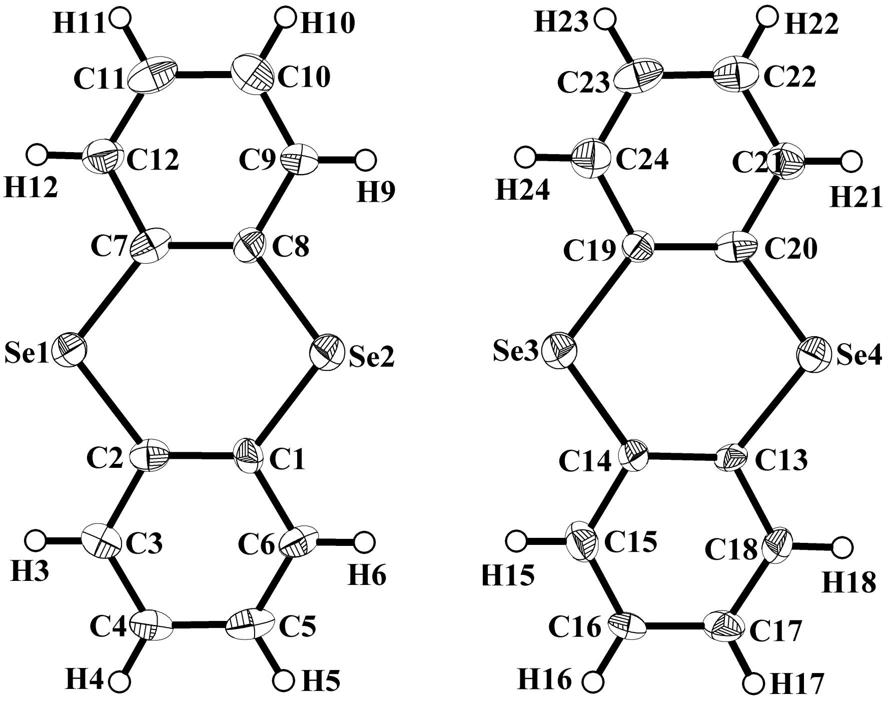
H11
H10
C11
C10
C12
C9
H12
H9
C7
C8
Se1
Se2
C2
C1
C3
C6
H3
H6
C4
C5
H4
H5
H23
H22
C23
C22
C24
C21
H24
H21
C19
C20
Se3
Se4
C14
C13
C15
C18
H15
H18
C16
C17
H16
H17

Figure 2.36: The two independent $SA^{\cdot+}$ molecules in the structure of $(SA^{\cdot})_2[SO_4(BF_3)_2] \cdot SO_2$. Thermal displacement ellipsoids are scaled to include 50% probability. H atoms are drawn with arbitrary radii.

file was transformed according to transformation matrix suggested by *ROTAX*[68] twinning tool and the structure was further refined with a BASF command giving a value of 0.33626. All hydrogen atoms were added in calculated positions and fixed to the carbon atoms of the benzene rings of the SA molecules.

Structure

The asymmetric unit of the structure consists of two selenanthrene radical cations and a rare anion $[F_3B{-}O(SO_2)O{-}BF_3]^{2-}$,[69] bis(selenanthreniumyl) bis(trifluoridoborate) (tetraoxidosulfate)(2–) mono(sulfurdioxide), $(SA^{\cdot})_2[SO_4(BF_3)_2] \cdot SO_2$ (**10**). The configuration of the cation molecule is similar to its homologue, thianthreniumyl. The molecule is flattened (Fig. 2.36) and paired via two Se$\cdots$Se interactions at a distance of 3.095 Å, comparable to the thianthreniumyl pair (Fig. 2.37). A small slippage in the pairs causes the four Se atoms to deviate from a rectangular arrangement. Thus,

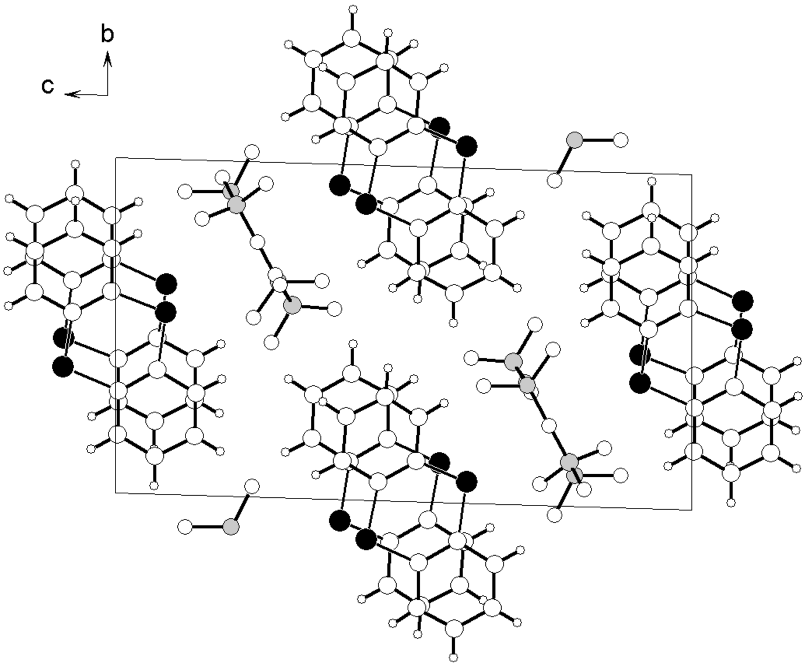

Figure 2.37: The arrangement the molecules in the structure of $(SA^{\bullet})_2[SO_4(BF_3)_2]\cdot SO_2$ in a view along the crystallographic *a*-axis.

the pair has only C_i symmetry but is close to the ideal D_{2h}. An interesting feature of the structure of **10** is that F5, B1, O4, S1, O1, B2, F2 and S2 are almost located in one plane, additionally, both selenanthreniumyl molecules are found at the same distance on the both side of the plane. A crystallographical mirror plane, however, is not present in the unit cell (Fig. 2.39).

The atom assignment in the anion of **10** based on the diffraction data turned out to be difficult, not only because of the limited quality of the diffraction data, but also by the nature of oxygen and fluorine, with only one electron difference making them almost indistinguishable by X-ray diffractometry. From the view of acid-base interaction, it is most probable that both bridging atoms are oxygen (Fig. 2.38) according to the formula $[F_3B{-}O(SO_2)O{-}BF_3]^{2-}$. In this case, the anion is composed of a strong Lewis-base SO_4^{2-} and two strong Lewis-acids BF_3. If both bridging atoms are fluorine according to the formula $[F_3B{-}F(SO_2)F{-}BF_3]^{2-}$, an unstable anion would result, since SO_2 is a Lewis-base as well as Lewis-acid at the same time and also

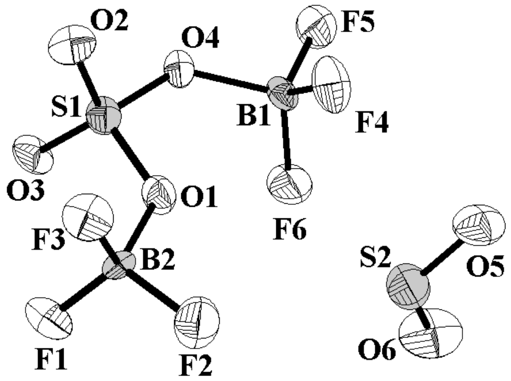

Figure 2.38: The anion $[F_3B{-}O(SO_2)O{-}BF_3]^{2-}$ and the SO_2 solvate molecule in the structure of $(SA^{\bullet})_2[SO_4(BF_3)_2] \cdot SO_2$. Thermal displacement ellipsoids are scaled to include 50% probability.

known as a weakly coordinating ligand.[55,70] On the other side, BF_4^- is also a weakly coordinating ligand, which means the ability to give an electron pair via the F atom for a dative bond is very low. In fact, the refinement calculation gave an insignificantly better R value if the bridging atoms between B and S are assigned as oxygen instead of fluorine. Details of structure determination are listed in Table 2.29. Table 2.30 and 2.31 list the selected bond lengths and angles in **10**, respectively.

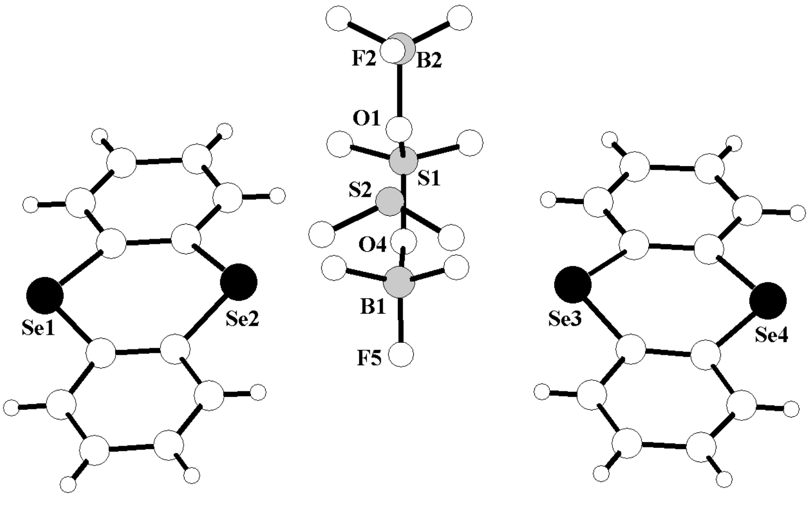

Figure 2.39: A view of the asymmetric unit in structure of $(SA^{\bullet})_2[SO_4(BF_3)_2] \cdot SO_2$. Atom B2 deviates most from the best plane through F5, B1, O4, S1, O1, B2, F2 and S2, by 0.0352 Å.

Table 2.29: Details of structure determination for $(\mathrm{SA}^{\bullet})_2[\mathrm{SO}_4(\mathrm{BF}_3)_2]\cdot\mathrm{SO}_2$.

Formula	$C_{12}H_8BF_3O_3SSe_2$
Cell lengths	a = 7.4144(4) Å, b = 10.5316(6) Å, c = 18.0659(9) Å
Cell angles	α = 88.071(4)°, β = 87.118(3)°, γ = 85.139(3)°
Volume of unit cell	1403.22(13) $Å^3$
Number of formula units, Z	4
Density (calc.), ρ	2.168 g cm^{-3}
Absorption coefficient, μ	5.46 mm^{-1}
Absorption correction	Multiscan[56] (empirical correction)
Crystal system, space group	triclinic, $P\bar{1}$ (No. 2)
Diffractometer	KappaCCD
Radiation, wave length (λ)	Mo–Kα, 0.71073 Å
Temp. of measurement, T	153 K
Range of data collection	$4.06° < \theta < 27.49°$
hkl range	$-9 \leqslant h \leqslant 9$; $-13 \leqslant k \leqslant 13$; $-22 \leqslant l \leqslant 23$
Number of data collected	35869
Number of ind. refl., R_{merge}	6369, 0.1236
Number of refined parameters	398
Ratio reflections/parameters	16.00
R values	$wR(F^2)= 0.221$
	$R(\|F\|) = 0.1748$ for all 35869 refl.
	$R(\|F\|) = 0.0870$ for 19435 refl. with $F_0 > 4\mathrm{sig}(F_0)$
GooF	1.015
Largest electron density difference peak and hole	+2.02/-1.54 $eÅ^{-3}$

Table 2.30: List of selected bond lengths/Å in $(\mathrm{SA}^{\bullet})_2[\mathrm{SO}_4(\mathrm{BF}_3)_2] \cdot \mathrm{SO}_2$.

Se3–C19	1.865(7)	C1–C2	1.391(9)	C15–C16	1.375(11)
Se3–C14	1.868(7)	C1–C6	1.406(10)	C16–C17	1.374(8)
Se2–C8	1.877(7)	C2–C3	1.407(10)	C17–C18	1.365(10)
Se2–C1	1.883(7)	C3–C4	1.385(11)	C19–C20	1.392(9)
Se1–C7	1.862(7)	C4–C5	1.395(10)	C19–C24	1.413(10)
Se1–C2	1.874(7)	C5–C6	1.370(11)	C20–C21	1.404(10)
Se4–C13	1.867(7)	C7–C8	1.396(9)	C21–C22	1.420(10)
Se4–C20	1.882(7)	C7–C12	1.428(10)	C22–C23	1.384(11)
S1–O3	1.424(5)	C8–C9	1.398(10)	C23–C24	1.346(10)
S1–O2	1.429(4)	C9–C10	1.374(11)	B1–F4	1.368(8)
S1–O4	1.517(4)	C10–C11	1.410(11)	B1–F6	1.385(8)
S1–O1	1.527(4)	C11–C12	1.340(11)	B1–F5	1.399(7)
S2–O5	1.418(6)	C13–C14	1.393(8)	B2–F3	1.326(8)
S2–O6	1.431(6)	C13–C18	1.423(10)	B2–F2	1.381(7)
O1–B2	1.553(7)	C14–C15	1.419(10)	B2–F1	1.382(9)
O4–B1	1.508(7)				

Table 2.31: List of selected bond angles/° in $(\mathrm{SA}^{\bullet})_2[\mathrm{SO}_4(\mathrm{BF}_3)_2] \cdot \mathrm{SO}_2$.

C19–Se3–C14	104.5(3)	C5–C6–C1	119.3(7)	C20–C19–Se3	127.7(6)
C8–Se2–C1	104.6(3)	C8–C7–C12	118.0(7)	C24–C19–Se3	113.6(5)
C7–Se1–C2	104.9(3)	C8–C7–Se1	128.3(6)	C19–C20–C21	120.4(7)
C13–Se4–C20	105.1(3)	C12–C7–Se1	113.8(5)	C19–C20–Se4	126.5(6)

O3–S1–O2	116.8(3)	C7–C8–C9	120.4(7)	C21–C20–Se4	113.2(5)
O3–S1–O4	107.4(3)	C7–C8–Se2	125.9(6)	C20–C21–C22	119.2(7)
O2–S1–O4	107.2(3)	C9–C8–Se2	113.6(5)	C23–C22–C21	119.1(7)
O3–S1–O1	110.6(3)	C10–C9–C8	120.8(7)	C24–C23–C22	121.5(8)
O2–S1–O1	110.9(3)	C9–C10–C11	118.5(8)	C23–C24–C19	121.2(7)
O4–S1–O1	102.9(2)	C12–C11–C10	121.9(8)	F4–B1–F6	112.5(5)
O5–S2–O6	116.9(3)	C11–C12–C7	120.4(7)	F4–B1–F5	110.0(5)
S1–O1–B2	126.5(3)	C14–C13–C18	120.2(7)	F6–B1–F5	109.2(5)
B1–O4–S1	130.1(4)	C14–C13–Se4	126.7(6)	F4–B1–O4	111.1(5)
C2–C1–C6	120.0(7)	C18–C13–Se4	113.1(4)	F6–B1–O4	108.9(5)
C2–C1–Se2	127.2(7)	C13–C14–C15	118.8(7)	F5–B1–O4	104.8(5)
C6–C1–Se2	112.6(5)	C13–C14–Se3	127.7(6)	F3–B2–F2	113.4(5)
C1–C2–C3	119.5(8)	C15–C14–Se3	113.5(5)	F3–B2–F1	113.7(5)
C1–C2–Se1	126.8(6)	C16–C15–C14	120.4(6)	F2–B2–F1	109.4(5)
C3–C2–Se1	113.7(5)	C17–C16–C15	119.6(8)	F3–B2–O1	110.1(5)
C4–C3–C2	120.3(7)	C18–C17–C16	122.8(8)	F2–B2–O1	102.8(4)
C3–C4–C5	119.1(8)	C17–C18–C13	118.2(6)	F1–B2–O1	106.7(5)
C6–C5–C4	121.7(8)	C20–C19–C24	118.6(7)		

2.3.4 Phenazinediium bis(hydrosulfate)

Preparation

The idea for this reaction was to see what will happen if bent and planar molecules are oxidized with $AgNO_3$ in the same reaction. The bent molecule is TA and the planar one is PAz.[71,72] Thianthrene (72.1 mg, 0.333 mmol) and phenazine (30 mg, 0.167 mmol) were placed in the same branch of an H-vessel whereas $AgNO_3$ (56.6 mg, 0.333 mmol) was in the other one. Liquid SO_2 was condensed in the first branch and dissolved both organic compounds. The resulting yellow colored solution was then transferred onto the silver salt. There was no observable color change of the solution. After about a week orange colored crystals appeared out of a solution of the same color. Single crystal selection was done under inert condition with the cold oil method (see A.4.1, p. 124). The crystal structure solution was done using the direct method.[54] All hydrogen atoms in the structure are directly found during the structure refinement.

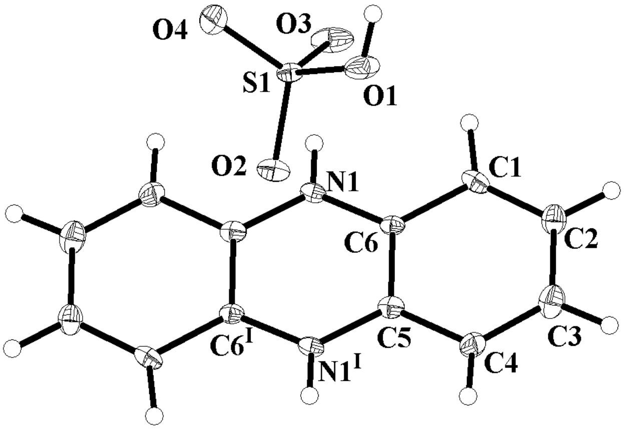

Figure 2.40: The asymmetric unit of the structure of $(H_2PAz)(HSO_4)_2$. Thermal displacement ellipsoids are scaled to include 50% probability. H atoms are drawn with arbitrary radii.

Structure

Phenazinediium bis(hydrosulfate), $(H_2PAz)(HSO_4)_2$ (**11**), crystallizes in the orthorhombic crystal system. The asymmetric unit of the crystal structure consists of one half phenazinediium molecule and a HSO_4^- unit (Fig. 2.40). The next HSO_4^- units are in a range of strong hydrogen bonding between O and N atoms[73] on both side of the phenazinediium molecule (Fig. 2.41). The molecule gains crystallographic C_i symmetry, but it is close to the ideal D_{2h}. In the unit cell there are four differently oriented H_2PAz^{2+} molecules. 8/8 molecules centered at all corners, 2/4 molecules centered at the midpoint of the cell edges at 0 0 $\frac{1}{2}$ and related positions, 2/2 molecules centered

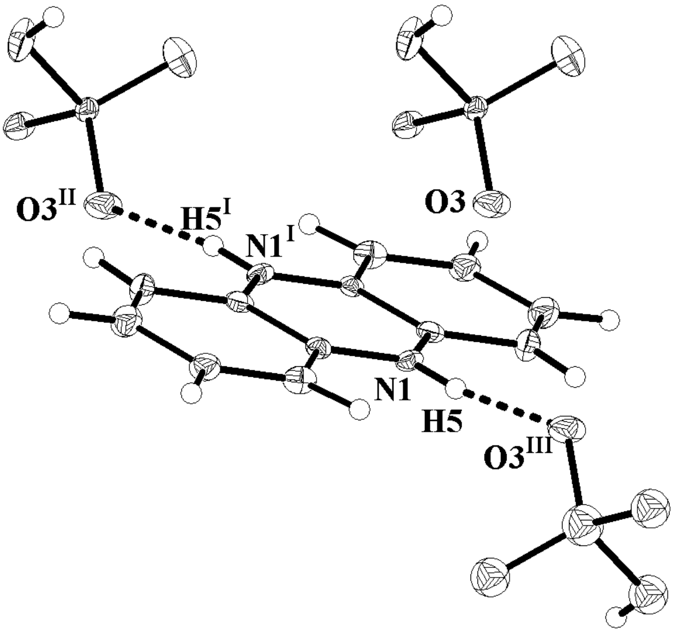

Figure 2.41: The H_2PAz^{2+} cation and the HSO_4^- anions in the structure of $(H_2PAz)(HSO_4)_2$. The dotted lines represent hydrogen bonds which connect both moieties. Thermal displacement ellipsoids are scaled to include 50% probability. H atoms are drawn with arbitrary radii. Symmetry operation I = 1-x, 1-y, 1-z; II = x, -1+y, z; III = 1-x, 2-y, 1-z.

in the midpoint of the a-b plane at $\frac{1}{2}\ \frac{1}{2}\ 0$ and 1 molecule in the midpoint of the cell, centered at $\frac{1}{2}\ \frac{1}{2}\ \frac{1}{2}$. Fig. 2.42. The HSO_4^- units form one dimensional chains parallel to *b*-axis direction via hydrogen bonds (Fig. 2.43). These chains are connected to the ions also via hydrogen bonds. Table 2.32 lists the details of structure determination, Table 2.33 and 2.34 for the selected bond lengths and angles, respectively, in the structure of **11**.

The reaction

Through this reaction phenazine molecule is protonated to phenazinediium molecule. The molecule with two benzene rings is obviously not a neutral phenazine any more since two hydrogen atoms attached to the N atoms of the molecule are clearly found during the structure refinement. It is also not a neutral dihydrophenazine, since

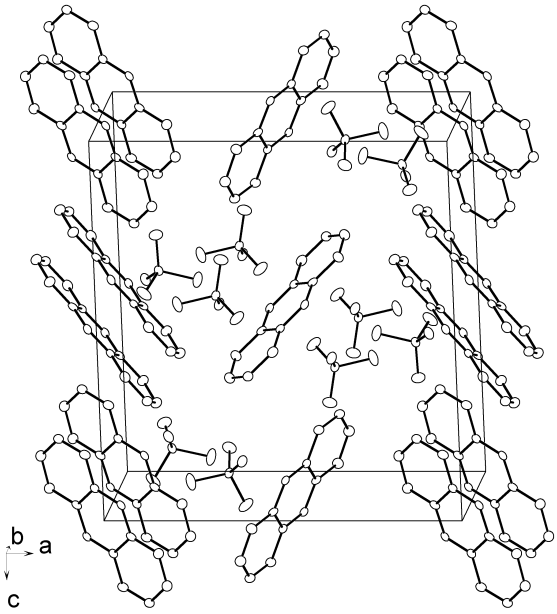

Figure 2.42: The molecular arrangement in the structure of $(H_2PAz)(HSO_4)_2$. H atoms are omitted for clarity.

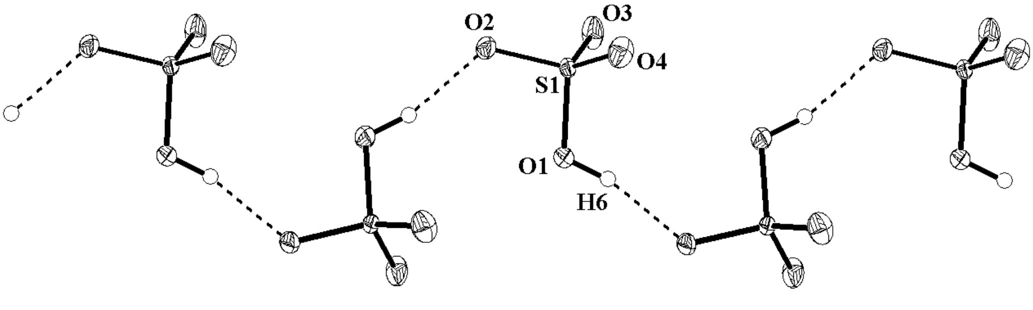

Figure 2.43: The chain of HSO_4^- in the structure of $(H_2PAz)(HSO_4)_2$ connected via hydrogen bonds. H atoms are drawn with arbitrary radii.

the molecule is planar. Dihydrophenazine is a puckered molecule with dihedral angle along the N$\cdots$N axis of 158°.[72] A part of the solvent molecules is apparently oxidized into HSO_4^-.

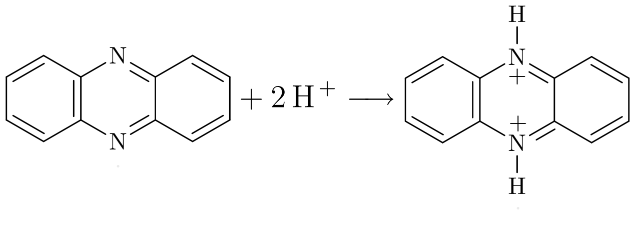

(2.1)

The reaction mechanism for the conversion of phenazine into phenazinediium is unlikely to involve any oxidation process (Reaction 2.1). On the other hand, the development or the presence of HSO_4^- and H_2SO_4 in the product from the reaction between $AgNO_3$ and TA in liquid SO_2 is already observed (see 2.2.1, p. 51), especially when liquid SO_2 purchased form *Air Product* was used (see Tab. A.1, Fig. A.1 and Fig. A.2). Therefore, an intermediate product in form of H_2SO_4 must have been involved in the reaction process. The proton transfer then occurred when the H_2SO_4 molecules were forming hydrogen bonds to the phenazine molecules and crystallized as phenazinediium. Up to 100% proton transfer of $OH\cdots N \rightleftharpoons O^-\cdots H^+N$ type is already known to occur between carboxylic acid and *N*-base.[74] The source for the protons will be explained in subsection 2.4.3 (p. 101).

Table 2.32: Details of structure determination for $(H_2PAz)(HSO_4)_2$.

Formula	$C_6H_6NO_4S$
Cell lengths	a = 13.0492(4) Å, b = 6.8773(2) Å, c = 15.3589(4) Å
Volume of unit cell	1483.99(7) $Å^3$
Crystal system, space group	orthorhombic, *Pbcn*(No. 60)
Number of formula units, Z	8
Density (calc.), ρ	1.685 g cm^{-3}
Absorption coefficient, μ	0.407 mm^{-1}
Absorption correction	Multiscan[56] (empirical correction)
Diffractometer	KappaCCD
Radiation, wave length (λ)	Mo–Kα, 0.71073 Å
Temp. of measurement, T	123 K
Range of data collection	$10.96° < \theta < 30.06°$
hkl range	$-19 \leqslant h \leqslant 19$; $-9 \leqslant k \leqslant 9$; $-21 \leqslant l \leqslant 21$
Number of data collected	53230
Number of ind. refl., R_{merge}	3539, 0.2982
Number of refined parameters	133
Ratio reflections/parameters	15.36
R values	$wR(F^2)$= 0.1327
	$R(\|F\|) = 0.1402$ for all 2045 refl.
	$R(\|F\|) = 0.0781$ for 1312 refl. with $F_0 > 4sig(F_0)$
GooF	1.211
Largest electron density difference peak and hole	+0.478/-0.438 $eÅ^{-3}$

Table 2.33: List of selected bond lengths/Å in $(H_2PAz)(HSO_4)_2$.

S1–O4	1.430(3)	N1–C5^I	1.340(5)	C2–C3	1.431(6)
S1–O2	1.459(2)	N1–C6	1.349(4)	C3–C4	1.359(6)
S1–O3	1.460(3)	C1–C2	1.358(5)	C4–C5	1.404(5)
S1–O1	1.557(3)	C1–C6	1.416(5)	C5–C6	1.430(5)

Table 2.34: List of selected bond angles/° in $(H_2PAz)(HSO_4)_2$.

O4–S1–O2	115.11(16)	C5^I–N1–C6	123.7(3)	N1^I–C5–C6	118.1(3)
O4–S1–O3	113.05(17)	C2–C1–C6	118.7(3)	C4–C5–C6	120.1(3)
O2–S1–O3	109.96(15)	C1–C2–C3	120.7(3)	N1–C6–C1	121.7(3)
O4–S1–O1	108.29(16)	C4–C3–C2	122.0(3)	N1–C6–C5	118.2(3)
O2–S1–O1	102.28(15)	C3–C4–C5	118.4(3)	C1–C6–C5	120.1(3)
O3–S1–O1	107.29(17)	N1^I–C5–C4	121.8(3)		

2.4 Analytical experiments

2.4.1 Qualitative analyses

Reactions in liquid SO_2

The yellow colored liquid SO_2 solution of thianthrene and the colorless solution of aluminum chloride react immediately into a dark violet colored mixture if both solutions are mixed. Metallic lustered crystals precipitate out of the solution within two minutes. This reaction is identical to that with selenanthrene (see chapter 2.3.1, p. 71).

The violet coloration indicates the development of thianthreniumyl pair, $(\mathrm{TA}^{\cdot+})_2$.[32] The crystals have been selected out and measured with X-ray diffractometry, and an identical structure to thianthrene radical cation tetrachloridoaluminate[9] was found.

To avoid any misinterpretation about the oxidation of TA, which occurs in the absence of an oxidizing agent, a small amount of liquid SO_2 was synthesized from $NaHSO_3$ and H_3PO_4. Although the second purchased solvent (later after the one from Air Product, see Tab. A.1, p. 119) was already the highest purity available in the market, with a content of less than 25 ppm H_2SO_4, the self-prepared liquid SO_2 contains certainly no trace of SO_3. The above described reaction of TA and aluminum chloride was repeated with the self-made liquid SO_2, yet the same crystals were obtained.

This finding raise a question: what is the oxidizing agent in the reaction? Since aluminum chloride is non-oxidative, the first investigation involved SO_2, which can be reduced into dithionite according to the following tentative reaction (2.2).

$$6\,\mathrm{C_{12}H_8S_2} + 8\,\mathrm{AlCl_3} + 6\,\mathrm{SO_2} \longrightarrow 6\,(\mathrm{C_{12}H_8S_2^{\cdot+}})[\mathrm{AlCl_4}]^- + \mathrm{Al_2(S_2O_4)_3} \tag{2.2}$$

Rongalit test

The known qualitative analytical test to detect dithionite is the reaction for Rongalit.[75] Dithionite reacts with formaldehyde into Rongalit or sodium hydroxy-methanesulfinate (reaction 2.3), which releases H_2S when heated (reaction 2.4).

$$\mathrm{Na_2S_2O_4} + 2\,\mathrm{CH_2{=}O} + \mathrm{H_2O} \longrightarrow \mathrm{NaO_2SCH_2OH} + \mathrm{NaO_3S{-}CH_2OH} \tag{2.3}$$

$$2\,\mathrm{NaO_2SCH_2OH} \longrightarrow 2\,\mathrm{CH_2O} + \mathrm{Na_2SO_4} + \mathrm{H_2S} \tag{2.4}$$

A special reaction setup has been established for this investigation. Similar to reaction described in subsection 2.3.1, 0.75 mmol for both compounds were used, but thianthrene was used instead of selenanthrene. After the completion of the reaction the solvent was released. One connector of the H-shaped vessel was connected to the argon source and both teflon valves were opened so that a constant flow of the inert gas isolated the sample from humidity as well as from oxygen. The cock of the valve to the second connector was then completely removed, to provide a large opening for further treatment. About 1 mL 50% NaOH solution and 1 mL 30% formaldehyde solution were added, and the vessel was heated until the boiling point of the solution. Afterwards, the cock was reset on its place and the connector was covered with paper wet with Pb(II) acetate solution before the vessel was heated further. There was no dark coloration on the paper even after the sample turned brown, which means no dithionite was detected.

Raman spectrometry

A Raman spectrometry analysis was performed in attempt to identify dithionite in the reaction product. Several reaction sets containing thianthrene and $AlCl_3$ in liquid SO_2 were prepared for this purpose. The solvent was removed from each vessel after the completion of the reaction. The remaining solid was then extracted with various solvent mixtures (Tab. 2.35) to isolate any dithionite from the residue. The extracts were freshly measured with Raman spectrometry. As the reference, spectra from literature were used.[76–78]

The measured values for dithionite were in good agreement with the calculated frequencies at 1058, 1041, 1005, 916, 580, 575, 472, 303 and 208 cm^{-1}.[77] The spectra of dithionite dissolved in solvent show shifts of peaks, however, the peaks are generally sharp and easily observable. The measurement results of the samples from this experiments show no detectable peak in the spectra, in comparison with the noise, originating from the solvent. This observations indicate that no dithionite can be detected. The qualitative Raman spectrometry results are summarized in Table 2.35.

Table 2.35: Raman spectrometry qualitative experiment for dithionite

Sample	extracted with	final form	result
Reaction product	water	water phase	not detected
	water + NaOH	water phase	
	toluene + water	dried toluene phase	
	toluene + water + NaOH	dried toluene phase	

Reaction with Pb(II) acetate solution

Another reaction setup and procedure as for the Rongalit test has been also performed for the following experiment, but a solution of Pb(II) acetate was used instead.

As the Pb(II) acetate solution was added to the sample, a white to yellow perturbation appeared, which in less than a minute turned to a pale brown milky suspension and then formed a precipitation. The mixture was then transferred into a small tube and a mild centrifugation let the dark solid particles to be at the bottom of the tube. This experiment confirms the evolution of sulfide in the reaction.

Ampoule experiments

Several ampoules were prepared containing equal molar amounts of thianthrene and aluminum chloride and processed as described in subsection 2.1.4.

When broken, from the ampoule evolved gas that blackened a paper wet with lead(II) acetate solution within about 5 minutes. The process occurred slowly. This can be understood by the following process. Water evaporated from the wrapping wet paper into the ampoule and reacted with aluminum chloride or a chloride-containing aluminate to release gaseous HCl. At the same time water reacted with a hydrolyzable sulfide and released hydrogen sulfide. Both gases finally reached the lead(II) acetate to give a black lead(II) sulfide smudge as well as white appearance at the middle of the outer fold layer, which consists most likely of colorless $PbCl_2$ crystals. This results indicate the existence of a sulfide as one of the reaction products (Fig. 2.44).

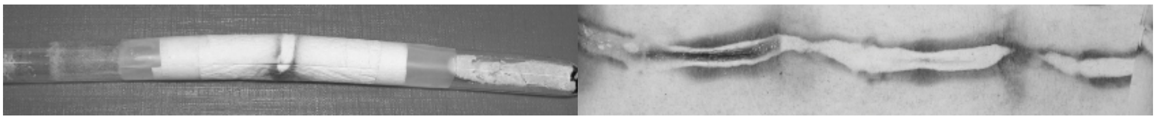

Figure 2.44: Photograph of a broken ampoule of the reaction of TA and $AlCl_3$ (left). When the wrapping paper was uncoiled and stretched, black smudge through the layers of the paper is visible (right).

Mass spectrometry

In order to identify the reaction products mass spectrometry was used. After the solvent was removed, the residue from the reaction between thianthrene and aluminum chloride in liquid SO_2 was extracted with toluene. The toluene was extracted and the residue, termed as the *extracted reaction products*, was taken as the sample for recording mass spectra. Fig. 2.45 shows the mass spectrum of purified thianthrene and Fig. 2.46 shows the spectrum of the *extracted reaction products*. Both spectra are almost identical, except for the intensity of the peak at $m/z = 184$ which corresponds to $C_{12}H_8S$, assigned most probably to dibenzothiophene. It was detected to a slightly higher amount in the mass spectrum of the *extracted reaction products* than in pure thianthrene. Here, the respective peak has a lower intensity (42.5%, scaled to $M^+ = 100\%$) in comparison to the spectrum of the *extracted reaction products* (47%).

This results imply the high probability of the evolution of $C_{12}H_8S$, and the possibility of $C_{12}H_8S$ as one of the reaction products in the reaction between TA and $AlCl_3$ in liquid SO_2.

2.4.2 Gravimetry

In an effort to find the side product formed in the reaction between thianthrene and aluminum chloride in liquid SO_2, a series of reactions has been performed in five

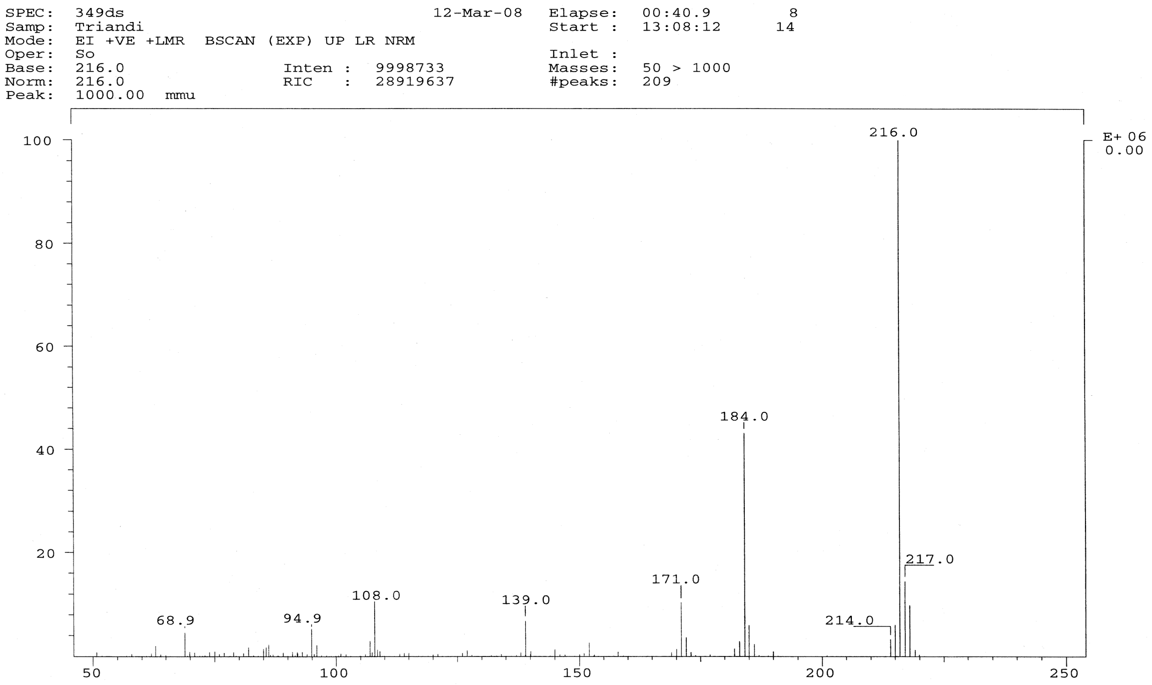

```
SPEC:  349ds                                  12-Mar-08  Elapse:  00:40.9      8
Samp:  Triandi                                           Start :  13:08:12     14
Mode:  EI +VE +LMR  BSCAN (EXP) UP LR NRM
Oper:  So                                                Inlet :
Base:  216.0               Inten :  9998733              Masses:  50 > 1000
Norm:  216.0               RIC   :  28919637             #peaks:  209
Peak:  1000.00  mmu
```

Figure 2.45: Mass spectrum of purified thianthrene.

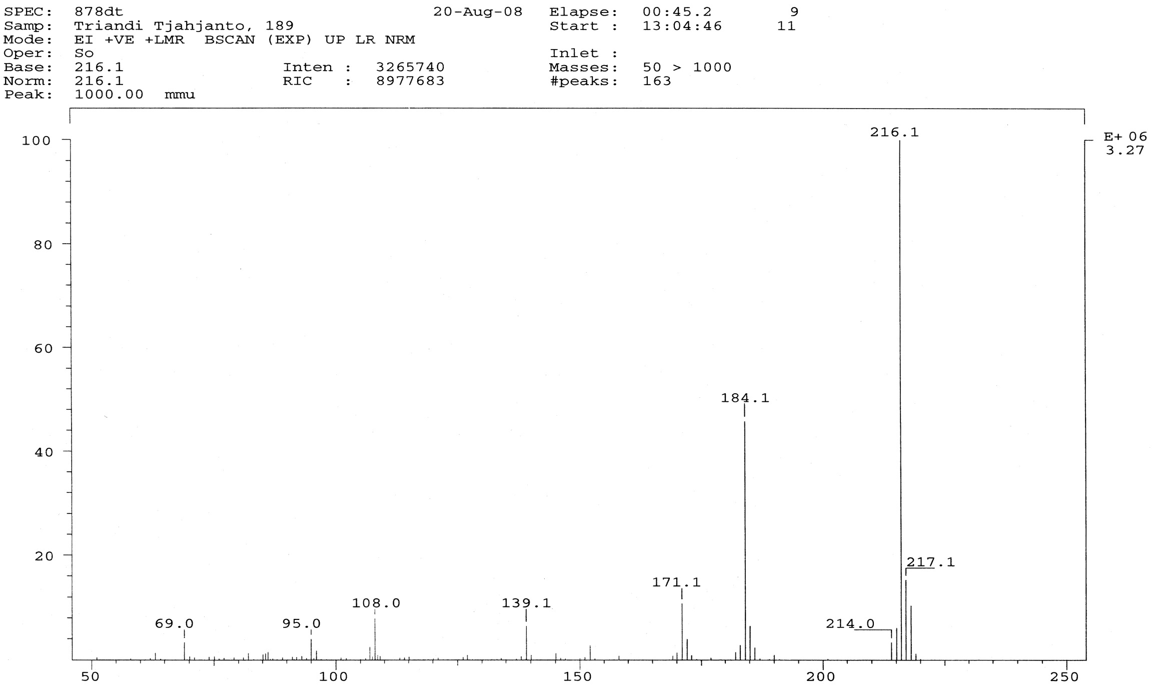

```
SPEC:  878dt                                  20-Aug-08  Elapse:  00:45.2      9
Samp:  Triandi Tjahjanto, 189                            Start :  13:04:46     11
Mode:  EI +VE +LMR  BSCAN (EXP) UP LR NRM
Oper:  So                                                Inlet :
Base:  216.1               Inten :  3265740              Masses:  50 > 1000
Norm:  216.1               RIC   :  8977683              #peaks:  163
Peak:  1000.00  mmu
```

Figure 2.46: Mass spectrum of the residue of the toluene extract of the reaction product of TA + $AlCl_3$ in liquid SO_2 (*extracted reaction products*).

small reaction tubes. All preparations were done in inert atmosphere. Liquid SO_2 was condensed into the five reaction tubes each inside a pressure tight vessel. The solution were aged at room temperature over night before the solvent was released. Each vessel was flushed out with a flow of argon gas, and evacuated to completely remove the SO_2 from the remained solids. The weighing after the reaction was done inside a glove box. In each reaction, $AlCl_3$ was made to be the limiting factor (the amount of TA was added in excess) since it is known that $AlCl_3$ will form a complex with SO_2,[51,79] and hence potentially invalidate the result.

Table 2.36: Gravimetry evaluation of the reaction between TA and $AlCl_3$ in liquid SO_2.

Reaction tube	1	2	3	4	5
Amount of Thianthrene/mg	71.2	61.7	56.9	63.5	60.4
Amount of $AlCl_3$/mg	45.4	29.8	37.1	31.9	31.3
Additional weight after the reaction/mg	15.8	10.7	13.5	11.5	11.0
n $AlCl_3$/mmol	0.341	0.224	0.278	0.239	0.235
n SO_2/mmol	0.247	0.167	0.211	0.180	0.172
mol ratio $AlCl_3$: SO_2	1.379	1.337	1.319	1.332	1.366
Averaged ratio	1.347				

The complete results of the gravimetry measurement are listed in Table 2.36. Molar amount, n, of $AlCl_3$ is calculated by dividing the corresponding amount with its molecular mass, 133.33 g/mol. The additional weight is attributed to the embedded SO_2 which has reacted either with TA or with $AlCl_3$ and n SO_2 is calculated by dividing the additional weight with its molecular mass, 64.07 g/mol. Interestingly, the calculation shows that the mol ratio of $AlCl_3$ to SO_2, embedded after the reaction, is 1.347 or approximately 4:3. It means, each 4 mol $AlCl_3$ react together with 3 mol SO_2. The molar ratio of $AlCl_3$ to SO_2 is, therefore, in agreement with the tentative reaction according to equation 2.2 (p. 95). However, since no dithionite could be detected, the reaction equation remains in doubt.

2.4.3 Coloration

A long time observation has been made with a solution of thianthrene and oxygen dissolved in liquid SO_2 in a pressure-tight NMR tube. The initial color of the solution was yellow and an NMR measurement was taken. After aging for more than 8 months at room temperature without protection from indirect sunlight a red coloration appeared and a second NMR spectrum was recorded. Fig. 2.47, representing the first NMR measurement, shows a relatively simple spectrum for TA on the left and a small amount of impurities on the right side. The high intensity resonances of H atoms attached to the benzene rings appear in the range of 6.8 – 7.1 ppm. In contrast, Fig. 2.48 shows a more complex spectrum from the second NMR measurement. The signals definitely arise from TA and the decompositon products of TA. Beside a shift of the resonance of the C-aromatic H atoms to the range of 7.6 – 8.0 ppm, there are additional resonances at 3.6, 2.7 and 2.57 ppm and a lot more of smaller resonances appearing at field higher than 8.0 ppm. This observation implies that thianthrene is slowly oxidized into its radical cation by oxygen at room temperature without protection against light. The decomposition of thianthrene is the most likely the source of H atoms in the structures of **5**, **9** and **11**.

Another observation has been made concerning the red colored solution of thianthrene in liquid SO_2 containing a trace of SO_3. About 20 mg of TA was placed in a narrow glass tube with one end closed and SO_3-containing liquid SO_2 was condensed into the tube before finally the second end was melted forming a closed ampoule. The solution became red just before reaching room temperature, indicating the formation of TA radical cations, oxidized by the SO_3. When the ampule was cooled below -60 °C, the color changed to green-blue. This observation shows that part of the dissolved thianthrene is oxidized into its radical cation, which is responsible for

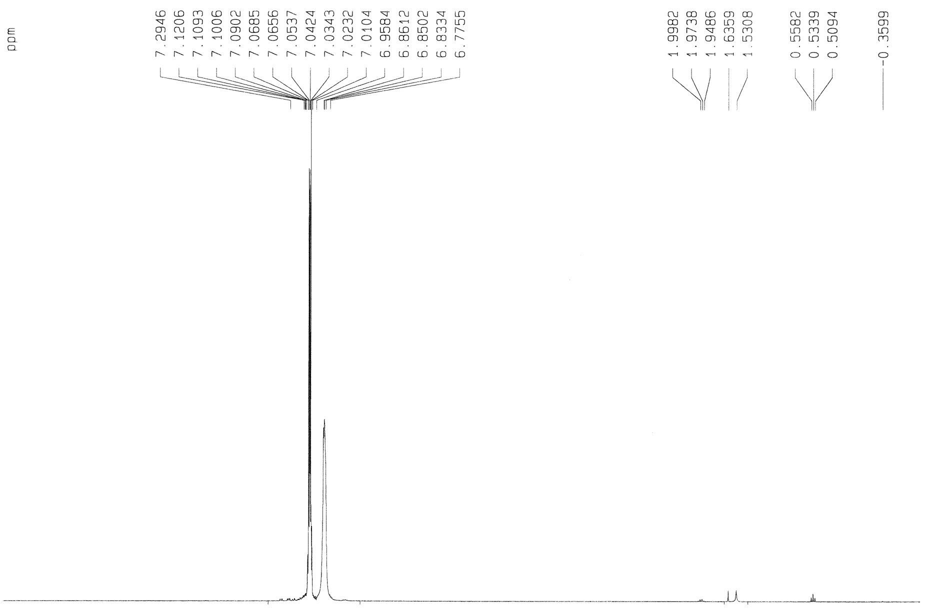

Figure 2.47: ^{1}H–NMR spectrum of a fresh solution of TA and O_2 in liquid SO_2.

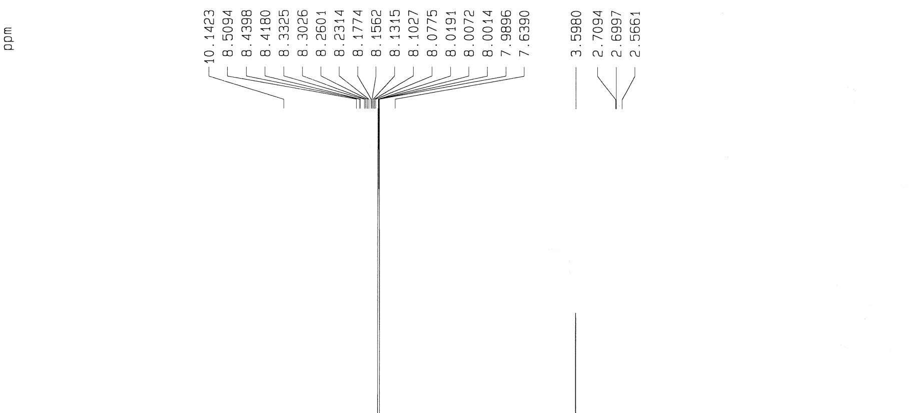

Figure 2.48: ^{1}H–NMR spectrum of a solution of TA and O_2 in liquid SO_2 after 8 months.

the red color. On cooling the cations are paired, losing the red color and become violet. A green-blue appearance was observable as a result of a color mix with the yellow solution of the unreacted thianthrene (in excess) in liquid SO_2. This coloration experiment is in agreement with the literature.[32] Without any oxidizing agent, the solution of thianthrene in liquid SO_2 remains yellow.

With a higher SO_3 concentration thianthrene was immediately oxidized in liquid SO_2 and precipitated as blue oily drops and metallic lustered crystals, identical to those described in subsection 2.2.1 (p. 51).

2.4.4 Cyclic voltammetry

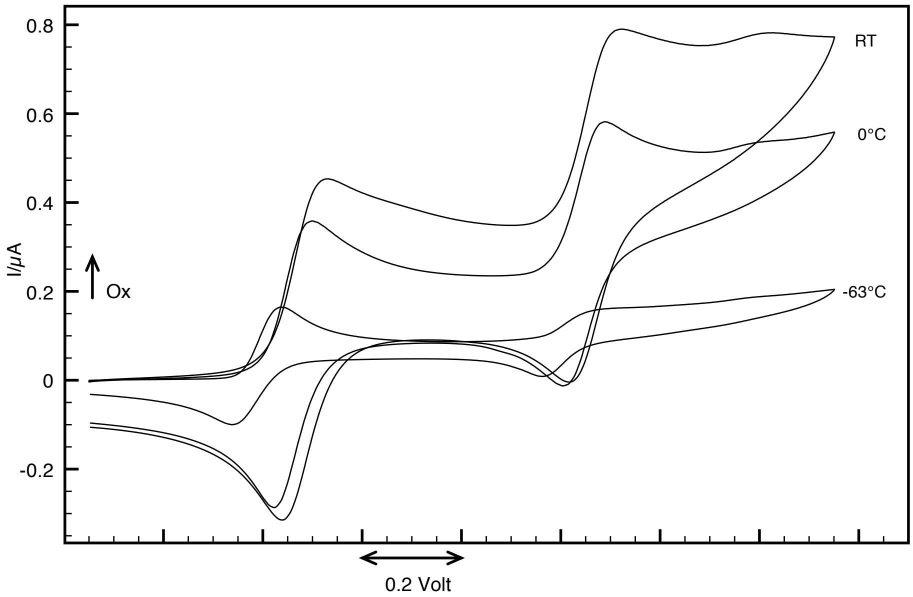

Figure 2.49: Cyclic voltammetry measurements of thianthrene in liquid SO_2. Single scans comparison at different temperatures.

To investigate whether the oxidation potential of thianthrene in liquid SO_2 is lower than that in a common organic solvent, a series of cyclic voltammetry measurements were performed. A special glass container was designed and built for this purpose, which allows for measurement under the equilibrium pressure of SO_2 at tempera-

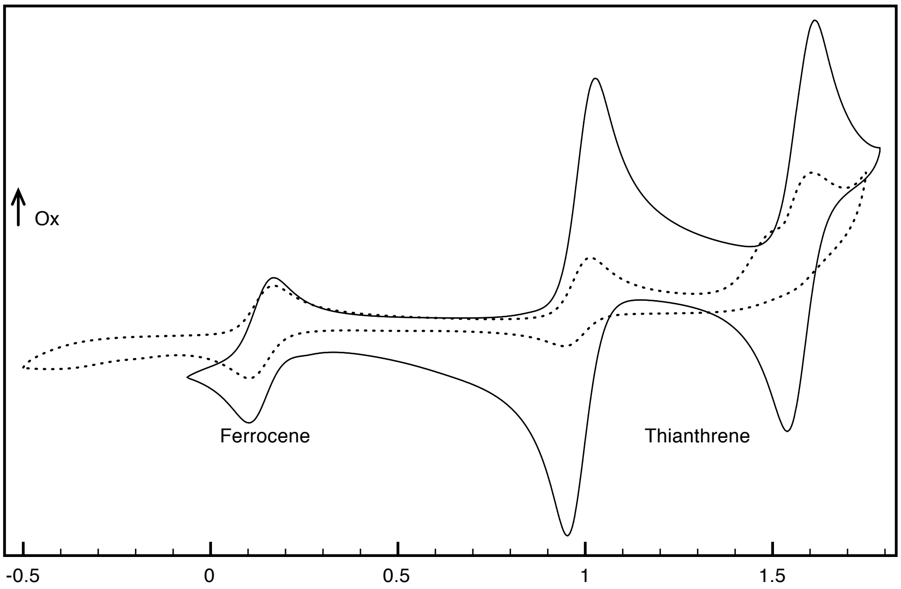

Figure 2.50: Cyclic voltammetry measurements of thianthrene in liquid SO_2 (continuous line) and in acetonitrile (dotted line) as well. Average of 5 scans at room temperature with ferrocene (Fc/Fc^+) as the reference redox system.

ture up to 40 °C. Since no reliable reference electrode is available for liquid SO_2 as the solvent, a solid state quasi-reference electrode[80] was constructed. To increase the reliability of the measurement results, an internal reference redox system,[81] ferrocene/ferrocenium (Fc/Fc^+), was added to the solution. The results are shown in Figures 2.49 and 2.50. Experimental parameters are thianthrene (5 mg, 0.023 mmol) in liquid SO_2 or in acetonitrile (10 ml, at RT). Working and counter electrodes are made of Pt (1.65 mm^2 surface area), the quasi-reference electrode is a home made Pt/polypyrrole,[80] and $[Bu_4N][PF_6]$ (968.6 mg, 2.5 mmol) is used as the electrolyte.

Fig. 2.49 shows that the first as well as the second redox potential of thianthrene shifted to the higher values on the increase of temperature. Additionally, the measured currents also varied with the temperature. The shift is in line with the Nernst Equation, $E = E^\circ + RT/zF \cdot ln(a_{Ox}/a_{Red})$, where temperature, T, and potential, E, are linearly correlated, whereas the increase of current is in line with the Cottrell Equation, $I = (nFA\sqrt{Dc*})/(\sqrt{\pi t})$, where viscosity, D, is linearly correlated with the current, I.[82] However, the shift of redox potential of TA in liquid SO_2 is only less than 0.1 V, in the range from -63 °C to room temperature, which can be considered as insignificant.

The measurement in the presence of internal reference redox system reveals the oxidation potential of thianthrene to be maintained in liquid SO_2. Each oxidation wave is followed by a similar magnitude of reduction current indicating that no irreversible reaction occurred in the system during the measurement. In separate experiments with acetonitrile, similar value has been found, 0.86 V. Fig. 2.50 shows both results to be coincident. The smaller current at the reduction wave in acetonitrile is probably caused by the reaction of the oxidized species with a water impurity.

Chapter 3

General Discussion

Most compounds obtained in the presented work are correlated in their properties and/or in the synthesis reactions. For these reasons, it is of importance to discuss the correlations separately, across the structures. The following discussion involves nine compounds: $[Ag_2(TA)_2][BF_4]_2 \cdot 3\,SO_2$ (**1**), $[Ag_2(TA)_3][SbF_6]_2 \cdot 5\,SO_2$ (**2**), $[AuCl_2(TA)_2]\,[AuCl_4]$ (**3**), $[AlCl_3TA]$ (**4**), $(TA^{\cdot})(HSO_4) \cdot H_2SO_4$ (**5**), $(TA^{\cdot})[FeCl_4]$ (**6**), $(TA)_3[Al_2Cl_7]_2$ (**7**), $SAO(HSO_4)_2$ (**9**) and $(SA^{\cdot})_2[SO_4(BF_3)_2]$ (**10**).

3.1 The solvent influence

The new complexes, **1** and **2**, are the first thianthrene complexes containing two metal atoms for each thianthrene ligand. The formation of these complexes is obviously influenced by the solvent used and, additionally, the counter ion chosen. All described thianthrene complexes in the literature were prepared using common organic solvents and the resulting metal complexes have the metal to ligand ratio of 1:1 up to 1:3. However, the bonding between the metal atom and thianthrene can only be ascertained by a crystallographic structure determination. Bis(μ-η^2-thianthrene)disilver(I) bis(perchlorate)[23] is an example of an unexpected coordination configuration of a complex with 1:1 metal to ligand ratio. Instead of exclusive coordination of the metal ion by S atoms, two C atoms of the benzene rings are also bound. Furthermore, the strong bond between the perchlorate molecule and the metal ion seems to reduce the available left space and hinder further $Ag^{+}\cdots TA$ interactions.

In fact, the stronger the folding of the thianthrene molecule the more space for the donor atoms of the ligand is available, giving the thianthrene a higher probability to bind two metal ions. However, the direction of the lone pair of the S atoms causes the configuration of the molecule to be in the opposite tendency. In the structure of bis(μ-η^2-thianthrene)disilver(I) bis(perchlorate),[23] where both S atoms simultaneously bind one metal ion, the folding of TA become slightly stronger with a dihedral angle of 126°, whereas in **1** and **2** the folding is weaker and the ligand molecules have, in average, a wider dihedral angle of about 132°. This suggests that in the reaction process, surrounded by SO_2 molecules, the attraction between Ag and S atoms is stronger than the repulsive force between the two cations and hence flattening of the thianthrene molecule occurs. The structure of **2** is very interesting, because the thianthrene ligands in the complex are therefore in the optimum distance to each other.

The obvious increase of the number of ligands for each metal ion on going from the common organic solvents to liquified SO_2 also occurs with the gold(III) complex. The weakly coordinating solvent accentuates the tendency of thianthrene to bind to the metal ion and finally a gold(III) complex with two coordinated thianthrene ligands precipitates. In comparison with the neutral complex prepared in acetonitrile,[9] liquid SO_2 increases the number of S atoms coordinated to Au^{3+}. Two metal ions on one TA molecule or a bidentate action of the ligand cannot be expected in the reaction with gold(III). Two closely bound metal ion arrangement as in the structure of **1** and **2** would cause a high cation–cation repulsion while exclusive coordination with only S atoms would not be stable since the charge density of Au^{3+} ion is too high to be compensated by TA only, therefore at least two covalent Au–Cl bonds are preserved.

Surprisingly, supported by its molecular arrangement, **3**, which consists of a cation and an anion complexes of gold(III), exhibits a valuable feature: a remarkable high electrical conductivity. At first glance, the salt-like character does not imply such behavior. Another advantageous feature of the gold complex over the previously invented neutral complex[9] is that **3** has no solvate molecule in the structure and with the exception of its hygroscopic nature it is stable in open atmosphere for weeks.

3.2 The oxidation reaction in liquid SO_2

The experimental results described in subsection 2.4.3 (p. 101) show the same color change behavior of thianthrene on oxidation in liquid SO_2 as it does in common organic solvents or in concentrated H_2SO_4. The liquid SO_2 solution of thianthrene cation radicals is pink at room temperature, and turns green to blue on dimerization at low temperature. While thianthrene dissolves in the common organic solvents as a colorless solution, the neutral molecule in liquid SO_2 is yellow.

The immediate pink coloration of the solution is an obvious sign of an oxidative process in the reaction involving thianthrene in the preparations of **1** and **2**. The more severe effect occurred in the preparations of **9** and **10** with the precipitation of oxidized selenanthrene molecules, although the silver salts used in those reactions were not oxidizing agents, because the precipitation of metallic silver was never observed. These incidents imply that the liquid SO_2 used for those reactions was contaminated with an oxidizing agent, which is most probably SO_3. Fig. A.1 confirms this conclusion. Did $AgNO_3$ oxidize thianthrene in the preparation of **5**? Since no precipitation of metallic silver was detected from the reaction using the purest available liquid SO_2, and no pink coloration occurred, the role of $AgNO_3$ in the reaction cannot be assigned. Anyway, neither Ag^+ nor NO_3^- were incorporated into the structure of **5**.

In the view of fact that **9** and **10** were obtained and no such structure for thianthrene, it can be inferred that selenanthrene is more easily oxidized than thianthrene.

3.3 The reaction with aluminum chloride

3.3.1 What oxidizes thianthrene?

A question arises from the experimental observations: why is thianthrene oxidized in the presence of aluminum chloride and not in the presence of gold(III) chloride?

The literature shows that thianthrene is oxidized in methylenechloride in the presence of aluminum chloride. An interpretation was given to this phenomenon, it was that the mixture of CH_2Cl_2 and $AlCl_3$ is strongly oxidizing with a potential of 1.6 V.[83] Considering the results from this work, this argument can be ignored since no reduction product of SO_2 – in form of dithionite – was found in the reaction between TA and $AlCl_3$ in liquid SO_2. Furthermore, the oxidation even occurs without solvent, in pre-evacuated ampoules.

The reaction between TA and $AlCl_3$ in liquid SO_2 seems to be quite similar to that in an ampoule without solvent. Liquid SO_2 can easily be released from the reaction vessel to obtain the solid reaction products for further experiments. The solid was examined for its dithionite content as the possible reduction product of SO_2. The qualitative analyses were done on a series of pre-concentrated samples with Raman spectrometry in addition to the conventional dithionite test,[75] and the results were all negative. These results confirm that two out of the three reaction components are non-oxidizing. It means, TA did not reduce any other reactant to be oxidized but underwent disproportionation, as the only possibility, in the presence of aluminum chloride. The low-coordinating solvent did not show any significant role in the redox process other than dissolving both reactants.

Since no thianthrenium radical ions occur in the preparation of **3**, it is unclear whether $FeCl_3$ oxidized thianthrene in the preparation of **6** or thianthrene was catalyzed by the Lewis acidic salt to oxidize itself. There is not enough information available in the literature to explain the nature of the reaction process between TA and a Lewis-acid in liquid SO_2.

3.3.2 A suggestion for the reaction mechanism

The reaction between TA and aluminum chloride is partly revealed. There was no dithionite detected in the reaction in liquid SO_2. The solid residue reacted with lead(II) acetate solution to give a dark precipitation. This observation is in agreement with the gas evolution which occurred in the opened ampoule after the reaction. The experiments to find any other reaction product by mass spectrometry resulted in spectra whith no significant difference to that of pure TA except the slight increase of the signal of $C_{12}H_8S$. Therefore, the only reactants are both starting materials and the so far identified products are **4**, **7**, the known thianthrene radical cation tetrachloridoaluminate,[9] hydrolyzable sulfide compound (see 2.4.1, *Reaction with Pb(II) acetate solution*, p. 94), and the yellow polygonal crystals (see 2.1.4, p. 40). Two possible sulfide compounds are known, Al_2S_3 and AlSCl. The latter is more likely to occur in this reaction, in line with the fact that AlSCl hydrolyzes in the presence of water to release H_2S. Finally, the complete reaction is proposed to follow the reaction equation 3.1.

$$8\,\mathrm{TA} + 9\,\mathrm{AlCl_3} \longrightarrow (\mathrm{TA})_3[\mathrm{Al_2Cl_7}]_2 + (\mathrm{TA})_2[\mathrm{AlCl_4}]_2 + [\mathrm{AlCl_3TA}] + 2\,\mathrm{AlSCl} + 2\,\mathrm{C_{12}H_8S} \tag{3.1}$$

No experiments has been performed to detect the existence, nor to confirm the structure of $C_{12}H_8S$. The last term in the reaction equation is only as a consequence of the stoichiometry, but the respective mass is always detectable with mass spectrometry as the second intensive line of the purified TA analysis as well as of the *extracted reaction products.* This should account for the so far unidentified yellow polygonal thin crystals in the ampoules. In the ampoule experiments, the thianthreniumyl dimer,[9] $(TA^+)_2$, is only a minor whereas in liquid SO_2 it is the major product. On the other hand, **4** and **7** are not observable in the reaction in liquid SO_2 but they are easily formed in the reaction without solvent.

In the reaction in liquid SO_2 a weight increase of the reaction products was observed through gravimetric analysis. However, the embedment of SO_2 molecules in reaction product remains unknown and hence, it is not included in the reaction equation above.

From the experimental observation one can conclude that the intermediate product of the reaction between thianthrene and aluminum chloride is **4** (equation 3.2). The two thianthreniumyl compounds, $(TA^{\cdot})_2[AlCl_4]_2$ and **7**, are formed in subsequent processes according to the tentative reaction equations 3.3 and 3.4, respectively. In liquid SO_2 **4** and **7** do not appear apparently, because of their high solubility.

$$\mathrm{TA} + \mathrm{AlCl_3} \longrightarrow [\mathrm{AlCl_3TA}] \tag{3.2}$$

$$3\,[\mathrm{AlCl_3TA}] \longrightarrow (\mathrm{TA}^{\cdot})_2[\mathrm{AlCl_4}]_2 + \mathrm{AlSCl} + \mathrm{C_{12}H_8S} \tag{3.3}$$

$$4\,[\mathrm{AlCl_3TA}] + \mathrm{AlCl_3} \longrightarrow (\mathrm{TA})_3[\mathrm{Al_2Cl_7}]_2 + \mathrm{AlSCl} + \mathrm{C_{12}H_8S} \tag{3.4}$$

The blue to violet color, appearing on mixing thianthrene and aluminum chloride is associated with the thianthreniumyl. In the solid state the thianthreniumyl molecules always form pairs.

3.4 Electrical conductivity

The chain-like arrangement of the cationic complexes $[AuCl_2(TA)_2]$ in the structure of **3** may be the reason why the compound is semi-conducting. Gold(III) can be reduced to Au(I) and both TA ligands in the coordination complex can be oxidized to the radical cation. This intra-molecular electron transfer would allow electrons to become mobile within the molecule. The process of the electron jump from a thianthrene ligand of one cation to the other thianthrene of the next cationic complex is probable, via the pairing of thianthrene radicals.

However, the pairing of thianthrene radical cations, so far, involves the central part of the molecules, the dithiin ring. According to a theoretical work both interactions are possible, with either the S$\cdots$S axes parallel or the S$\cdots$S axes orthogonal to each other.[34] Interestingly, the close TA$\cdots$TA arrangement of neighboring complex cations in **3** is almost identical to that in **4**. In both structures, the dithiin ring of thianthrene of one complex faces the benzene ring of thianthrene of the neighboring complex. The dihedral angles between the best planes of the two rings are close to parallel alignment, 5.96° and 2.22° in the structures of **3** and **4**, respectively. The slippage of adjacent thianthrene molecules from a perfect dithiin$\cdots$dithiin 'face-to-face' arrangement is a barrier for strong interaction as soon as the molecules are oxidized.

Another barrier for the ideal pairing of the thianthreniumyl molecules in **3** and **4** in the conduction process is that thianthrene flattens on oxidation. This would continuously change almost all atomic positions of both thianthrene molecules in form of vibrations, which means a high energy requiring movement. These two barriers, the slightly slipped dithiin$\cdots$dithiin arrangement and the impossibility of flattening for the TA molecule in the crystals, are unlikely to be overcome by the heat supplied during the electrical conductivity measurement, since no endothermic effect was observed from the DSC curve in the temperature range. However, the conductivity of the compound was substantially increased at higher temperature. This fact implies an interaction of other type that allows TA$\cdots$TA electrons transfer, which is presently unknown.

Especially for **4**, there is another obstacle for the conductivity. The electrons are not able to move across the $-\mathrm{AlCl}_3\cdots\mathrm{Cl}_3\mathrm{Al}-$ intermolecular interaction of which the shortest distance amounts to 3.7 Å, slightly bigger than the sum of van der Waals radii of two Cl atoms. Concerning the low activation energy for both compounds, no clear mechanism on the electrons transfer can be given.

The thermal activation energy of semiconducting materials corresponds to the band gap between the conduction and the valence bands. Electron can be exited to the conduction band and this process is accompanied by the absorption of light. Thus, small gap semiconductor generally are dark colored. The black color of compound **3** is in line with the semiconducting behavior. The transparent, colorless compound **4** is expected to have a large activation energy for the electrical conduction process. The actual activation energy of only 0.8 eV is therefore inconsistent with the colorless appearance of the compound. There is presently no explanation for this discrepancy.

Chapter 4

Summary

Thianthrene (TA) is a synthetic heterocyclic compound which was firstly reported in 1869. On oxidation the TA molecule, which is bent at the S$\cdots$S axis in its neutral form, flattens and changes its color. The pink and violet color of the oxidized species are associated with the thianthrene radical cation and the pair of the radicals, respectively. The large amount of literature reports about the oxidation of thianthrene is indicating the ease of the reaction.

Apart form the results of this work, there are only two compounds with crystallographically determined structures bearing thianthrene as a ligand available in the literature: thianthrene-gold(III)chloride[17] and bis(μ-η^2-thianthrene)disilver(I) bis(perchlorate),[23] both were prepared in common organic solvents. The thianthrene ligand of both structures is in its neutral form. Besides the two complexes of neutral thianthrene, there are also two crystallographic structures containing oxidized thianthrene, thianthrenium tetrachloridoaluminate[9] and tris(thianthrene)(2+) bis(dodecamethylcarba–*closo*–dodecaborate) di-chloromethane tetrasolvate,[34] which were also prepared in usual solvents.

There is a lack of literature concerning the reactions of thianthrene in liquid SO_2, probably because thianthrene had been reported erroneously to be insoluble in the solvent.[53] The experimental results obtained during this work show that thianthrene is well soluble in liquid SO_2 at room temperature giving a bright yellow colored solution. Selenanthrene, the heavier homologue of thianthrene, also dissolves in liquid SO_2 giving the same bright yellow colored solution.

In the present work, reactions in liquid SO_2 were performed in pressure-tight reaction vessels at room temperature. The reactants were placed in different branches of the vessels and the reaction was done by mixing both solutions. The crystalline products which precipitated from the solution were selected under inert conditions with the cold oil method to be investigated by X-ray diffractometry. Several experiments of the reaction between TA and $AlCl_3$ were done in pre-evacuated ampoules, at 100 °C. The reactants were filled into the ampoule in an argon-filled glove box. The resulting products which are adhered on the wall of the ampoule were selected under inert conditions at room temperature.

To study the reaction between TA and $AlCl_3$, qualitative analyses were conducted, including sulfide and dithionite detection, mass spectrometry, NMR spectrometry and Raman spectrometry. Products of the reactions performed in this work, which are stable in ambient pressure and temperature, were characterized for their electrical conductivity. The method used was the conventional two electrodes technique. The resulting conductivity values were evaluated using the Arrhenius equation to calculate the thermal activation energy. To study the redox properties of thianthrene in liquid SO_2, cyclic voltammetry was used. The experiments were done in a self-constructed pressure tight vessel equipped with pressure tight electrodes, at temperatures up to 25 °C.

The reactions performed in liquid SO_2 between TA and silver salts, AgX (X = BF_4^-, SbF_6^-), resulted in two new complexes, $[Ag_2(TA)_2][BF_4]_2 \cdot 3\,SO_2$, (**1**), and $[Ag_2(TA)_3][SbF_6]_2 \cdot 5\,SO_2$, (**2**). The reaction with gold(III) chloride provided the complex salt $[AuCl_2(TA)_2][AuCl_4]$, (**3**). Besides these complexes containing neutral TA

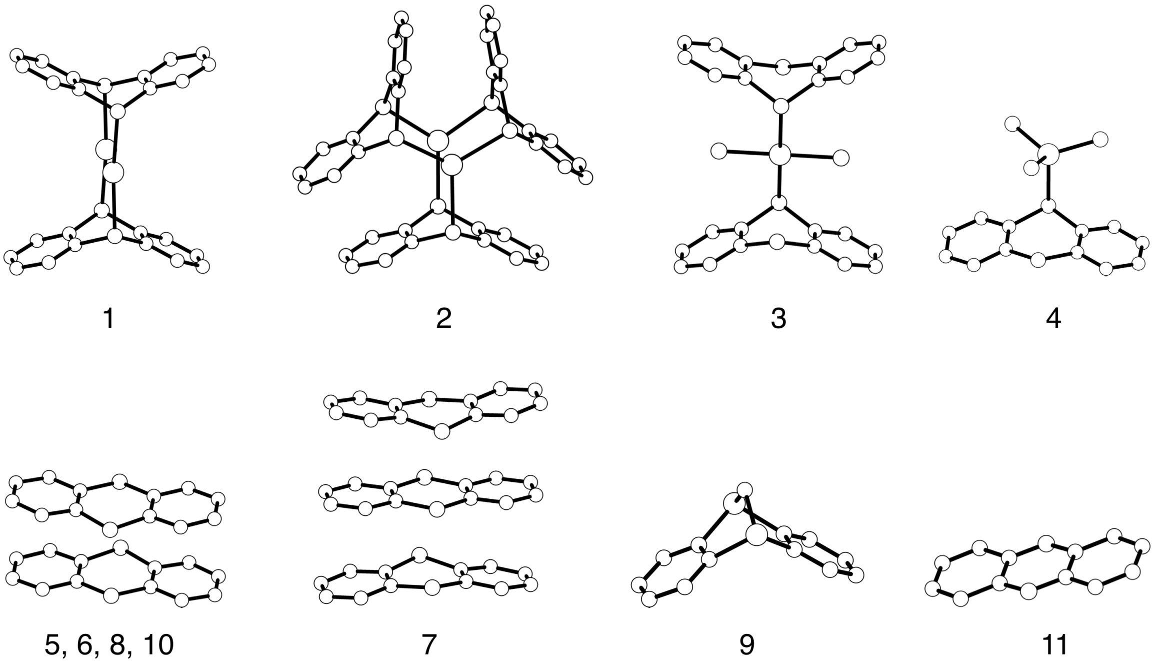

Figure 4.1: Molecular entities present in the crystal structures of (**1**): dinuclear complex cation $[Ag_2(TA)_2]^{2+}$ in $[Ag_2(TA)_2][BF_4]_2 \cdot 3\,SO_2$, (**2**): dinuclear complex cation $[Ag_2(TA)_3]^{2+}$ in $[Ag_2(TA)_3][SbF_6]_2 \cdot 5\,SO_2$, (**3**): complex cation $[AuCl_2(TA)_2]^+$ in $[AuCl_2(TA)_2][AuCl_4]$, (**4**): neutral complex $[AlCl_3TA]$, (**5**, **6**, **8**, **10**): radical cation pair $(TA^{\cdot+})_2$ in $(TA^{\cdot})(HSO_4) \cdot H_2SO_4$, $(TA^{\cdot})[FeCl_4]$ and $(SA^{\cdot+})_2$ in $(SA^{\cdot})[AlCl_4]$ and $(SA^{\cdot})_2[SO_4(BF_3)_2]$, (**7**): stacked trimer $(TA)_3^{2+}$ in $(TA_3)[Al_2Cl_7]_2$, (**9**): μ-oxy-selenanthrene(2+) in $SAO(HSO_4)_2$, and (**11**): phenazinediium in $(H_2PAz)(HSO_4)_2$.

as ligand, reactions leading to the formation of the radical cation of thianthrene in form of salts were also performed: $(TA^{\cdot})(HSO_4) \cdot H_2SO_4$ (**5**) as a result from the reaction between TA and $AgNO_3$, and $(TA^{\cdot})[FeCl_4]$ (**6**), from TA and $FeCl_3$. The solid state reaction between TA and $AlCl_3$ without solvent resulted in the neutral complex $[AlCl_3TA]$ (**4**) and a "triple decker" structure $(TA_3)[Al_2Cl_7]_2$ (**7**). In addition to these results obtained with thianthrene, four new compounds resulting from reactions involving selenanthrene and phenazine could be isolated: $(SA^{\cdot})[AlCl_4]$ (**8**), $SAO(HSO_4)_2$ (**9**), $(SA^{\cdot})_2[SO_4(BF_3)_2]$ (**10**) and $(H_2PAz)(HSO_4)_2$ (**11**) (Fig. 4.1).

Taking into account the obtained products from the reaction between TA and $AlCl_3$ and the observations of the qualitative analyses, a possible reaction mechanism with a respective reaction equation was set up.

$$8\,\mathrm{TA} + 9\,\mathrm{AlCl_3} \longrightarrow \mathrm{(TA)_3[Al_2Cl_7]_2} + \mathrm{(TA)_2[AlCl_4]_2} + \mathrm{[AlCl_3TA]} + 2\,\mathrm{AlSCl} + 2\,\mathrm{C_{12}H_8S}$$

Liquid SO_2 does not play any role in the oxidation of TA in the presence of $AlCl_3$, since the results from cyclic voltammetry measurements show only an insignificant shift of reduction potential of TA in liquid SO_2 in comparison with that in acetonitrile.

The electrical conductivity measurements show that **3** and **4** are semiconductors with remarkably small activation energies of 0.43 and 0.845 eV, respectively. While the black appearance of **3** is in line with its the electrical properties, the colorless crystals of **4** remains unexplainable.

The following conclusions can be drawn based on the results of the experimental works. (1) Thianthrene coordinates metal ion(s) mainly via S atom(s). (2) The number of S atoms coordinated to the metal ion increases when the reaction is performed in liquid SO_2, in comparison with the reaction performed in common organic solvents. (3) Liquid SO_2 is inert. The oxidation reactions which occur in liquid SO_2 are actually an impact of the oxidant impurities in the solvent or even because of the nature of the dissolved molecule it self in the presence of other compound. (4) Liquid SO_2 does not lower the oxidation potential of thianthrene. (5) Thianthrene undergoes a self-oxidation process in the presence of $AlCl_3$ with or without solvent, putting the previously claimed *one-electron-oxidation-system* $AlCl_3/CH_2Cl_2$[9] in doubt. (6) The old known phenomenon of the violet color resulting from heating dry mixture of thianthrene and $AlCl_3$ is revealed. It originates actually from the paired radicals of thianthrene. (7) The semiconductive nature of thianthrene complexes is remarkable though not completely understood. (8) Selenanthrene is apparently oxidized easier in comparison with thianthrene. (9) The formation of hydrogen bonds involving proton transfer was observed in the structure of phenazinediium hydrosulfate.

Appendix A

Experimental work

A.1 Chemicals

Table A.1: List of chemicals used

Acetonitrile	Riedel-de Haën	refluxed over P_4O_{10}
$AgCF_3SO_3$	Across Organics	used as received
$AgBF_4$	Aldrich	used as received
$AgNO_3$	Aldrich	used as received
$AgSbF_6$	Across Organics	used as received
$AlCl_3$	Fluka	sublimated before use
$AuCl_3$	synthesized	sublimated before use
Bu_4NPF_6	Aldrich	used as received
$FeCl_3$	synthesized	sublimated before use
Ferrocene	Across Organics	used as received
Phenazine	Aldrich	re-crystallized from ethanol
SO_2	Air Product & Praxair (3.8)	stored over P_4O_{10} for at least 3 days
Selenanthrene	synthesized	used as obtained
Thianthrene	Aldrich	re-crystallized from ethanol/toluene

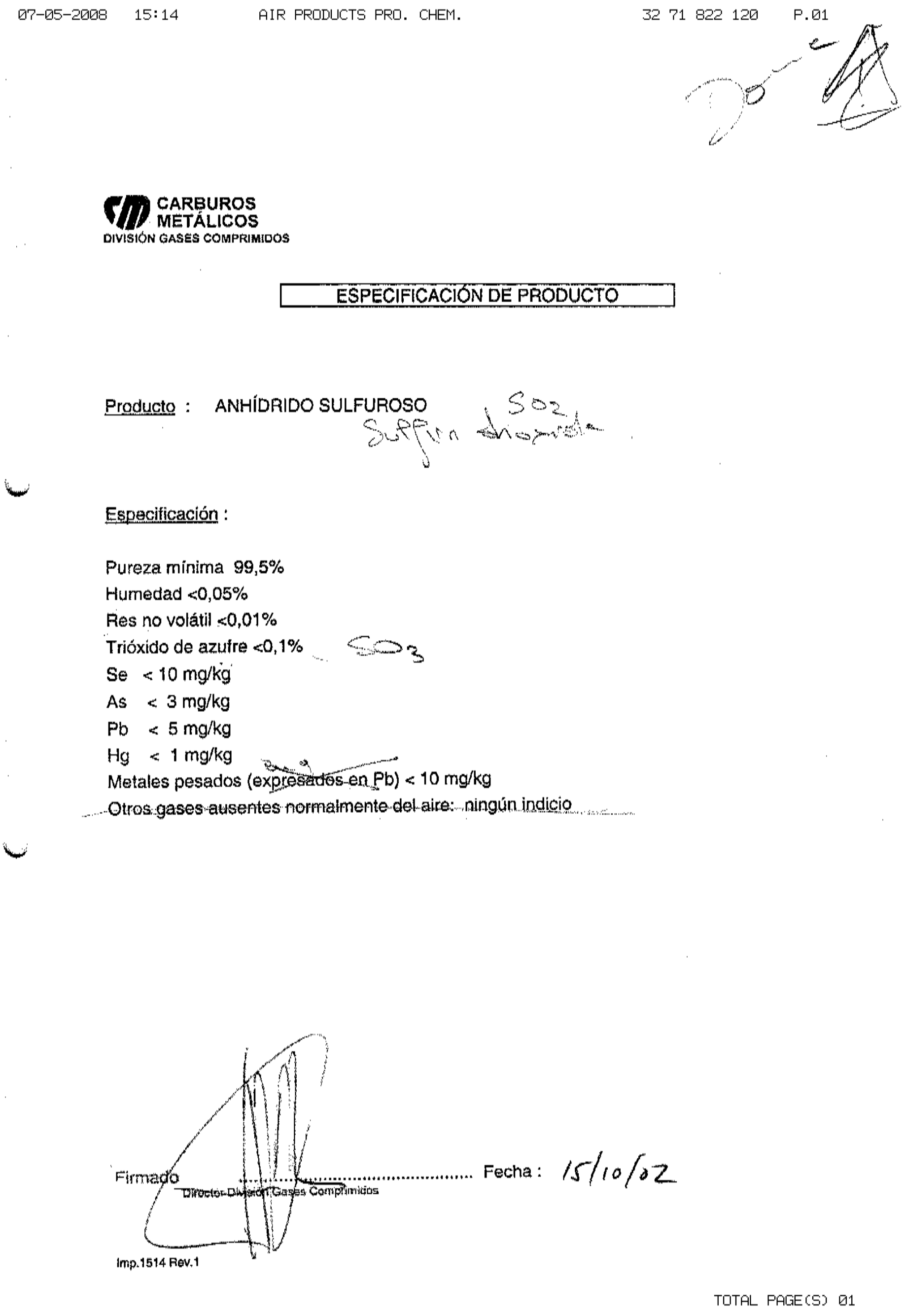

07-05-2008 15:14 AIR PRODUCTS PRO. CHEM. 32 71 822 120 P.01

CARBUROS METÁLICOS
DIVISIÓN GASES COMPRIMIDOS

ESPECIFICACIÓN DE PRODUCTO

Producto : ANHÍDRIDO SULFUROSO SO2
Sulfur dioxide

Especificación :

Pureza mínima 99,5%
Humedad <0,05%
Res no volátil <0,01%
Trióxido de azufre <0,1% SO3
Se < 10 mg/kg
As < 3 mg/kg
Pb < 5 mg/kg
Hg < 1 mg/kg
Metales pesados (expresados en Pb) < 10 mg/kg
Otros gases ausentes normalmente del aire: ningún indicio

Firmado .... Fecha : 15/10/02
Director División Gases Comprimidos

Imp.1514 Rev.1

TOTAL PAGE(S) 01

Figure A.1: Specification of the liquid SO_2 by the supplier AirProducts Inc. The SO_3 content is reported to be less than 0.1%.

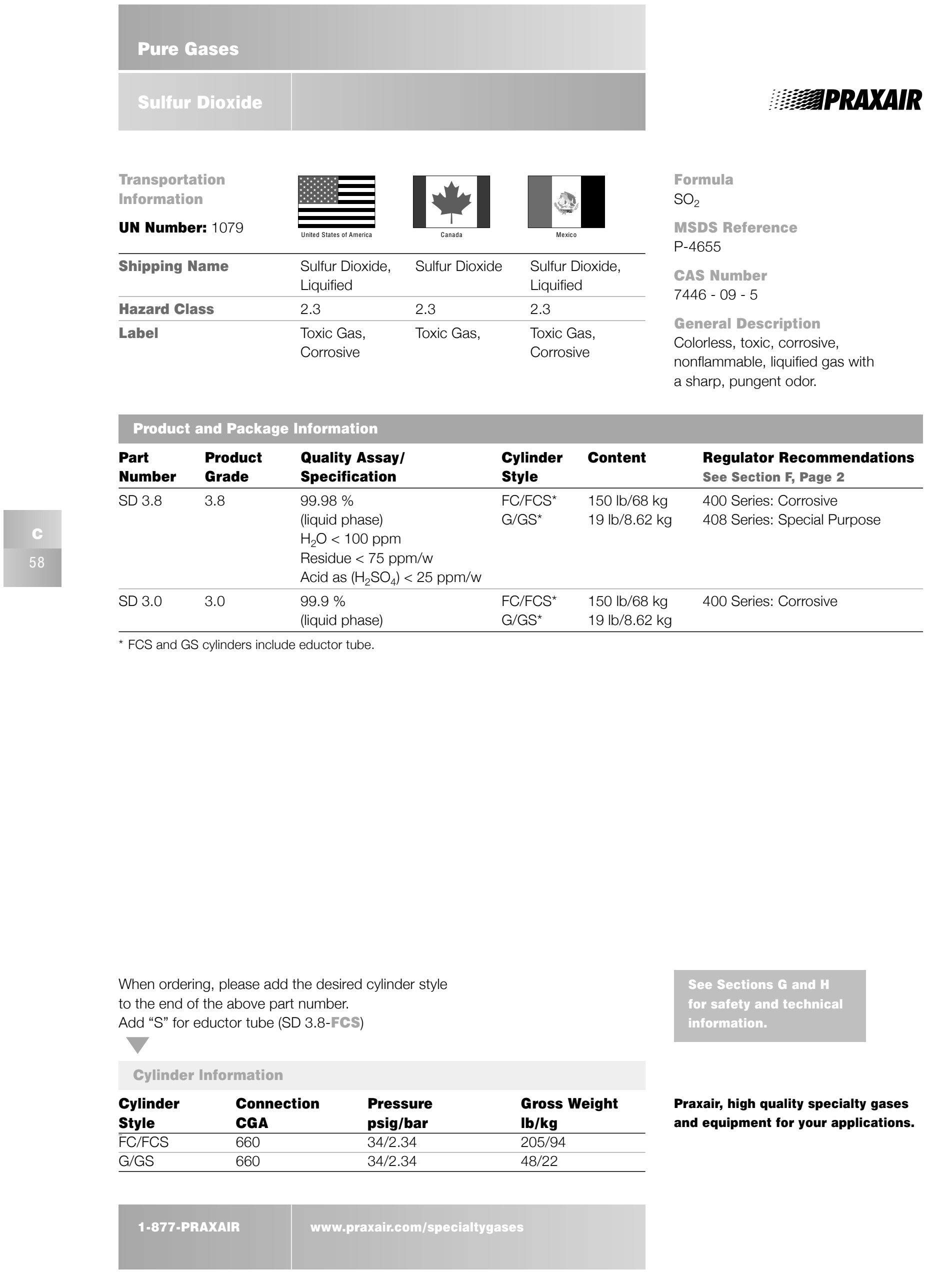

Pure Gases

Sulfur Dioxide

PRAXAIR

Transportation Information

UN Number: 1079

	United States of America	Canada	Mexico
Shipping Name	Sulfur Dioxide, Liquified	Sulfur Dioxide	Sulfur Dioxide, Liquified
Hazard Class	2.3	2.3	2.3
Label	Toxic Gas, Corrosive	Toxic Gas,	Toxic Gas, Corrosive

Formula
SO_2

MSDS Reference
P-4655

CAS Number
7446 - 09 - 5

General Description
Colorless, toxic, corrosive, nonflammable, liquified gas with a sharp, pungent odor.

Product and Package Information

Part Number	Product Grade	Quality Assay/ Specification	Cylinder Style	Content	Regulator Recommendations See Section F, Page 2
SD 3.8	3.8	99.98 % (liquid phase) H_2O < 100 ppm Residue < 75 ppm/w Acid as (H_2SO_4) < 25 ppm/w	FC/FCS* G/GS*	150 lb/68 kg 19 lb/8.62 kg	400 Series: Corrosive 408 Series: Special Purpose
SD 3.0	3.0	99.9 % (liquid phase)	FC/FCS* G/GS*	150 lb/68 kg 19 lb/8.62 kg	400 Series: Corrosive

* FCS and GS cylinders include eductor tube.

C
58

When ordering, please add the desired cylinder style
to the end of the above part number.
Add “S” for eductor tube (SD 3.8-**FCS**)

See Sections G and H for safety and technical information.

Cylinder Information

Cylinder Style	Connection CGA	Pressure psig/bar	Gross Weight lb/kg
FC/FCS	660	34/2.34	205/94
G/GS	660	34/2.34	48/22

Praxair, high quality specialty gases and equipment for your applications.

1-877-PRAXAIR **www.praxair.com/specialtygases**

Figure A.2: Specification of the liquid SO_2 by the supplier Praxair Inc. The SO_3 content of the 3.8 grade in form of H_2SO_4 is less than 25 ppm/w.

A.2 Instruments

Table A.2: List of analytical instruments used

Cyclic voltammeter	Metrohm Autolab μ-III
DSC	Netzsch DSC 204 F1 Phoenix
Elemental analyzer	ICP-OES IRIS Advantage, Thermo Jarrel Ash Corporation
FTIR spectrometer	Bruker IFS 113v FTIR spectrometer
Glovebox	labmaster130 mbraun
Manometer	Thermovac TM 20
Microscope	Hund Wetzlar h33
Raman spectrometer	Bruker RFS100 FT-Raman spectrometer
UV-Vis spectrometer	Dr. Gröbel UV-Elektronik GmbH PC-Spectrometer
Vacuum pump	vacuubrand RD4
X-ray diffractometer	Bruker-Nonius Kappa-CCD diffractometer equipped with an Oxford Cryostream cooling device

A.3 Laboratory equipment

A.3.1 Vacuum line installation

For the experimental work vacuum and argon lines were essential. Both were installed as a unity. Argon line installation comprises *an argon gas source, a filter system, and an argon line.* A 99.994% pure argon gas obtainable from the *source* is piped to the *filter system* through a T-connector, of which the third branch is equipped with a flow indicator and a manometer that also acts as a pressure controller. The highest pressure of the source is limited to 0.3 bar. At higher pressure the excess gas is released automatically and the flux of released gas can be seen on the indicator.

The *filter system* consists of a flow indicator and four glass columns (40 cm long and 4 cm diameter) filled with silica gel, potassium hydroxide pellets, molecular sieve, phosphorus pentoxide and titanium sponge in a quartz tube at 600 °C. The glass columns are set vertically and are interconnected as a horizontal serial line. The rough estimation of the argon flow in the filter is seen on the indicator, silica gel traps traces of water, potassium hydroxide retains carbon dioxide impurities, molecular sieve binds water, phosphor pentoxide absorbs the rest of water and the hot titanium metal removes traces of oxygen and nitrogen from the gas. Highly purified argon gas is provided through the system, and piped into the *argon line*.

The vacuum line installation comprises a pressure gauge, cold trap and a vacuum pump. The cold trap is cooled with liquid nitrogen to condense any gas and thus prevents the vacuum pump from losing performance. The vacuum and argon lines are set parallel and interconnected at two points each with a split outlet pipe equipped with two valves. Both outlet ends are ground cuts. As a result, up to two reaction vessels can be connected to the outlets and by regulating the valves the vessels can be evacuated or flushed with argon independently. When a dry reaction vessel is needed, evacuation, heating and flushing are repeated several times before filling in air sensitive compounds in a glove box.

A.3.2 Glove box

The glove box is equipped with airlocks for allowing to bring in and out laboratory devices without degrading the quality of the atmosphere inside. There are laboratory equipments in the working chamber available to manipulation of air sensitive compounds which are used in this work: scale, microscope, micro oven and electrodes for conductivity measurement, and a hot tungsten wire for melting glass. Pressure inside the glove box is kept slightly higher than that of outside atmosphere to make sure that no air, oxygen, or humidity can enter the working chamber.

A.3.3 H-shaped vessel

In most cases, reactions were handled in H-shaped vessels. It consists of two vertical columns, separated by a glass filter in the horizontal connecting line. Each column is closed at the bottom and equipped with Young valve at the top. The other end of the valves are attached with a female NS-14,5/23 cut as a connector to the vacuum line or other glass equipment. The overall volume of the vessel is about 70 mL (Fig. A.3).

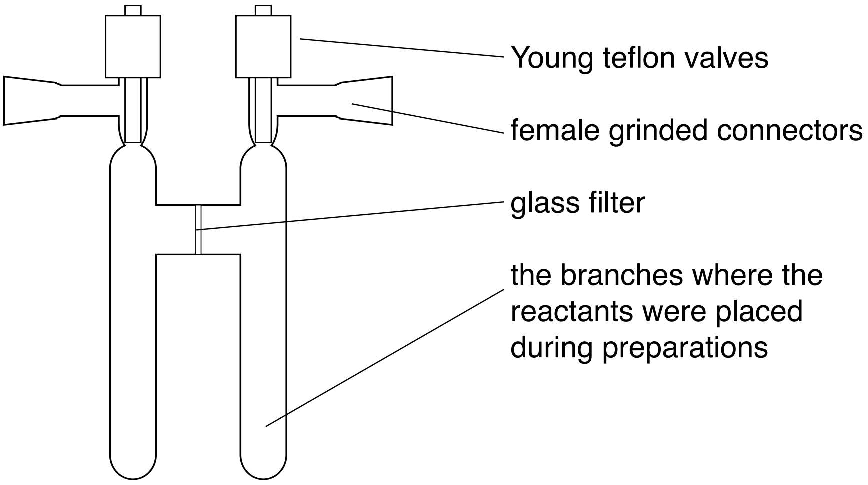
Young teflon valves
female grinded connectors
glass filter
the branches where the reactants were placed during preparations

Figure A.3: Schematic view of the pressure-tight H-shaped reaction vessel.

A.4 Methods

A.4.1 Crystal selection under inert conditions

Crystal selections performed in this experimental work were done under inert conditions with the cold oil method. With this method, crystals containing solvent of

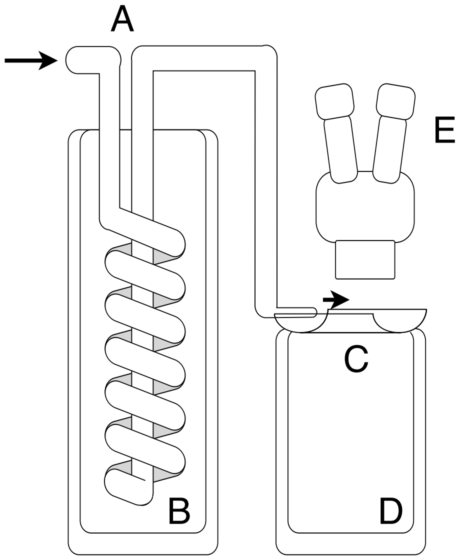

Figure A.4: A schematic view of the equipment for single crystal selection under inert conditions at low temperature. (A) Metal pipe, (B) large Dewar flask, (C) concave glass dish, (D) short Dewar flask and (E) microscope. The Dewar flasks are filled with liquid nitrogen. Arrows show the flow of the nitrogen gas.

crystallization with high vapor pressure (e.g. SO_2) can be preserved and securely selected for X-ray diffraction measurements. The first step is to transfer the crystal from a cooled H-shaped vessel with long metal spoon quickly onto a dish of a concave glass containing perfluorinated oil. The oil is isolated from open air with a continuous stream of cold nitrogen gas. The nitrogen gas flows according to the small arrow in Fig. A.4 into a metal pipe immersed in liquid nitrogen inside a Dewar flask. The cold nitrogen stream coming out of the pipe simultaneously cools and protects the crystals on the glass dish from open air. The crystals generally remain unchanged in drops of fluorinated oil for a considerable long duration. The concave glass dish is kept cold on top of another Dewar flask filled with liquid nitrogen. The crystal selection is performed with the help of a microscope.

The selected single crystal is picked up with a glass needle and stored inside liquid nitrogen in a small Dewar flask during transport to the X-ray diffractometer.

A.4.2 Electrical conductivity measurements

The electrical conductivity measurements were performed using conventional two electrodes technique. The sample was placed in a 30 mm long quartz tube with outer and inner diameter of 4.05 and 2.0 mm respectively, and was pressed manually between the electrodes, made of stainless steel, from opposite directions. Both electrodes were held by two metal springs to keep the sample under constant static pressure in the middle of the quartz tube. The disc shaped samples had a thickness of 0.70 mm. Variation of temperature was done using a cylindrical micro-oven equipped with a thermocouple as a temperature sensor. The length and the outer diameter of the micro oven are 24 mm and 15 mm respectively. The central hole for the quartz tube with the sample had an inner diameter of 4.10 mm. The measured values were evaluated using the Arrhenius equation, $\sigma = \sigma_0 \cdot \mathrm{e}^{-E/(kT)}$. Applying natural logarithm to both side give ln σ = ln σ_0 - E/(kT), and x = 1/T, y = ln(σ), A = ln σ_0 and B = -E/k for the linear regression line y = A + Bx. The Boltzmann constant is 8.617343×10^{-5} eVK^{-1}.

A.4.3 Electrochemical technique

The pressure tight-electrodes used in this work were home-made. Each is composed of platinum wire of diameter 0.3 mm and about 4 cm long, platinum rod of diameter 1.45 mm and 1 cm long, 30 cm long insulated copper cable, elastic Teflon tube and a 4 mm diameter glass tube. The platinum rod is melted at one end to make it round and bigger as seen on Fig. A.5, and the platinum wire is attached at the other end of the rod. The wire is soldered to the copper cable. This connection is inserted into the glass tube, the Teflon tube is positioned between the metal and the glass. The seal is tightened with the elastic Teflon tube by pressing the metal into the glass pipe. The whole glass tube is then inserted through a hole drilled along the axis in the middle of the Young Teflon cock. In this work, the platinum opening at the end of the glass

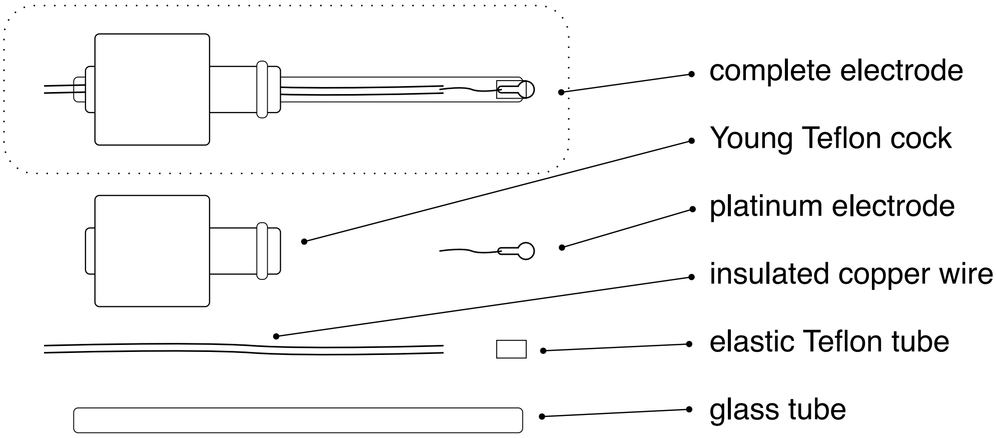
complete electrode
Young Teflon cock
platinum electrode
insulated copper wire
elastic Teflon tube
glass tube

Figure A.5: Schematic view of the components of the home made–pressure tight–electrode.

tube had a surface area of 1,65 mm^2 and was used as the working electrode. The counter electrode is identical to the working electrode.

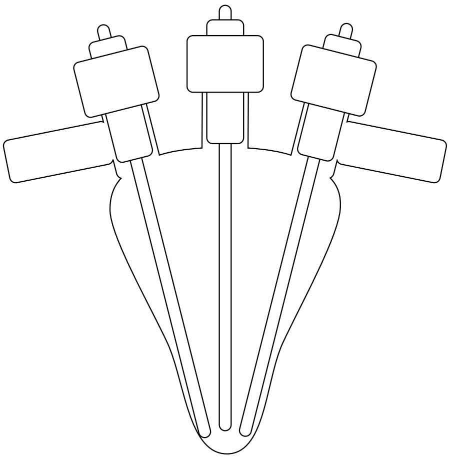

Figure A.6: Schematic view of the voltammetry cell.

For the reference electrode the same construction was also used, but additionally, conductive polymer[84] was layered onto the opening metal surface. The preparation of the polypyrrole layer for the electrode followed that described in literature.[80] The three electrodes are arranged as seen in Fig. A.6. The cell can hold the equilibrium pressure of liquid SO_2 at least until 40 °C, which corresponds to 6.2 bars.

Appendix B

Software

Table B.1: List of software used

MacOS X 10.4.11	Mac operating system
Microsoft Windows 2000	PC operating system
iWork 8 (Pages 3.0.2)	page layout editor for Mac
TeXShop 2.18	$\LaTeX\ 2_\varepsilon$ program for Mac
BibDesk 1.3.19 (1329)	reference manager program for Mac
Plot 0.997	plotting program
Microsoft Word	word processor application program
Microsoft Excel	spreadsheet application program
Inkscape 0.46-3	vector graphic program
Diamond 3.1f	chemical structure visualization program
Mercury 1.4.2 (build 2)	chemical structure visualization program
EasyChem 0.6	chemical formula structure editor
WinGX 1.70.01[85]	crystallographic packet program
Platon[86]	crystallographic packet program
Shelx-97[87]	crystal structure solution & refinement program
SciFinder	literature database
CCDC	chemical structure database
ICSD	chemical structure database

Bibliography

(1) Stenhouse, J. *Proceedings of the Royal Society of London* **1868**, *17*, 62–67.

(2) Graebe, C. *Justus Liebigs Annalen der Chemie* **1875**, *179*, 178–183.

(3) Krafft, F.; Lyons, R. E. *Berichte der deutschen chemischen Gesellschaft* **1896**, *29*, 435–442.

(4) Breslow, D. S.; Skolnik, H. In *The Chemistry of Heterocyclic Compounds*; John Willey & Sons., 1966; Vol. 21, Chapter 12, pp 1155–1228.

(5) Schönenberg, A.; Mustafa, A. *Journal of the Chemical Society (Resumed)* **1949**, 889–892.

(6) Larson, S. B.; Simonsen, S. H.; Martin, G. E.; Smith, K.; Puig-Torres, S. *Acta Crystallographica Section C* **1984**, *40*, 103–106.

(7) Schaefer, T.; Sebastian, R.; Beaulieu, C. *Canadian Journal of Chemistry* **1991**, *69*, 927.

(8) Amato, M. E.; Grassi, A.; Irgolic, K. J.; Pappalardo, G. C.; Radics, L. *Organometallics* **1993**, *12*, 775–780.

(9) Bock, H.; Rauschenbach, A.; Näther, C.; Kleine, M.; Havlas, Z. *Chemische Berichte* **1994**, *127*, 2043–2049.

(10) Mastryukov, V. S.; Chen, K.-H.; Simonsen, S. H.; Allinger, N. L.; Boggs, J. E. *Journal of Molecular Structure* **1997**, *413–414*, 1–12.

(11) Ito, A.; Ino, H.; Ichiki, H.; Tanaka, K. *Journal of Physical Chemistry A* **2002**, *106*, 8716–8720.

(12) Kim, S.; Kwon, Y.; Lee, J.-P.; Choi, S.-Y.; Choo, J. *Journal of Molecular Structure* **2003**, *655*, 451–458.

(13) de Vondele, J. V.; Lynden-Bell, R.; Meijer, E. J.; Sprik, M. *Journal of Physical Chemistry B* **2006**, *110*, 3614–3623.

(14) Joule, J. A. *Advances in Heterocyclic Chemistry* **1990**, *48*, 301–393.

(15) Hosoya, S. *Acta Crystallographica* **1963**, *16*, 310–312.

(16) Kacholdt, H.; Berges, P.; Klar, G.; Hinrichs, W. *Transition Metal Chemistry* **1987**, *12*, 515–520.

(17) Alcock, N. W.; Ang, K. P.; Mok, K. F.; Tan, S. F. *Acta Crystallographica Section B* **1978**, *34*, 3364–3366.

(18) Miles, M. G.; Wilson, J. D. *Inorganic Chemistry* **1975**, *14*, 2357–2360.

(19) Kwik, W.-L.; Tan, S.-F. *Journal of the Chemical Society and Dalton Transactions* **1976**, 1072–1075.

(20) Root, M. J.; Deutsch, E. *Inorganic Chemistry* **1985**, *24*, 1464–1471.

(21) Tan, S.-F.; Kwik, W.-L.; Ang, K.-P. *Journal of the Less-Common Metals* **1980**, *75*, 29–35.

(22) Hill, Z. D.; MacCarthy, P. *Journal of Chemical Education* **1986**, *63*, 162–167.

(23) Munakata, M.; Yan, S. G.; Ino, I.; Kuroda-Sowa, T.; Maekawa, M.; Suenaga, Y. *Inorganica Chimica Acta* **1998**, *271*, 145–150.

(24) Hirshon, J. M.; Gardner, D. M.; Fraenkel, G. K. *Journal of the American Chemical Society* **1953**, *75*, 4115.

(25) Shine, H. J.; Piette, L. *Journal of the American Chemical Society* **1962**, *34*, 4798–4806.

(26) Kinoshita, M.; Akamatu, H. *Bulletin of the Chemical Society of Japan* **1962**, *35*, 1040–1041.

(27) Bock, H.; Rauschenbach, A.; Ruppert, K.; Havlas, Z. *Angewandte Chemie Intenational Edition* **1991**, *30*, 714–716.

(28) Hinrichs, W.; Berges, P.; Klar, G. *Zeitschrift für Naturforschung, B* **1986**, *41*, 1133–1141.

(29) Hinrichs, W.; Berges, P.; Klar, G. *Zeitschrift für Naturforschung, B* **1987**, *42*, 169–176.

(30) Glass, R. S. In *Organosulfur Chemistry II*; Springer Berlin / Heidelberg, 1999; Vol. 205, Chapter Sulfur Radical Cations, pp 1–87.

(31) Tinker, L. A.; Bard, A. J. *Journal of the American Chemical Society* **1979**, *101*, 2316.

(32) Rapta, P.; Kress, L.; Hapiot, P.; Dunsch, L. *Physical Chemistry Chemical Physics* **2002**, *4*, 4181–4185.

(33) Hübler, P.; Heinze, J. *Berichte der Bunsengesellschaft für Physikalische Chemieer Bunsengesellschaft Für Physikalische Chemie* **1998**, *102*, 1506–1509.

(34) Rosokha, S. V.; Lu, J.; Rosokha, T. Y.; Kochi, J. K. *Acta Crystallographica Section C* **2007**, *63*, o347–o349.

(35) Fava, A.; Sogo, P. B.; Calvin, M. *Journal of the American Chemical Society* **1957**, *75*, 1078–1083.

(36) Sato, Y.; Kinoshita, M.; Sano, M.; Akamatu, H. *Bulletin of the Chemical Society of Japan* **1967**, *40*, 2539.

(37) Balch, A. L.; Cornman, C. R.; Latos-Grażyński, L.; Olmstead, M. M. *Journal of the American Chemical Society* **1990**, *112*, 7552–7558.

(38) Kuratsu, M.; Suzuki, S.; Kozaki, M.; Shiomi, D.; Sato, K. *Inorganic Chemistry* **2007**, *46*, 10153–10157.

(39) Hammerich, O.; Parker, V. D. *Electrochimica Acta* **1973**, *18*, 537–541.

(40) Murata, Y.; Hughes, L.; Shine, H. J. *Inorganic and Nuclear Chemistry Letters* **1968**, *4*, 573–576.

(41) Rundel, W.; Scheffler, K. *Tetrahedron Letters* **1963**, 993–995.

(42) Lucken, E. A. C. *Journal of the Chemical Society* **1962**, 4963.

(43) Boduszek, B.; Shine, H. J. *Journal of Organic Chemistry* **1988**, *53*, 5142–5143.

(44) Bandlish, B. K.; Shine, H. J. *Journal of Organic Chemistry* **1977**, *42*, 561–563.

(45) de Sorgo, M.; Wasserman, B.; Szwarc, M. *Journal of Physical Chemistry* **1972**, *76*, 3468.

(46) Martin, R. P.; Sawyer, D. T. *Inorganic Chemistry* **1972**, *11*, 2644–2647.

(47) Tapsoba, I.; Haouas, B.; Boujlel, K. *Journal of Electroanalytical Chemistry* **2004**, *574*, 107–112.

(48) Zao, B.-J.; Evans, D. H.; Maícias-Ruvalcaba, N. A.; Shine, H. J. *Journal of Organic Chemistry* **2006**, *71*, 3737–3742.

(49) Friedrich, R.; Janietz, S.; Wedel, A. *Macromolecular Chemistry and Physics* **1999**, *200*, 739–744.

(50) Giauque, W. F.; Stephenson, C. C. *Journal of the American Chemical Society* **1938**, *60*, 1389–1394.

(51) Burow, D. F. In *The Chemistry of Nonaqueous Solvents*; Lagowski, J. J., Ed.; Academic Press, New York and London, 1970; Vol. 3, Chapter 2, pp 137–185.

(52) Leftin, H. P.; Lichtin, N. N. *Journal of the American Chemical Society* **1957**, *79*, 2475–2480.

(53) Chan, S.; Gooley, C. M.; Keyzer, H. *Tetrahedron Letters* **1975**, *13*, 1193–1196.

(54) Sheldrick, G. M. *Acta Crystallographica Section A* **1990**, *46*, 467–473.

(55) Mews, R.; Lork, E.; Watson, P. G.; Görtler, B. *Coordination Chemistry Reviews* **2000**, *197*, 277–320.

(56) Blessing, R. H. *Acta Crystallographica Section A* **1995**, *51*, 33–38.

(57) Shannon, R. D.; Gumerman, P. S. *Journal of Inorganic Nuclear Chemistry* **1976**, *38*, 699–703.

(58) Jansen, M. *Angewandte Chemie Intenational Edition* **1987**, *26*, 1098–1110.

(59) Pyykkö, P. *Chemical Reviews* **1997**, *97*, 597–636.

(60) Amthor, S.; Lambert, C.; Graser, B.; Leusser, D.; Selinka, C.; Stalke, D. *Organic & Biomolecular Chemistry* **2004**, *2*, 2897–2901.

(61) Bertinelli, F.; Bizzari, P. C.; Casa, C. D.; Fiorini, M. *Journal of Polymer Science Part B: Polymer Physics* **1988**, *26*, 2203–2214.

(62) S.Kinugasa,; K.Tanabe,; T.Tamura, *Spectral Database for Organic Compounds SDBS*, 2008.
`http://riodb01.ibase.aist.go.jp/sdbs/cgi-bin/cre_index.cgi`.

(63) Brown, I. D. *Acta Crystallographica Section A* **1976**, *32*, 24.

(64) Shannon, R. D. *Acta Crystallographica Section A* **1976**, *32*, 751–767.

(65) Jenkins, H. D. B.; Roobottom, H. K.; Passmore, J.; Glasser, L. *Inorganic Chemistry* **1999**, *38*, 3609–3620.

(66) Marcus, Y.; Jenkins, H. D. B.; Glasser, L. *Journal of Chemical Society, Dalton Transaction* **2002**, 3795–3798.

(67) Bergson, G. *Acta Chemica Scandinavica* **1957**, *11*, 580–581.

(68) Cooper, R. I.; Gould, R. O.; Parsons, S.; Watkin, D. J. *Journal of Applied Crystallography* **2002**, *35*, 168–174.

(69) Gutmann, V.; Mayer, U.; Krist, R. *Synthesis and Reactivity in Inorganic and Metal-Organic Chemistry* **1974**, *4*, 523–533.

(70) Schenk, W. A. *Angewandte Chemie* **1987**, *99*, 101–112.

(71) Uchida, T.; Kimura, K. *Acta Crystallographica Section C* **1984**, *40*, 139–140.

(72) Thalladi, V. R.; Smolka, T.; Gehrke, A.; Boese, R. *New Journal of Chemistry* **2000**, *24*, 143–147.

(73) Emsley, J. *Chemical Society Reviews* **1980**, *9*, 91–124.

(74) Lindemann, R.; Zundel, G. *Journal of Chemical Society, Faraday Transaction 2* **1977**, *73*, 788–803.

(75) Denk, G. *Fresenius' Journal of Analytical Chemistry* **1956**, *153*, 367.

(76) Weinrach, J. B.; Meyer, D. R.; Joseph T. Guy, J.; Michalski, P. E.; Carter, K. L.; Grubisha, D. S.; Bennett, D. W. *Journal of Crystallographic and Spectroscopic Research* **1992**, *22*, 291.

(77) Hodgeman, W. C.; Weinrach, J. B.; Bennett, D. W. *Inorganic Chemistry* **1991**, *30*, 1611–1614.

(78) Peter, L.; Meyer, B. *Journal of Molecular Structure* **1982**, *95*, 131–139.

(79) Boyle, T. J.; Andrews, N. L.; Alam, T. M.; Tallant, D. R.; Rodriguez, M. A.; Ingersoll, D. *Inorganic Chemistry* **2005**, *44*, 5934–5940.

(80) Ghilane, J.; Haplot, P.; Bard, A. J. *Analytical Chemistry* **2006**, *78*, 6868–6872.

(81) Gritzner, G.; Kuta, J. *Pure & Applied Chemistry* **1984**, *56*, 461–466.

(82) Compton, R. G.; Banks, C. E. *Understanding Voltammetry*, illustrated ed.; World Scientific, 2007.

(83) Bock, H.; Lechner-Knoblauch, U. *Journal of Organometallic Chemistry* **1985**, *294*, 295–304.

(84) Zhou, M.; Pagels, M.; Geschke, B.; Heinze, J. *Journal of Physical Chemistry B* **2002**, *106*, 10065–10073.

(85) Farrugia, L. J. *Journal of Applied Crystallography* **1999**, *32*, 837–838.

(86) Spek, A. L. *Journal of Applied Crystallography* **2003**, *36*, 7–13.

(87) Sheldrick, G. M. *SHELX-97, A program for crystal structure refinement*; 1997.

List of Figures

1.1 Molecular formula of thianthrene (a), including the atom numbering scheme (according to *Chemical Abstracts*) and some of its substitution derivates; selenanthrene (b), phenoxathiin (c) and phenazine (d). . . . 3

1.2 The structure of the thianthrene-gold(III)chloride complex.[17] 5

1.3 Bis(μ-η^2-thianthrene)disilver(I) bis(perchlorate),[23] a dimer with a center of inversion. Hydrogen atoms are not shown. 6

1.4 The structure of thianthrene radical ion dimer in the structure of thianthrene radical cation tetrachloridoaluminate.[9] 7

1.5 Tris(thianthrene)(2+), a trimer with an inversion center in the structure of tris(thianthrene)(2+) bis(dodecamethylcarba–*closo*–dodecaborate) dichloromethane tetrasolvate.[34] The anion and solvate molecules are omitted. 8

1.6 Curve of vapor pressure of SO_2 derived from literature.[51] The investigation ranges from –70° to +40 °C (203–313 K) which corresponds to 0.02 to 6.22 bar. 10

1.7 Curve of density and viscosity of SO_2 derived from literature.[51] The laboratory work ranges from –70° to +40 °C (203–313 K) which corresponds to 1.61 to 1.32 g/cm^3 and 6.57 to 2.58 mP, respectively. . . 10

2.1 An individual complex in the structure of $[Ag_2(TA)_2][BF_4]_2 \cdot 3\,SO_2$. Thermal displacement ellipsoids are scaled to include 50% probability. Symmetry operation I = 1.5-x, 0.5-y, 1-z. 14

2.2 The BF_4 unit in $[Ag_2(TA)_2][BF_4]_2 \cdot 3\,SO_2$ is shown as a superimposition of two orientations. F3, F4, F5 and F6 are each refined as a half occupied atoms. Thermal displacement ellipsoids are scaled to include 50% probability. 15

2.3 The SO_2 units in $[Ag_2(TA)_2][BF_4]_2 \cdot 3\,SO_2$, one of them is shown as a superimposition of two orientations. O3 and O4 are each refined as a half occupied. Thermal displacement ellipsoids are scaled to include 50% probability. Symmetry operation I = 2-x, y, 1.5-y. 16

2.4 View of the unit cell of $[Ag_2(TA)_2][BF_4]_2 \cdot 3\,SO_2$ along *b*-axis. H atoms are omitted for clarity, the dotted line represents weak interaction between SO_2 molecule through O atom and Ag ions. 17

2.5 The $[Ag_2(TA)_3]^{2+}$ unit in the structure of $[Ag_2(TA)_3][SbF_6]_2 \cdot 5\,SO_2$. Thermal displacement ellipsoids are scaled to include 50% probability. H atoms are drawn with arbitrary radii. 21

2.6 Two independent $[SbF_6]^-$ ions and the five independent SO_2 molecules in the structure of $[Ag_2(TA)_3][SbF_6]_2 \cdot 5\,SO_2$. Thermal displacement ellipsoids are scaled to include 50% probability. 21

2.7 View of the unit cell of $[Ag_2(TA)_3][SbF_6]_2 \cdot 5\,SO_2$ along the *b*-axis. H atoms are omitted for clarity. The SO_2 molecules and SbF_6 anions fill up the space between layers of the complex cations. 23

2.8 The two independent $[AuCl_2(TA)_2]^+$ complex cation in the structure of $[AuCl_2(TA)_2][AuCl_4]$. Thermal displacement ellipsoids are scaled to include 50% probability. H atoms are drawn with arbitrary radius. Symmetry operation I = 1-x, 2-y, 2-z; II = 2-x, 1-y, 1-z 30

2.9 Two independent $[AuCl_4]^-$ units in the structure of $[AuCl_2(TA)_2][AuCl_4]$. Thermal displacement ellipsoids are scaled to include 50% probability. Symmetry operations: III = 1-x, 1-y, 2-z; IV = 1-x, 1-y, 1-z 31

2.10 The cationic complexes in the structure of $[AuCl_2(TA)_2][AuCl_4]$ make up a chain-like arrangement along the –111 direction and the cations are located on special positions on the center of the unit cell, four edges and four faces of the unit cell. H atoms are omitted for clarity. 32

2.11 DSC measurement of $[AuCl_2(TA)_2][AuCl_4]$ was done in 3 cycles. Each cycle started from room temperature to a certain value and back to the initial temperature at rate of 10 K per minute, up and down as well. The highest temperatures were 383 K, 403 K and 423 K at the top of 1st, 2nd and 3rd cycle, respectively. 36

2.12 The remission profile of $[AuCl_2(TA)_2][AuCl_4]$ (continuous line) evaluated with Kubelka-Munk function. In the background the intensity profile of the Xe-lamp is given (dotted line). The dotted and the continuous lines are scaled differently with respect to the y-axis. 38

2.13 Specific conducitivity of $[AuCl_2(TA)_2][AuCl_4]$ as a function of temperature, $ln(\sigma) = f(T^{-1})$. Applied potential was 1 V. 40

2.14 The two crystallographically independent complexes in $[AlCl_3TA]$. Thermal displacement ellipsoids are scaled to include 50% probability. H atoms were drawn with arbitrary radii. 41

2.15 The configuration of two independent complexes in the structure of $[AlCl_3TA]$ shown in different views: along Al–S bonds (top) and along the plane of the TA ligands (bottom). H atoms are omitted for clarity. 42

2.16 The arrangement of complexes in the structure of $[AlCl_3TA]$. H atoms are omitted for clarity. 43

2.17 The thermal behavior of colorless [$AlCl_3TA$] crystals. The DSC measurement was done in two cycles of heating and cooling each between 303 – 383 K. 47

2.18 The conductivity measurement of the colorless [$AlCl_3TA$] crystals. The measured values are plotted as the function of *specific resistivity = f(temperature)*. Applied potential was 1 V. 48

2.19 The Arrhenius plot of the conductivity function of [$AlCl_3TA$] according to $ln(\sigma) = f(T^{-1})$. 48

2.20 The color change of the colorless crystalline sample of [$AlCl_3TA$] in quartz tube in open air at ambient temperature after the conductivity measurement. The dark area is referred to violet color. 49

2.21 The Raman spectra of [$AlCl_3TA$] crystals and pure thianthrene. The insets show enlarged ranges of the spectra containing vibrations of C–S bonds of thianthrene, ticked with black marks. 50

2.22 The asymmetric unit of the structure of $(TA^{\cdot +})(HSO_4) \cdot H_2SO_4$. Thermal displacement ellipsoids are scaled to include 50% probability. H atoms are drawn with arbitrary radii. 53

2.23 The pair of cations in the structure of $(TA^{\cdot +})(HSO_4) \cdot H_2SO_4$, generated through an inversion center. The S···S distances amount 3.05 Å. Thermal displacement ellipsoids are scaled to include 50% probability. H atoms are drawn with arbitrary radii. Symmetry operation I = -x, 2-y, 2-z. 53

2.24 The arrangement of molecules in $(TA^{\cdot +})(HSO_4) \cdot H_2SO_4$. The SO_4 units are shown as polyhedra, hydrogen atoms are omitted for clarity. . . . 54

2.25 The $HSO_4^- \cdot H_2SO_4$ hydrogen bridged network in the structure of $(TA^{\cdot})(HSO_4) \cdot H_2SO_4$. The hydrogen bonds are drawn in the same way as the other bonds. Thermal displacement ellipsoids are scaled to include 50% probability. H atoms are drawn with arbitrary radii. Symmetry operation I = -x, 3-y, 1-z; II = 1+x, y, z; III = -x, 3-y, 2-z. 55

2.26 The thianthrene radical cations pair in $(TA^{\cdot})[FeCl_4]$. Thermal displacement ellipsoids are scaled to include 50% probability. H atoms are drawn with arbitrary radii. 59

2.27 The arrangement of the ions in the unit cell of $(TA^{\cdot})[FeCl_4]$. 60

2.28 The $[FeCl_4]^-$ anions in the structure of $(TA^{\cdot})[FeCl_4]$. Thermal displacement ellipsoids are scaled to include 50% probability. 60

2.29 The view of cationic thianthrene trimer and the $[Al_2Cl_7]^-$ ion in the structure of $(TA_3)[Al_2Cl_7]_2$. Thermal displacement ellipsoids are scaled to include 50% probability. H atoms are drawn with arbitrary radii. Symmetry operation I = 1-x, 1-y, 1-z. 65

2.30 Arrangement of the ions in the structure of $(TA_3)[Al_2Cl_7]_2$ in a view along crystallographic and *b*-axis (top), along the stack of the thianthrene trimer (middle) and along crystallographic *a*-axis (bottom). 66

2.31 The selenanthrene radical cation pair in the structure of $SA^{\cdot}[AlCl_4]$. Thermal displacement ellipsoids are scaled to include 50% probability. H atoms are drawn with arbitrary radii. 72

2.32 The two independent $[AlCl_4]^-$ anions in the structure of $(SA^{\cdot})[AlCl_4]$. Thermal displacement ellipsoids are scaled to include 50% probability. 72

2.33 The molecular moiety in the structure of $SAO(HSO_4)_2$. Thermal displacement ellipsoids are scaled to include 50% probability. H atoms are drawn with arbitrary radii. I = 1-x, 2-y, 1-z; II = -x, 2-y, 2-z; III = 1-x, 1-y, -z. 78

2.34 The unit cell view in the $\mathrm{SAO(HSO_4)_2}$. Thermal displacement ellipsoids are scaled to include 50% probability. H atoms are drawn with arbitrary radii. 79

2.35 The Lewis structure of $\mathrm{SAO(HSO_4)_2}$ (left) and selenanthrene-5,10-dioxide (right). 79

2.36 The two independent $\mathrm{SA}^{\bullet+}$ molecules in the structure of $\mathrm{(SA^{\bullet})_2[SO_4(BF_3)_2] \cdot SO_2}$. Thermal displacement ellipsoids are scaled to include 50% probability. H atoms are drawn with arbitrary radii. 83

2.37 The arrangement the molecules in the structure of $\mathrm{(SA^{\bullet})_2[SO_4(BF_3)_2] \cdot SO_2}$ in a view along the crystallographic *a*-axis. 84

2.38 The anion $\mathrm{[F_3B{-}O(SO_2)O{-}BF_3]^{2-}}$ and the $\mathrm{SO_2}$ solvate molecule in the structure of $\mathrm{(SA^{\bullet})_2[SO_4(BF_3)_2] \cdot SO_2}$. Thermal displacement ellipsoids are scaled to include 50% probability. 85

2.39 A view of the asymmetric unit in structure of $\mathrm{(SA^{\bullet})_2[SO_4(BF_3)_2] \cdot SO_2}$. Atom B2 deviates most from the best plane through F5, B1, O4, S1, O1, B2, F2 and S2, by 0.0352 Å. 85

2.40 The asymmetric unit of the structure of $\mathrm{(H_2PAz)(HSO_4)_2}$. Thermal displacement ellipsoids are scaled to include 50% probability. H atoms are drawn with arbitrary radii. 89

2.41 The $\mathrm{H_2PAz^{2+}}$ cation and the $\mathrm{HSO_4^-}$ anions in the structure of $\mathrm{(H_2PAz)(HSO_4)_2}$. The dotted lines represent hydrogen bonds which connect both moieties. Thermal displacement ellipsoids are scaled to include 50% probability. H atoms are drawn with arbitrary radii. Symmetry operation I = 1-x, 1-y, 1-z; II = x, -1+y, z; III = 1-x, 2-y, 1-z. 90

2.42 The molecular arrangement in the structure of $\mathrm{(H_2PAz)(HSO_4)_2}$. H atoms are omitted for clarity. 91

2.43 The chain of HSO_4^- in the structure of $(H_2PAz)(HSO_4)_2$ connected via hydrogen bonds. H atoms are drawn with arbitrary radii. 91

2.44 Photograph of a broken ampoule of the reaction of TA and $AlCl_3$ (left). When the wrapping paper was uncoiled and stretched, black smudge through the layers of the paper is visible (right). 98

2.45 Mass spectrum of purified thianthrene. 99

2.46 Mass spectrum of the residue of the toluene extract of the reaction product of TA + $AlCl_3$ in liquid SO_2 (*extracted reaction products*). . . 99

2.47 ^{1}H–NMR spectrum of a fresh solution of TA and O_2 in liquid SO_2. . . 102

2.48 ^{1}H–NMR spectrum of a solution of TA and O_2 in liquid SO_2 after 8 months. 102

2.49 Cyclic voltammetry measurements of thianthrene in liquid SO_2. Single scans comparison at different temperatures. 103

2.50 Cyclic voltammetry measurements of thianthrene in liquid SO_2 (continuous line) and in acetonitrile (dotted line) as well. Average of 5 scans at room temperature with ferrocene (Fc/Fc^+) as the reference redox system. 104

4.1 Molecular entities present in the crystal structures of (**1**): dinuclear complex cation $[Ag_2(TA)_2]^{2+}$ in $[Ag_2(TA)_2][BF_4]_2 \cdot 3\,SO_2$, (**2**): dinuclear complex cation $[Ag_2(TA)_3]^{2+}$ in $[Ag_2(TA)_3][SbF_6]_2 \cdot 5\,SO_2$, (**3**): complex cation $[AuCl_2(TA)_2]^+$ in $[AuCl_2(TA)_2][AuCl_4]$, (**4**): neutral complex $[AlCl_3TA]$, (**5**, **6**, **8**, **10**): radical cation pair $(TA^{\bullet +})_2$ in $(TA^{\bullet})(HSO_4) \cdot H_2SO_4$, $(TA^{\bullet})[FeCl_4]$ and $(SA^{\bullet +})_2$ in $(SA^{\bullet})[AlCl_4]$ and $(SA^{\bullet})_2[SO_4(BF_3)_2]$, (**7**): stacked trimer $(TA)_3^{2+}$ in $(TA_3)[Al_2Cl_7]_2$, (**9**): μ-oxy-selenanthrene(2+) in $SAO(HSO_4)_2$, and (**11**): phenazinediium in $(H_2PAz)(HSO_4)_2$. 117

A.1 Specification of the liquid SO_2 by the supplier AirProducts Inc. The SO_3 content is reported to be less than 0.1%. 120

A.2 Specification of the liquid SO_2 by the supplier Praxair Inc. The SO_3 content of the 3.8 grade in form of H_2SO_4 is less than 25 ppm/w. . . 121

A.3 Schematic view of the pressure-tight H-shaped reaction vessel. 124

A.4 A schematic view of the equipment for single crystal selection under inert conditions at low temperature. (A) Metal pipe, (B) large Dewar flask, (C) concave glass dish, (D) short Dewar flask and (E) microscope. The Dewar flasks are filled with liquid nitrogen. Arrows show the flow of the nitrogen gas. 125

A.5 Schematic view of the components of the home made–pressure tight–electrode. 127

A.6 Schematic view of the voltammetry cell. 127

List of Tables

2.1 Details of structure determination for $[Ag_2(TA)_2][BF_4]_2 \cdot 3\,SO_2$. 18

2.2 List of selected bond lengths/Å in $[Ag_2(TA)_2][BF_4]_2 \cdot 3\,SO_2$. 19

2.3 List of selected bond angles/° in $[Ag_2(TA)_2][BF_4]_2 \cdot 3\,SO_2$. 19

2.4 Details of structure determination for $[Ag_2(TA)_3][SbF_6]_2 \cdot 5\,SO_2$. . . . 25

2.5 List of selected bond lengths/Å in $[Ag_2(TA)_3][SbF_6]_2 \cdot 5\,SO_2$. 26

2.6 List of selected bond angles/° in $[Ag_2(TA)_3][SbF_6]_2 \cdot 5\,SO_2$. 27

2.7 Details of structure determination for $[AuCl_2(TA)_2][AuCl_4]$. 33

2.8 List of selected bond lengths/Å in $[AuCl_2(TA)_2][AuCl_4]$. 34

2.9 List of selected bond angles/° in $[AuCl_2(TA)_2][AuCl_4]$. 34

2.10 A comparison of IR absorption bands of pure thianthrene according to literature and the spectrum of $[AuCl_2(TA)_2][AuCl_4]$. 37

2.11 Details of structure determination for $[AlCl_3TA]$. 44

2.12 List of bond lengths in $[AlCl_3TA]$. 45

2.13 List of selected bond angles/° in $[AlCl_3TA]$. 45

2.14 Details of structure determination for $(TA^{\bullet})(HSO_4) \cdot H_2SO_4$. 57

2.15 List of selected bond lengths/Å in $(TA^{\bullet})(HSO_4) \cdot H_2SO_4$. 58

2.16 List of selected bond angles/° in $(TA^{\bullet})(HSO_4) \cdot H_2SO_4$. 58

2.17 Details of structure determination for $(TA^{\bullet})[FeCl_4]$. 62

2.18 List of selected bond lengths/Å in $(TA^{\bullet})[FeCl_4]$. 63

2.19 List of selected bond angles/° in $(TA^{\bullet})[FeCl_4]$. 63

2.20 Details of structure determination for $(TA_3)[Al_2Cl_7]_2$. 69

2.21 List of selected bond lengths/Å in $(TA_3)[Al_2Cl_7]_2$. 70

2.22 List of selected bond angles/° in $(TA_3)[Al_2Cl_7]_2$. 70

2.23 Details of structure determination for $(SA^{\bullet})[AlCl_4]$. 74

2.24 List of selected bond lengths/Å in $(SA^{\bullet})[AlCl_4]$. 75

2.25 List of selected bond angles/° in $(SA^{\bullet})[AlCl_4]$. 76

2.26 Details of structure determination for $SAO(HSO_4)_2$. 80

2.27 List of selected bond lengths/Å in $SAO(HSO_4)_2$. 81

2.28 List of selected bond angles/° in $SAO(HSO_4)_2$. 81

2.29 Details of structure determination for $(SA^{\bullet})_2[SO_4(BF_3)_2] \cdot SO_2$. 86

2.30 List of selected bond lengths/Å in $(SA^{\bullet})_2[SO_4(BF_3)_2] \cdot SO_2$. 87

2.31 List of selected bond angles/° in $(SA^{\bullet})_2[SO_4(BF_3)_2] \cdot SO_2$. 87

2.32 Details of structure determination for $(H_2PAz)(HSO_4)_2$. 93

2.33 List of selected bond lengths/Å in $(H_2PAz)(HSO_4)_2$. 94

2.34 List of selected bond angles/° in $(H_2PAz)(HSO_4)_2$. 94

2.35 Raman spectrometry qualitative experiment for dithionite 97

2.36 Gravimetry evaluation of the reaction between TA and $AlCl_3$ in liquid SO_2. 100

A.1 List of chemicals used 119

A.2 List of analytical instruments used 122

B.1 List of software used 128